SCUOLA INTERNAZIONALE SUPERIORE DI STUDI AVANZATI
INTERNATIONAL SCHOOL FOR ADVANCED STUDIES
Elementary Particle Theory Sector
Statistical Physics Curriculum

Quench dynamics of many-body systems

Thesis submitted for the degree of
Doctor Philosophiæ

ADVISORS:
Prof. Giuseppe Santoro
Prof. Rosario Fazio
Dr. Alessandro Silva

CANDIDATE:
Elena Canovi

27th September 2010

Contents

List of Figures

Introduction

In the last few years the study of condensed matter systems has received an exceptional boost due to some experimantal breakthroughs in the field of cold atoms. The unprecedented level of accuracy and precision reached in this field allows to realize perfectly tunable quantum systems described e.g. by the Hubbard, Bose-Hubbard, Luttinger and Kondo models. It is worth stressing that until some decades ago such models were toy-models, i.e. theoretical simplified models proposed to capture the low energy physics of more complex systems. At present, one of the long-term goals of this experimental work is to concretly implement devices supporting quantum computation. But most interestingly, the situation is now that the continuous experimental advances explore new frontiers of condensed matter physics, which call for a theoretical understanding. The non-equilibrium dynamics in closed quantum systems lies indeed at one of such frontiers. On the theoretical side, while a lot of tools (mean field theory, renormalization group, conformal field theory, just to mention some of them) help in understanding equilibrium systems, much less is known for systems out of equilibrium.

Out of the several ways in which an interacting quantum system may be pushed out of equilibrium, here we concentrante on the case of a *quantum quench*. This is nothing but a change in one of the system parameters: it could happen slowly, through a continuous time dependence of a part of the Hamiltonian, or suddenly. Both the slow and sudden quenches disclose very rich physics linking different ingredients (e.g. quantum phase transitions, thermalization, integrability) and stimulating the development of beautiful theories.

In the case of a slow quench, the Hamiltonian visits differents points in the phase space during its evolution. A particularly intriguing situation is when at a given time the system crosses a phase transition: the initial and final states are thus macroscopically different. An experimental milestone in the observation of quantum phase transitions is the work by Greiner *et al.* [78]. They succeeded in realizing the superfluid-insulator phase transition

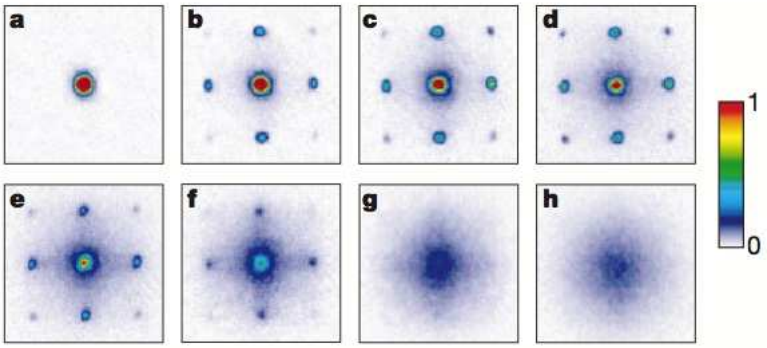

Figure 1: Absorption images of multiple matter wave interference patterns, showing the Mott insulating phase and the superfluid phase. Adapted from Ref. [78]

in the Bose-Hubbard model, see Fig. 1. Following this seminal work, other experiments have been performed in this direction [133, 146, 121], for a review see Ref. [10].

The interest in slow quenches is also related to quantum computation protocols, as in Adiabatic Quantum Computation [65, 134, 135]. The idea is to map a the solution of a classical optimization problem into the ground state of a quantum Hamiltonian. The way to find this (complex) unknown state is buidling a time-dependent Hamiltonian, such that at the initial time it possesses a known and very simple ground state and such that the ground state of the final Hamiltonian is the solution of the complex problem. The fundamental ingredient is the quantum adiabatic theorem. Starting the evolution in the (known) ground-state, if the Hamiltonian is always gapped and the Hamiltonian changes not too quickly, then the system will remain in the ground state throughout the whole evolution, thus leading to the solution of the optimization problem. Crossing a quantum phase transition spoils this scheme, because in the thermodynamic limit the gap is known to vanish.

From the theoretical point of view, universality, which is at the deep roots of quantum phase transitions, is the key for understanding the dynamics of quenches involving critical points. On the grounds of simple arguments based on universality, it is possible to predict the scaling of many observables related to the loss of adiabaticity at critical points, like the number of topological defects. This is the main finding of the two seminal works in this context [157, 115], which set the foundations of two equivalent theoretical frameworks known as Kibble-Zurek mechanism (KZM) and Adia-

batic Perturbation Theory (APT) respectively. The KZM, originally formulated for classical transitions driven by thermal fluctuations [156] and then adapted to quantum systems at zero temperature, assumes that the evolution of a system driven through a quantum phase transition becomes diabatic when the time scale at which the Hamiltonian is varied is of the order of the relaxation time, determined by the inverse of the instantaneous gap. Adiabaticity is recovered only when, after the critical point has been crossed, the relaxation time comes back to be smaller than the time scale of the variation of the Hamiltonian, τ, and the defect density can be estimated via the correlation length ξ at the instant of the loss of adiabaticity. KZM has been tested in various models through both analytical and numerical studies [30, 33, 39, 40, 51, 52, 56, 59, 93, 104, 115, 157] and it is also supported by experiments [133] and, in generalized formulations, in Refs. [4, 22, 40, 43, 57, 60, 140]. Adiabatic perturbation theory [115, 117], appeared almost contemporarily to the quantum rielaboration of KZM, moves instead from a different perspective: the excitation probability during the dynamics is estimated by considering only transitions involving the instantaneous ground state and neglecting the contribution of direct population exchange between excited states. Then general scaling arguments can be invoked in order to extract the dependence of the defect density on the quench time scale τ. The crossing of critical points is actually only one of the applications of APT, which also works for both gapped and gapless systems with quasi-particle excitations, sudden quenches with small amplitude and finite temperature systems [39, 40, 41, 42, 127, 128] . It should be mentioned that recent studies have highlighted particular transitions apparently not describable with these approaches [23, 25, 45, 49, 50, 104, 110, 141].

In the opposite limit, when a closed quantum system undergoes a sudden quench, the energy after the quench is constant and is distributed among the various degrees of freedom during the evolution. Different questions arise in this case. Are the interactions within the degrees of freedom of the system sufficient to establish ergodicity? Does the system reach asymptotically a steady state? Is this steady state thermal? The definition of quantum ergodicity is a very subtle topic which has been discussed from the early days of quantum mechanics until now [47, 76, 97, 111, 144, 151]. A crucial result of this theoretical discussion is that, differently from classical systems, in quantum systems ergodicity must be defined with respect to macroscopic observables rather than to states.

The issue of thermalization in closed quantum systems has triggered a lot of attention after the experiment by Kinoshita *et al.*, in which they realized a nearly integrable system which does not thermalize, see Fig. 2. Indeed

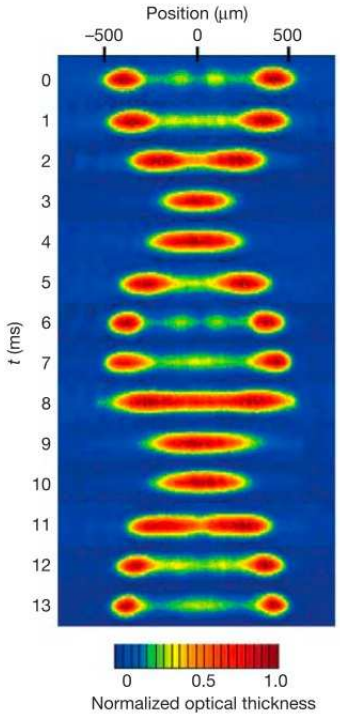

Figure 2: Time-of-flight absorption images of an ensemble of 1D Bose gases after the atoms were placed in a superposition of $\pm 2p_0$ momentum states. Adapted from Ref. [89]

integrability implies an infinite number of conserved quantities, so that specifying the initial state through its energy is not enough to make predictions about the asymptotic state. Nevertheless a characterization of the steady state and of the asymptotic bahavior of some local observables is possible through the generalized Gibbs ensemble (GGE), proposed by Rigol *et al.* in Ref. [125]. The GGE is a statistical ensemble that keeps track of all the integrals of motion. The conditions of applicability and the drawbacks of this ensemble have been extensively investigated [5, 16, 18, 27, 35, 61, 70, 75]. For nonintegrable systems, thermalization is expected to occur for all the observables, as numerically confirmed in many circumstances [26, 62, 91, 96, 124, 123, 126]. The mechanism underlying thermalization is related to quantum chaos, as originally proposed in Ref. [111]. The presence of quantum chaos means that simple observables are represented by random matrices in the eigenbasis of the Hamiltonian. More recently thermalization in nonintegrable systems has been precisely formulated in terms of the eigenstate

thermalization hypothesis (ETH). It states that the expectation value of some natural observable is a smooth function of the energy of the eigenstates [47, 144, 9], so thermalization in quantum chaotic systems happens at the level of individual eigenstates. In this context an interesting direction of research involves the crossover from integrability to non-integrability and the correspondent thermal or non thermal behavior in relation with quantum chaos [8, 91, 96, 123, 124]. Indeed is has been known for long [114] that integrable systems are characterized by a Poisson distribution of the level statistics, while the distribution is Wigner-Dyson in non-integrable systems.

The results discussed in this Thesis, developed during the PhD course, focus on both the adiabatic and the sudden quench dynamics. In the former case we test the applicability of the scaling relations of the KZM and its generalizations for a system related to the Bose-Hubbard model, which, as we mentioned above, is of primary experimental importance. In the latter case we focus on the issue of thermalization and the way it is entangled with integrabilty. We find that the problem of thermalization can be successfully formulated in the language of many-body localization. We also suggest that disorder may affect significantly the way non-local observables reach their asymptotic state in integrable systems.

The contents of the Thesis are organized as follows. In Chapter 1 we review the state of the art about the dynamics both in the adiabatic case and after a sudden quench.
In Chapter 2 we study the adiabatic dynamics of an anisotropic spin-1 chain across a second order quantum phase transition of the Berezinskii-Kosterlitz-Thouless type. We consider a linear quench in the single spin anisotropy and characterize the loss of adiabaticity after the quench through the excess energy. We will show that, for sufficiently large system sizes, the excess energy admits a non-trivial scaling behavior that is not predictable by standard Kibble-Zurek arguments for isolated critical points or extended critical regions. This emerges from a competing effect of many accessible low-lying excited states, inside the whole continuous line of critical points.
In Chapter 3 we concentrate on the study of the dynamics following a sudden quench and to its interplay with integrability. We will describe the onset of thermalization in terms of localization-delocalization transition in quasi-particle space [2, 6] induced by the integrability breaking term. We will further show that, in order to observe such a transition, one has to investigate the behavior of observables which are local in terms of quasi-particles. Indeed, as it is known from previous studies [129, 130], non-local quantities do thermalize also in the integrable case. We will test the validity of our conjecture in the XXZ model in the presence of an integrability breaking

term. We will first characterize the breaking of integrability in detail and quantify the delocalization in quasi-particle space in terms of some statistical quantities, and then look at the behavior of two observables, a local and a non-local one, in order to verify their different sensitivity to the the breaking of integrability and their possibility of thermalization. In Appendix B we further support our conjecture in different non-integrable models.
In Chapter 4 we will present some preliminary results about the dynamics of the disordered Ising model after a sudden quench of the transverse field. First of all we will compare the real-time dynamics of the model with a constant Hamiltonian at $T = 0$ and at finite temperature to the imaginary time dynamics [85, 153, 152]. Building on the known results for the ordered case [129, 130], we will then numerically investigate the effect of disorder on the time-evolution and the asymptotics of a non-local observable.

Chapter 1

Quantum quenches in many-body systems

1.1 Adiabatic dynamics close to a quantum phase transition

The subject of this section is the dynamics of a closed quantum system whose Hamiltonian possesses a continuous time dependence in one of its parameters, in particular here we will be interested in the situation in which the system crosses a quantum phase transition during its evolution. In what follows we will briefly recall the concept of quantum phase transition and then review the major theoretical achievements describing with simple physical arguments the non-equilibrium dynamics of this kind of systems. We will see that it is possible to characterize the scaling of observables through the knowledge of the critical exponents of the phase transition. Some very recent revews can be found in Refs. [58, 79, 118], see also Ref [20].

1.1.1 Dynamics thorugh a quantum phase transition.

A phase transition is a drastic change in the structure and/or properties of a system: the simplest example from common experience is the change of state of substances from the gaseous to the liquid state, from liquid to solid, etc. Classical transitions are driven by thermal fluctuations and occur at a finite temperature, called critical temperature. On the contrary quantum phase transitions (QPT) occur at $T = 0$ and are entirely driven by quantum fluctuations. Both classical and quantum phase transitions are characterized by the existence of an order parameter which becomes non-zero in the ordered phase. The order parameter can be continuous or show a jump at

the transition point depending on whether the transition is of second or first order respectively. Only second order phase transitions [131] are considered in this Thesis. Indeed they involve a very rich physics and can be studied through a variety of powerful theoretical tools, which turn out to capture also the non-equilibrium dynamics.

A second order quantum phase transition can be studied by means of two quantities: the correlation length ξ and the energy scale Δ, which typically is the gap, i.e. the energy difference between the ground state and the first excited state. The correlation length ξ is a characteristic length scale which for example determines the exponential decay of equal time correlations in the ground state or the length scale at which some characteristic crossover occurs to the correlations at the longest distances. Consider a parameter dependent Hamiltonian $H(\lambda)$, where λ is dimensionless. At a QPT the correlation length diverges as:

$$\xi^{-1} \propto |\lambda - \lambda_c|^{\nu} \tag{1.1.1}$$

where ν is a *critical exponent*. Generally speaking, the fundamental feature of critical exponents is that they are universal, i.e. they do not depend on most of the microscopic details of the Hamiltonian, but for example on the dimensionality of the system and on its symmetries. In correspondence with the divergence of the correlation length, the gap Δ vanishes in the thermodynamic limit according to:

$$\Delta \sim \xi^{-z} \,, \tag{1.1.2}$$

where z is the dynamical critical exponent. In terms of the distance from the critical point, Eq. 1.1.2 can be rewritten as:

$$\Delta \sim |\lambda - \lambda_c|^{z\nu} \,. \tag{1.1.3}$$

The time scale on which a system is able to adjust its state to the variation of a parameter is measured by the inverse of the minimum instantaneous gap. The adiabatic theorem establishes that a system can be adiabatically driven without introducing excitations only if the transformation rate is much larger than the minimum gap encountered during the whole dynamics [99]. The critical closure of the gap then sets up an insurmountable obstacle for the adiabaticity condition: no matter how slow the system is driven through the transition, its evolution becomes impulsive.

A QPT takes place when the governing Hamiltonian is characterized by two (or more) competing parts: in Bose-Hubbard-like models the kinetic term copes with the onsite repulsion; in ferromagnetic Ising-like models the

coupling between spins along a particular direction has to struggle with a transverse field. Typically when the relative weight of one term with respect to the other is very large the system belongs to one phase; the transition happens when the intensity of the competing forces is of the same order. The dynamics through a QPT can be then performed by introducing a time modulation of the relative strength of the two terms.

In this section we will consider Hamiltonians with the following structure:

$$\mathcal{H}(t) = \mathcal{H}_0 + \lambda(t)\mathcal{H}_{\rm t} \tag{1.1.4}$$

where λ is typically chosen to vary linearly in time. We are interested in the case in which a given time, say $t = 0$ for convenience, $\lambda(t)$ is such that the Hamiltonian crosses a critical point. The dynamics of a system crossing a quantum critical point, i.e. with the known initial state and the unknown final state belonging to different phases, is characterized by the loss of adiabaticity due to the closure of the gap. In this situation the system becomes unavoidably excited with respect to the instantaneous ground state. In terms of the order parameter of the phase transition, the consequence is the production of defects. An intense theoretical effort has been devoted to quantifying the loss of adiabaticity by studying the scaling of suitable quantities which we will now recall.

A first measure of the loss of adiabaticity is the difference between the instantaneous energy of the system and the energy of the instantaneous ground state, whose normalized definition, the *excess energy*, is given by:

$$E_{\rm exc}(t) = \frac{\langle\psi(t)|\mathcal{H}(t)|\psi(t)\rangle - \langle\psi_{GS}(t)|\mathcal{H}(t)|\psi_{GS}(t)\rangle}{\langle\psi_0|\mathcal{H}(t)|\psi_0\rangle - \langle\psi_{GS}(t)|\mathcal{H}(t)|\psi_{GS}(t)\rangle} \tag{1.1.5}$$

This quantity, which we will study for a specific system in Chapter 2, depends on how fast the Hamiltonian is varied in time: the slower the variation, the smaller the excess energy. In particular, if the system remains always in its ground state $E_{\rm exc}$ is zero, while if the state of the system never changes (apart from phases) from the initial state, the excess energy is unity.

Another quite useful way of measuring the degree of adiabaticity of the evolution is in terms of the *infidelity*, that measures the total excitation probability of the evolved state with respect to the ground state of the final Hamiltonian

$$I = 1 - |\langle\psi(t_{\rm fin})|\psi_{GS}(t_{\rm fin})\rangle|^2 \tag{1.1.6}$$

where $|\psi_{GS}(t_{\rm fin})\rangle$ represents the ground state of $\mathcal{H}(t_{\rm fin})$. This quantity is commonly used in studying optimization problems involving an initial state and a target state to be reached after unitary evolution (see for example Ref. [24]).

Nevertheless the most widely used quantities used in literature to study nonadiabaticity are the total number of excitations $n_{\rm ex}$ and its density $\rho_{\rm ex}$, which for example may count the (density) of topological defects if they are well defined, or the number of created quasiparticles in theories which predict them. These quantities have been studied for example in the seminal papers [157, 115, 117]. Their definition is strongly dependent on the model in analysis and on what is considered as a defect. For instance in Ising chains, with the transverse field along the z direction, the defect density is identified with the kink density and can be defined as:

$$\rho_k = \frac{1}{N}\sum_{i}^{N-1}\langle\psi(t_{\rm fin})|\frac{1}{2}(1-\sigma_i^x\sigma_{i+1}^x)|\psi(t_{\rm fin})\rangle \tag{1.1.7}$$

where N is the size of the chain and σ_i^α are the Pauli operators.

Finally, non-adiabaticity can be accounted for studying the entropy, since it is conserved only for adiabatic processes, while it is expected to increase as the system passes through a quantum critical point. Identifying a suitable definition entropy is nevertheless quite subtle and two definitions have been used in literature: the diagonal entropy [116] and the entanglement entropy. The first is generated only due to nonadiabatic transition and in some cases satisfies the same scaling relations of the density of quasi-particles [40, 41, 42, 105]. The other definition consists in the entanglement entropy, i.e. the Von Neumann entropy of the reduced density matrix of a part of the system, which has been studied in the context of time independent conformal field theories at quantum phase transitions [148, 120, 14] and in sudden quenches in Refs. [15, 16, 31, 17, 19, 64, 63].

1.1.2 Kibble-Zurek mechanism and its generalizations.

Assuming that the non-adiabatic behavior manifests only nearby the critical point, it is natural to wonder whether the loss of adiabaticity can be described in terms of the static features of the transition, for instance through its critical exponents. The Kibble-Zurek mechanism [156] addressed exactly this issue, providing an elegant connection between statics and non-equilibrium properties. According to KZM the time scale at which the system is able to react to an external change diverges at the transition point as a manifestation of the critical slowing down, observed also in the classical case [157]. The main idea behind KZM is distinguishing two regimes for the evolution: the *adiabatic regime*, in which the system is able to follow the variation of the time dependent Hamiltonian, so that there is no population transfer between the instantaneous energy eigenstates, and the *impulse*

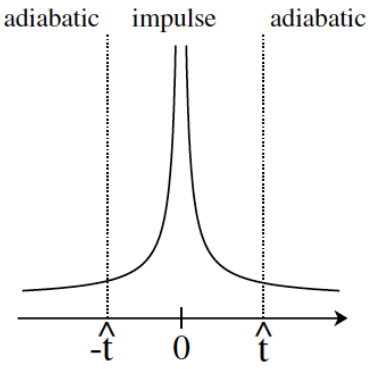

Figure 1.1: (color online). Relaxation time scale from KZM theory; $\hat{t}$ represents the freeze-out time (picture from Ref.[37]).

regime, which contains the critical point, where the relaxation times are so long that there is no change in the wave function except for an overall phase factor. The instant of the evolution which signals the boundary between the two regimes is called the freeze-out time, $\hat{t}$, see Fig.1.1.
According to the KZM, the adiabaticity is lost when the time remaining to the transition is equal to the relaxation time, given by the inverse of the instantaneous gap Δ. Calling $\epsilon \equiv \lambda - \lambda_c$ the dimensionless parameter measuring the distance from the transition, near the critical point ($\epsilon = 0$) its time dependence can be linearized:

$$\epsilon = t/\tau \tag{1.1.8}$$

where τ represents the quench time. The freeze-out time is thus given by:

$$\hat{t} \sim \Delta^{-1}(\hat{t}) = |\epsilon(\hat{t})|^{-z\nu} \tag{1.1.9}$$

or, in terms of τ:

$$\hat{t} \sim \tau^{-z\nu/(1+z\nu)} \tag{1.1.10}$$

$z\nu$ being the critical exponents entering in Eq.1.1.3. The correlation length at the freezing time, giving an estimate of the size of the typical ordered domain, can be employed to evaluate the defect density $\rho_{\rm ex}$, assuming that on average one defect per domain is produced. The Kibble-Zurek prediction is then

$$\rho_{\rm ex} \sim \xi^{-d}(\hat{t}), \tag{1.1.11}$$

where d is the space dimension and by using $\xi(\hat{t}) \sim |\epsilon(\hat{t})|^{-\nu}$ it finally leads to

$$\rho_{\rm ex} \sim \tau^{-d\nu/(1+z\nu)}. \tag{1.1.12}$$

As an example, for the ordered quantum Ising chain[157], in which $z = \nu = 1$, Eq.1.1.12 gives the well known result[56] $\rho_{\rm ex} \sim \tau^{-1/2}$.

The formula Eq. 1.1.12 was also independently found by means of adiabatic perturbation theory [115] (see Sec. 1.1.4) and has been tested in a variety of models through both analytical and numerical studies, in particular for the Ising model [157, 115, 56, 33], for the XY spin 1/2 model [104, 30], for periodic optical lattices [59], for a spinor condensate [93], for the sine-Gordon model [39, 40] and very recently for graphene [51, 52] and it is also supported by experiments [133].

The KZM formula 1.1.12 has been generalized for different time and space dependences. Dziarmaga *et al.* [60] get a modified scaling equation for the case in which the dimensionless distance from the critical point ϵ is not homogeneous in space, a more realistic condition for the experimental setup. An application of these results can be found in the study the structural defects in ion crystals [43]. If the time dependence of the tuning parameter λ is not linear, $\lambda(t) \sim \lambda_{\rm c} \pm \delta|t|^r$, arguments similar to those leading to Eq. 1.1.12 and adiabatic perturbation theory (see below) [4, 40, 140] give:

$$\rho_{\rm ex} \sim |\delta|^{d\nu/(z\nu r+1)} \tag{1.1.13}$$

A power-law time dependence of the tuning parameter turns out to be optimal in order to minimize the number of defects generated passing through a critical point [4]. Finally, the KZM scaling can be generalized to disordered systems, like a disordered Ising chain, where it is found that the density of kinks scales as $\rho_k \sim 1/\log^2(\tau)$ [22, 57], as expected from Eq.1.1.12 due to the divergence of the exponent z near the critical point [72].

1.1.3 Landau Zener approximation

In Ref. [157] an alternative approach based on the quantum tunneling effect has been also proposed. For finite-size systems with a small but non-vanishing gap, the thermodynamical critical closure of the gap is rounded off in an avoided level crossing that can be locally approximated with a Landau-Zener model [155]. Under the assumption that only the first gap accessible during the dynamics is responsible for the loss of adiabaticity, the Landau-Zener formula can be used to give a lower bound to the true, global excitation probability of the system:

$$P_{ex} = e^{-\pi(\Delta/2)^2\tau} \tag{1.1.14}$$

where Δ represents the amplitude of the gap at the finite size critical point and τ is the rate of the linear quench. Notice that for particular models,

like the ordered Ising chain [56], or the $1d$ Kitaev model [140], the first instananeous gap can be exactly mapped onto a LZ-like Hamiltonian. Then once the scaling of the critical gap with the size is known, $\Delta = f(N)$, Eq. 1.1.14 can be exploited to determine the behavior of the maximum defect-free size after a quench, $N_{\rm free}$, as a function of τ. Once an arbitrary small but fixed probability $\tilde{P}$ is chosen, it turns out that

$$\tilde{P}_{\rm ex} = e^{-\pi (f(N_{\rm free})/2)^2 \tau} \Rightarrow N_{\rm free} \sim f^{-1}\left(\sqrt{\frac{\kappa}{\tau}}\right) \tag{1.1.15}$$

with $\kappa = -4(\ln \tilde{P})/\pi$. Finally, once the relation connecting $N_{\rm free}$ and the selected measure of the loss of adiabaticity (excess energy, defect density, infidelity, etc.) is established, the desired behavior is obtained. For instance, for the ordered Ising chain it is known that [53] $\Delta \sim N^{-1}$ and $\rho_{\rm ex} \sim N_{\rm free}^{-1}$, so Eq. 1.1.15 leads to the correct result $\rho_{\rm ex} \sim \tau^{-1/2}$.

1.1.4 Adiabatic perturbation theory

The KZM results emerge in the more general context of the adiabatic perturbation theory (APT), first introduced in [115] and then fully developed in [117, 39, 128, 40, 42, 127]. In the KZM arguments there is a velocity δ (which in the linear quench case is proportional to $1/\tau$) which is implicitly assumed to be small: this is indeed the small parameter at the heart of adiabatic perturbation theory (APT) which we will briefly recall in a while following Ref. [42] in detail. APT is a very powerful tool for studying the scaling of quantities like excitations, entropy, heat, in the general case of linear quenches [42, 40] starting from the ground state or finite (small) temperature states. APT turns out to be very general, because it is able to capture the role of dimensionality and its interplay with universality at low dimensionality. Indeed, for low dimensional systems the adiabatic dynamics induces few transitions and the systems effectively explore only the low energy part of the spectrum, which can be characterized by a small number of parameters in some effective low energy theory. The situation becomes different in high dimensional systems [117], because the density of low energy states is small. As a result the transitions to high energy states dominate the dynamics, universality is lost and the scaling of excitations is quadratic. The arguments of APT also show that there exist a direct analogy between slow quenches (with small velocity) and sudden quenches with small amplitude λ^*, through the identification $\lambda^* \sim |\delta|^{1/(z\nu+1)}$ and an analogous role of dimensionality emerges.

Given an Hamiltonian $\mathcal{H}(t) = \mathcal{H}_0 + \lambda(t)V$, with $\mathcal{H}_0$ stationary, the following linear dependence for $\lambda(t)$ is assumed:

$$\lambda(t) = \begin{cases} \lambda_i & t < 0 \\ \lambda_i + t\delta(\lambda_f - \lambda_i) & 0 \leq t \leq 1/\delta \\ \lambda_f & t > 1/\delta \end{cases} \tag{1.1.16}$$

where δ is the rate of change of the parameter $\lambda(t)$. Since λ_i and λ_f can be arbitrarily far from each other, one cannot rely on conventional perturbation theory in the difference $|\lambda_f - \lambda_i|$. In the limit of slow quenches, the "good" small parameter for developing a perturbative approach and finding an approximate solution of the Schrödinger equation $i\partial_t|\psi\rangle = \mathcal{H}(t)|\psi\rangle$ is in turn the velocity δ. It is convenient to introduce the adiabatic (instantaneous) basis:

$$|\psi(t)\rangle = \sum_n a_n(t)|\phi_n(t)\rangle \tag{1.1.17}$$

where $|\phi_n(t)\rangle$ are instantaneous eigenstates of the Hamiltonian $\mathcal{H}(t)|\phi_n(t)\rangle = E_n(t)|\phi_n(t)\rangle$ corresponding to the instantaneous eigenvalues $E_n(t)$. These eigenstates implicitly depend on time through the coupling $\lambda(t)$. Substituting this expansion into the Schrödinger equation and multiplying it by $\langle\phi_m|$ one finds:

$$i\partial_t a_m(t) + i\sum_n a_n(t)\langle\phi_m|\partial_t|\phi_n\rangle = E_m(t)a_m(t). \tag{1.1.18}$$

Through the gauge transformation $a_n(t) = \alpha_n(t)\exp(-i\Theta_n(t))$, where

$$\Theta_n(t) = \int_{t_i}^{t} E_n(\tau)d\tau \tag{1.1.19}$$

the Schrödinger equation becomes:

$$\dot{\alpha_n}(t) = -\sum_m \alpha_m(t)\langle n|\partial_t|m\rangle \exp[i(\Theta_n(t) - \Theta_m(t))], \tag{1.1.20}$$

which may also be rewritten as an integral equation:

$$\alpha_n(t) = -\int_{t_i}^{t} dt' \sum_m \alpha_m(t')\langle n|\partial_{t'}|m\rangle e^{i(\Theta_n(t') - \Theta_m(t'))}. \tag{1.1.21}$$

If the energy levels $E_n(\tau)$ and $E_m(\tau)$ are not degenerate, the matrix element $\langle n|\partial_t|m\rangle$ can be written as

$$\langle n|\partial_t|m\rangle = -\frac{\langle n|\partial_t\mathcal{H}|m\rangle}{E_n(t) - E_m(t)} = -\dot{\lambda}(t)\frac{\langle n|V|m\rangle}{E_n(t) - E_m(t)}, \tag{1.1.22}$$

where we emphasize that the eigenstates $|n\rangle$ and eigenenergies $E_n(t)$ are instantaneous. If $\lambda(t)$ is a monotonic function of time the in Eq.1.1.21 one can change variables from t to $\lambda(t)$ and derive:

$$\alpha_n(\lambda) = -\int_{\lambda_i}^{\lambda} d\lambda' \sum_m \alpha_m(\lambda')\langle n|\partial_{\lambda'}|m\rangle e^{i(\Theta_n(\lambda')-\Theta_m(\lambda'))} \tag{1.1.23}$$

where

$$\Theta_n(\lambda) = \int_{\lambda_i}^{\lambda} d\lambda' \frac{E_n(\lambda')}{\dot{\lambda}'}. \tag{1.1.24}$$

Formally exact, Eqs.1.1.21 and 1.1.23 cannot be solved in the general case. However, they allow for a systematic expansion of the solution in the small parameter $\dot{\lambda}$. Indeed, in the limit $\dot{\lambda} \to 0$ all the transition probabilities are suppressed because the phase factors are strongly oscillating functions of λ, the only exception occurring for degenerate levels. In the leading order in $\dot{\lambda}$ only the term $m = n$ should be retained in the sums in Eqs. 1.1.21 and 1.1.23. [1].

We now compute the first order correction to the wave function assuming for simplicity that initially the system is in the ground state $n = 0$, so that $\alpha_0(0) = 1$ and $\alpha_n(0) = 0$ for $n \neq 0$. In the leading order in $\dot{\lambda}$ we can keep only one term with $m = 0$ in the sums in Eqs. 1.1.21 and 1.1.23 and derive:

$$\alpha_n(t) \approx -\int_{t_i}^{t} dt' \langle n|\partial_{t'}|0\rangle e^{i(\Theta_n(t')-\Theta_0(t'))}, \tag{1.1.25}$$

or alternatively

$$\alpha_n(\lambda) \approx -\int_{\lambda_i}^{\lambda} d\lambda' \langle n|\partial_{\lambda'}|0\rangle e^{i(\Theta_n(\lambda')-\Theta_0(\lambda'))}. \tag{1.1.26}$$

The transition probability from the level $|\phi_0\rangle$ to the level $|\phi_n\rangle$ as a result of the process is determined by $|\alpha_n(\lambda_f)|^2$. As mentioned before, Eqs.1.1.25 and 1.1.26 are derived for a generic linear quench. First of all one can show that the Landau-Zener transition probabilities for both infinite and finite times (see Sec.1.1.3 and App.A) can be recovered [40, 42]. The situation in which a quantum critical point (QCP) is crossed, which is recalled below, is a particular case of these APT equations, but other very interesting cases may be treated as well, for example gapless systems with quasiparticle excitations and gapped systems. Keeping in mind Eqs.1.1.3 and 1.1.1 and locating for convenience the critical point at $\lambda = 0$, a scaling analysis of Eq.1.1.26 can be performed assuming that quasiparticles generated from the quench are

[1] This term results in the emergence of the Berry phase

created in opposite momenta. The phase factor in Eq.1.1.26 is rewritten as $\Theta_k(\lambda') - \Theta_0(\lambda) = \frac{1}{\delta}\int_{\lambda_i}^{\lambda} d\lambda'(\varepsilon_k(\lambda') - \epsilon_0(\lambda'))$. From general scaling arguments [115] the energy difference may be written as:

$$\varepsilon_k(\lambda) - \varepsilon_0(\lambda) = \lambda^{z\nu} F(k/\lambda^{\nu}) \tag{1.1.27}$$

such that $F(x) \propto x^z$ for $x \gg 1$ and $F(x) \to$ const for $x \ll 1$ if the system in gapped away from the QCP. Another scaling ansatz can be done for the matrix element:

$$\langle k|\partial_\lambda|0\rangle = -\frac{\langle k|V|0\rangle}{\varepsilon_k(\lambda) - \varepsilon_0(\lambda)} = \frac{1}{\lambda} G(k/\lambda^{\nu}), \tag{1.1.28}$$

where $G(x) \propto x^{-1/\nu}$ at $x \gg 1$ and $G(x) \propto x^{\beta}$ for $x \ll 1$ and β is some non-negative number. With the change of variables $\lambda = \xi\delta^{1/(z\nu+1)}$, $k = \eta\delta^{\nu/(z\nu+1)}$ the number of quasiparticles reads:

$$n_{\text{ex}} \sim \int \frac{d^d k}{(2\pi)^d} |\alpha_k|^2 = |\delta|^{\frac{d\nu}{z\nu+1}} \int \frac{d^d \eta}{(2\pi)^d} |\alpha(\eta)|^2 \tag{1.1.29}$$

where

$$\alpha(\eta) = \int_{\xi_i}^{\xi_f} d\xi \frac{1}{\xi} G(\frac{\eta}{\xi^{\nu}}) \exp\left[i \int_{\xi_i}^{\xi} d\xi_1 \xi_1^{z\nu} F(\eta/\xi_1^{\nu}) \right]. \tag{1.1.30}$$

The KZM scaling of the quasiparticles Eq. 1.1.12 is recovered if the integral in η is convergent (the integration in ξ being always convergent). This happens for $d < d^*$, otherwise a quadratic scaling is found [40], the crossover dimension being by $d^* = 2z + 2/\nu$, since α scales as

$$\alpha(\eta) \propto \frac{1}{\eta^{z+1/\nu}}. \tag{1.1.31}$$

1.1.5 Cases eluding the KZM or APT

An interesting issue arising from the KZM is investigating what happens trying different paths in the parameter space spanned by the Hamiltonian, and verifying whether the KZM formulas still hold. For instance in the XY spin 1/2 model [30] a quench can be performed not only by modulating the transverse field along the z direction but also the anisotropy in the XY plane. The idea behind the procedure is to investigate the possibility of finding a gentle way to cross the transition in order to reduce the impact of the loss of adiabaticity. For the ordered Ising model the issue has been recently analyzed [104], enlightening the existence of peculiar paths, specifically through

a multicritical point, for which the anomalous τ^{-6} decay of the defect density with the quench time cannot be described via usual KZM or adiabatic perturbation theory, which would predict a $1/\sqrt{\tau}$ behavior. And this is not an isolated case. Other patological situations, unmanageable with standard tools have been revealed, such as while crossing a multicritical point [104, 50] or a $(d-m)$ dimensional critical surface [141, 102], quenching along a gapless line [49, 45, 46], or going through a BKT phase transition [110, 25], see also Chapter 2. Moreover the KZM or adiabatic perturbation theory cannot be used for infinetely coordinate systems, i.e. without a definite space dimensionality d [23].
The problem with these situations is that the critical exponents and also the effective model dimension characterizing the quantum phase transition turns out to be dependent on the path followed during the quench in the Hamiltonian parameter space [45, 46]. Unluckily, this issue cannot be easily cured within KZM derivation of Eq. 1.1.12: the only possibility is to introduce *ad hoc* substitutions. It turns out that crossing a multicritical point the exponent z has to be changed by a new dynamical exponent z_2 [50]; instead, going thorugh a $(d-m)$ dimensional critical surface not all phase space is at disposal and this influences the scaling of the variables in such a way that d must be corrected with m [141, 102]. In many situations, for finite size systems, the issue can be cured by exploiting Landau-Zener (LZ) effective models (see Sec. 1.1.3) locally approximating the dynamical critical gap [157, 22, 23, 110, 32]. Although based on the assumption that the contribution to the non adiabatic behavior is due only to the first minimum gap, this approach is quite more general, bypassing the knowledge of critical exponents and dimension, and focussing the attention only on the spectral properties of the system: the path dependence of the critical exponents is directly taken into account by the spectrum shape close to the critical point. There are still cases where an effective theory is still lacking, for example in presence of a BKT transition [110, 25], in which it is not possible to identify a dominant gap, see also Chapter 2.

1.2 Thermalization after a sudden quench

While in the previous section we considered the adiabatic dynamics due to a slowly varying Hamiltonian, here we focus on the dynamics of closed quantum systems when one of the control parameters of the Hamiltonian is

suddenly changed, i.e. a *sudden quench* according to the following scheme:

$$\mathcal{H}(t) = \begin{cases} \mathcal{H}(\lambda_0) \equiv \mathcal{H}_0 & \text{for} \quad t < 0 \\ \mathcal{H}(\lambda) \equiv \mathcal{H} & \text{for} \quad t \geq 0 \end{cases} \tag{1.2.1}$$

where λ is a control parameter and is put initially (for $t < 0$) in the ground state $|\psi_0\rangle$ of H_0. In this case the energy of the system after the quench

$$E_0 \equiv \langle \psi_0 | \mathcal{H} | \psi_0 \rangle \tag{1.2.2}$$

is *conserved* throughout the evolution. The most natural question that arises is whether and how the system under study relaxes at long times, that is, if the behavior of the observables reaches a steady state and whether it coincides with some thermal distribution[2]. As we will show below, the study of these systems entangles the issues of ergodicity, thermalization, integrability and localization, as discussed for example in the review [118].

1.2.1 Ergodicity

If we put an ideal classical gas in one part of a box diveded in two parts and then remove the wall separating the two chambers, soon the particles will occupy the whole box and acquire a Maxwell-Boltzmann distribution of momentum. The same equilibrium situation will take place irrespectively of the initial conditions, depending only on the total energy of the system and on the number of particles. This "thermodynamical universality" is explained in classical physics[74] as a consequence of the non-linearity of the equations of motion, which forces all the trajectories to explore uniformly the hypersurface at constant energy in phase-space. However, if the system possesses further conserved quantities which are functionally independent of the Hamiltonian and of each other, then time evolution is confined to a highly restricted hypersurface of the energy manifold, so that microcanonical predictions fail and thermalization is not possible. This is what happens for example in the celebrated Fermi-Pasta-Ulam numerical experiment [68]. Thus thermalization in classical systems is essentially made possible by the emergence of *dynamical* chaos. On the contrary, Schrödinger equation is linear, so a definition of ergodicity in quantum mechanics is not at all straightforward. The most obvious generalization of ergodicity leads to deep difficulties [151]. One needs first to define the microcanonical density

[2] The case of sudden quenches starting from initial thermal states in Ref. [143] where it is found that any finite subsystem eventually reaches a stationary thermal state with a momentum-dependent effective temperature.

matrix for a system with Hamiltonian $\mathcal{H}$ and eigenstates $|\psi_\alpha\rangle$ as:

$$\rho_{\rm mc} = 1/\mathcal{N} \sum_{\alpha \in \mathcal{H}(E)} |\psi_\alpha\rangle\langle\psi_\alpha| \tag{1.2.3}$$

where $\mathcal{H}(E)$ denotes the set of eigenstates of $\mathcal{H}$ with energy in the coarse-grained energy shell $[E, E+\delta E]$ and $\mathcal{N}$ is the number of such states. Given a generic initial state $|\psi_0\rangle = \sum_{\alpha\in\mathcal{H}(E)} c_\alpha |\psi_\alpha\rangle$, superposition of eigenstates with energy in the microcanonical shell, it is obvious to compare the long time average of the density matrix with the microcanical prediction. As already observed in 1929 by Von Neumann [151, 76], the two quantities almost never coincide. Given the time average of the density matrix:

$$\overline{|\psi(t)\rangle\langle\psi(t)|} = \sum_\alpha |c_\alpha|^2 |\psi_\alpha\rangle\langle\psi_\alpha| \equiv \rho_{\rm diag} \ , \tag{1.2.4}$$

also known in recent times as *diagonal ensemble* [125, 124], the obvious generalization of ergodiciy would require $\rho_{\rm mc} = \rho_{\rm diag}$, implying $|c_\alpha|^2 = 1/\mathcal{N}$ for every α, which is almost never true [151, 76].
A sensible definition of quantum ergodicity turns out to be nevertheless possible, concentrating on *observables* rather than on states [151, 97, 111]. Given a set of macroscopic observables $\{M_\beta\}$ and for every $|\psi_0\rangle$ on the microcanonical shell $\mathcal{H}(E)$, ergodicity would mean:

$$\langle\psi(t)|M_\beta|\psi(t)\rangle \stackrel{t\to\infty}{\longrightarrow} {\rm Tr}[M_\beta \rho_{\rm diag}] = \langle M_\beta\rangle_{\rm mc} \tag{1.2.5}$$

if the long time limit exists. A more precise definition is obtained referring to the time average of the density matrix:

$$\overline{\langle\psi(t)|M_\beta|\psi(t)\rangle} = {\rm Tr}[M_\beta\rho_{\rm mc}] \equiv \langle M_\beta\rangle_{\rm mc} \tag{1.2.6}$$

1.2.2 Generalized Gibbs ensembles

In a very famous experiment with arrays of 1D Bose gases [89], Kinoshita *et al.* succeded in realizing a quantum system, the quantum Newton cradle, which does not thermalize. The reason for the absence of thermalization is that the system is nearly integrable, namely there is an infinite number of conserved quantities. The consequence on the dynamics is that the knowledge of the initial energy of the system is not enough to characterize the asymptotic state. Does the system relax to some kind of equilibrium state? Is it possible to predict with some statistical ensemble the mean value of observables? As a possible answer to these questions, Rigol *et al.* [125] have introduced the generalized Gibbs ensemble (GGE). Sketching their argument,

if an equilibrium state exists, it must satisfy the standard prescription of statistical mechanics, i.e. it must maximize the entropy $S = -k_B \mathrm{Tr}[\rho \ln(\rho)]$ subject to the constraints imposed by the integrals of motion. This amounts to the following density matrix:

$$\rho = Z^{-1} \exp[-\sum_m \Lambda_m \hat{\mathcal{I}_m}] \tag{1.2.7}$$

where $\left\{\hat{\mathcal{I}_m}\right\}$ is the *full* set of the integrals of motion, $Z = \mathrm{Tr}[\exp(-\sum_m \Lambda_m)\hat{\mathcal{I}_m}]$ is the partition function, and $\{\Lambda_m\}$ are the Lagrange multipliers, fixed by the initial conditions via:

$$\mathrm{Tr}[\hat{\mathcal{I}_m}\rho] = \langle \hat{\mathcal{I}_m} \rangle (t = 0). \tag{1.2.8}$$

The GGE reduces to the usual grand-canonical ensemble for a generic system where only the total energy, the number of particles. If translation invariance holds, momentum is also conserved. In Ref. [125] a system of hard-core bosons is considered in order to verify that the correct asymptotic momentum distribution functions are correctly reproduced by the GGE.

The quantum Ising model is another prototypical system in which it is possible to analitically confirm the validity of the GGE for a local observable, as shown in Ref. [118], the argument of which we recall below. The Hamiltonian $\mathcal{H}_\mathrm{I} = -\sum_i \sigma_i^x \sigma_{i+1}^x + g\sigma_i^z$, can be expressed as a system of free fermions [131] after a Jordan-Wigner transformation. In terms of the fermionic operators c_k relative to modes of momentum $k = 2\pi n/L$ the Hamiltonian takes the form:

$$H_\mathrm{I} = 2\sum_{k>0}(g - \cos(k))(c_k^\dagger c_k - c_{-k}c_{-k}^\dagger) + i\sin(k)(c_k^\dagger c_k^\dagger - c_{-k}c_k) \tag{1.2.9}$$

Under this mapping the transverse magnetization becomes

$$M^z = -2\sum_{k>0}(c_k^\dagger c_k - c_{-k}c_{-k}^\dagger). \tag{1.2.10}$$

The eigenmodes γ_k of energy $E_k = 2\sqrt{(g - \cos(k))^2 + \sin(k)^2}$ diagonalizing the Hamiltonian are related to the fermionic operators c_k by a Bogoliubov transformation. In Heisenberg representation the operators γ_k acquire a simple time dependence: $\gamma_k(t) = \gamma_k(0)\exp[-iE_k t]$. If the energies are incommensurate, at sufficiently long times different momentum modes become statistically independent from each other. This statement does not apply to modes with opposite momenta k and $-k$ which have identical energies. However, if these correlations are not important then in the long time limit

each mode can be characterized by a conserved quantity $n_k = \langle \gamma_k^\dagger \gamma_k \rangle$. If the unitary dynamics starts with a generic initial condition $|\psi_0\rangle$, then the time evolution in terms of the eigenmodes of the Hamiltonian is:

$$\begin{aligned} M^z(t) \quad &= -2\textstyle\sum_{k>0} \cos(2\theta_k)(\gamma_k^\dagger \gamma_k - \gamma_{-k}\gamma_{-k}^\dagger) \\ &+ i \sin(2\theta_k)(\gamma_{-k}\gamma_k e^{-2iE_k t} - \gamma_k^\dagger \gamma_{-k}^\dagger e^{2iE_k t}). \end{aligned} \tag{1.2.11}$$

The GGE reproduces the correct asymptotic expectation value of the magnetization because in the long time limit only the diagonal terms in the sum survive, while the off-diagonal ones, describing creation or destruction of two fermions average to zero. So for any initial condition $|\psi_0\rangle$ the asymptotic value of the transverse magnetization is:

$$\overline{\langle M^z(t) \rangle} = -2 \sum_{k>0} \cos(2\theta_k)(\langle \gamma_k^\dagger \gamma_k \rangle - \langle \gamma_{-k}\gamma_{-k}^\dagger \rangle). \tag{1.2.12}$$

hence it is perfectly described by the GGE, the integrals of motion being fixed by $n_k = \langle \psi_0 | \gamma_k^\dagger \gamma_k | \psi_0 \rangle$.

The validity of the GGE has been verified in many situations: Luttinger liquids [27], Hubbard-like models [61, 90] and in the Bose-Hubbard model for a special class of quenches (from the Mott quantum phase to the free strong superfluid regime) [35]; in these cases correct predictions are found for the momentum distribution functions. In continuum integrable models, integrability means that the system has well defined quasi-particles which scatter elastically [106, 145]. In some specific integrable models, the quench dynamics can be exactly solved [66, 67] without invoking the GGE, but exploiting the Bethe Ansatz solution, which in particular gives access to simple expressions for the scalar product of eigenstates of two different Hamiltonians. Generalizing a previous results by Calabrese and Cardy [18], Barthel and Schollwöck [5] have proven rigorously that for Gaussian initial state and quadratic (fermionic or bosonic) systems the GGE does work, being the integrals of motion the occupation numbers of each quasi-particle state, and suggested that the GGE should also be generalized for Bethe Ansatz integrable systems. In a very recent work [70] the GGE has been shown to give correct results in one-dimensional integrable field theories for a special class of translationally invariant states, the so-called integrable boundary states.

Although the GGE gives correct predictions in many different contexts, there are some caveats and still open questions. As pointed out in Ref. [118], the choice of the integrals of motion in the GGE is strongly constrained by the fact that conserved quantities must be *additive*, in order to guarantee the

statistical independence and invariance of the ensemble with respect to the subsystem. Another case in which the GGE does not provide correct results is when the Hamiltonian is translationally invariant, but the initial condition is not, for example in the Ising case wheh $|\psi_0\rangle$ has broken translational invariance and the observable is $\delta n_k \delta n_{k'}$, with $\delta n_k = \gamma_k^\dagger \gamma_k - \langle \gamma_k^\dagger \gamma_k \rangle$ [118].

A very important issue is whether all observables behave necessarily non-ergodically. In two recent papers [129, 130] it has been shown both numerically and analitically that at low energies the autocorrelation function of the order parameter of the Ising model after a sudden quench of the transverse magnetic field perfectly thermalizes, while the transverse magnetization is non ergodic. These results maybe understood taking into account the locality of the observables in terms of the quasi-particles of the model. Indeed the order parameter σ^x is non-local in terms of fermions because it contains all the strings factors from the Jordan-Wigner transformation, although it is local in terms of spins. As we shall see in Chapter 3 (see also Ref. [26]) for the disordered XXZ model a different behavior of local and non-local quantities in terms of quasi-particles seems to take place. We will see that in this context a relation between thermalization and many-body localization in quasi-particle space may be conjectured.

1.2.3 Eigenstate thermalization hypothesis

When a system is far from the integrable limit, thermalization is expected to occur for all the observables [91, 96, 62, 124, 123, 126]. The intense theoretical efforts [111, 47, 144, 124] towards understanding the necessary conditions for thermalization focus on the connection with quantum chaos, a link originally proposed in Ref. [111]. In the latter work quantum chaos is defined intrinsically in quantum mechanics language as the situation in which simple dynamical variables are represented by pseudorandom matrices in the eigenbasis of the Hamiltonian. The consequences of chaos on thermalization have been described more precisely by conjecturing that thermalization in quantum chaotic systems occurs eigenstate-by-eigenstate, i.e. the expectation value of a natural observable $\langle \psi_\alpha | A | \psi_\alpha \rangle$ on an eigenstate $|\psi_\alpha\rangle$ is a smooth function of its energy E_α, being essentially constant on each microcanonical shell [47, 144]. If this happens, then ergodicity and thermalization in the asymptotic state follow for every initial condition sufficiently narrow in energy. This hypothesis is called *eigenstate thermalization hypothesis* (ETH), independently introduced by Deutsch[47] and Srednicki[144]. Deutsch [47] considers a model with an integrable Hamiltonian perturbed by a real symmetric random matrix, with elements drawn from a random Gaussian en-

semble. The idea is to show that, for a large enough number of degrees of freedom, this perturbation ensures ergodicty, i.e. the time average of an observable equals the microcanonical average, without invoking any ensemble average (differently from the classical case). This is possible because the random pertubation mixes with random phases an exponentially large number of eigenstates of the integrable Hamiltonian with energy in a given window, so that the fluctuations of $\langle\psi_\alpha|A|\psi_\alpha\rangle$ around the microcanonical average can be made arbitrarily small. For an integrable system the fluctuations are much larger.

The emergence of ETH can be also found in a quantum gas of N particles of mass m [144], with an initial condition sufficiently narrow in energy, under the assumption that Berry's conjecture holds. The latter states that each energy eigenfunction $\psi_\alpha(\mathbf{X})$ is a superposition of plane waves (in the $3N$ coordinate space $\mathbf{X} = (\mathbf{x_1}, \dots, \mathbf{x_N})$), with random phase and gaussian random amplitude, but fixed wavelength. Thus the eigenfunctions have the form:

$$\psi_\alpha(\mathbf{X}) = \mathcal{N}_\alpha \int d^{3N} P A_\alpha(\mathbf{P}) \delta(\mathbf{P}^2 - 2mU_\alpha) \exp(i\mathbf{P}\cdot\mathbf{X}/\hbar) \tag{1.2.13}$$

where $\mathbf{P} = \mathbf{p_1}, \dots, \mathbf{p_N}$ are the $3N$ conjugate momenta and $A_\alpha(\mathbf{P})$ being pseudo-random variables with gaussian statistics, $\langle A_\alpha(\mathbf{P}) A_\beta(\mathbf{P'})\rangle = \delta_{\alpha\beta}\delta^{3N}(\mathbf{P}+\mathbf{P'})/\delta(\mathbf{P}^2 - \mathbf{P'}^2)$. Berry's conjecture is expected to hold only for systems which exhibit classical chaos in all or at least most of the classical phase space. The validity of Berry's conjecture allows to show that the momentum distribution function relaxes to the Maxwell Boltzmann distribution[3]:

$$\langle f(\mathbf{p})\rangle = \int d\mathbf{p}_2 d\mathbf{p}_3 \dots \langle|\psi_\alpha(\mathbf{p}, \mathbf{p}_2 \dots)|^2\rangle \tag{1.2.14}$$

$$= \frac{e^{-\frac{p^2}{2mkT}}}{(2\pi mkT)^{3/2}} = f_{\mathrm{MB}}(p) \tag{1.2.15}$$

where the temperature is set by the equipartition law $E_\alpha = 3/2NkT$.

A recent paper [9] sheds further light on the precise definition of ETH and to its relation with finite-size effects. In particular two versions, a weak and a strong formulation, of the ETH are proposed. The weak formulation (WETH) states that the matrix elements $A_\alpha = \langle\psi_\alpha|A|\psi_\alpha\rangle$ of a few body observable have vanishing fluctuations over eigenstates close in energy in the thermodynamic limit. The WETH does not imply thermalization, because states with a value of A_α different from the microcanonical one actually do exist, even if they are rare, and, weighted by the c_α of the diagonal ensemble,

[3] Here we do not make any assumption on the symmetry of the wavefunctions under exchange of particles; for further details on bosons and fermions see Ref. [144]

they may shift microcanonical average away from the diagonal expectation value. The WETH is indeed verified even for integrable systems and some finite-size non integrable systems like the Bose-Hubbard model[9]. Instead the stronger version of the ETH (SETH) implies thermalization, because it holds if the WETH is valid and the support of the distribution of the A_α shrinks around the thermal microcanonical value in the thermodynamic limit.

Keeping in mind both the scenarios for thermalization in the integrable and in the nonintegrable case, it is very interesting to investigate the crossover between the two situations. A useful tool is represented by the study of the level statistics, since the breaking of integrability is associated to quantum chaotic behavior [114]. In particular, integrable systems are characterized by Poisson spectral distributions, while the breaking of integrability emerges at finite sizes as a gradual crossover to the Wigner Dyson distribution. Numerous recent works specifically investigate the crossover from non-ergodic to thermal behavior as integrability is gradually broken and on the origin of ergodicity in systems sufficiently far from integrability [8, 91, 96, 123, 124, 136, 126, 26]. We will come back to this point later in the Thesis, see Chapter 3.

Besides the characterization of the asymptotic state, a complementary problem is the behavior of the relaxation time, in particular in the thermodynamic limit. In a series of studies of relaxation in fermionic Hubbard model subject to quenches in the interaction strength it has been argued that, for sufficiently rapid quenches, relaxation towards thermal equilibrium occurs through a pre-thermalized phase [100, 101].

Chapter 2

Adiabatic dynamics in a spin-1 chain with uniaxial single-spin anisotropy

2.1 Introduction

In this chapter we study the adiabatic dynamics of a one-dimensional XY spin-1 system with single-spin uniaxial anisotropy [138, 44], exhibiting (in equilibrium) a QPT of the Berezinskii-Kosterlitz-Thouless (BKT) type. The interest in the dynamics of this specific spin-chain is motivated by the fact that it describes quite accurately the properties of the Bose-Hubbard (BH) Hamiltonian both in the limit of strong interaction and close to the Mott-to-superfluid QPT [1, 83]; understanding the nonlinear response of such system to slow quenches may reveal itself as a powerful tool to probe Bose condensates loaded in optical lattices [39]. Interestingly, the results presented below suggest that the knowledge of the static properties of the system, in particular of the BKT transition, may not be sufficient to predict and fully characterize the dynamical behavior.

Some dynamical properties of the BH model after a quasi-adiabatic crossing of the QPT have been analyzed both from the superfluid to the Mott insulator [139], and in the opposite direction [34], where topological defects arise. Other works focused on the emergence of universal dynamical scaling, when quenching to the superfluid phase: they started using the original KZ mechanism [115, 36], but then realized that, for non-isolated critical points or critical surfaces, a generalization in terms of dynamical critical exponents characterizing the whole critical region was necessary [141, 45, 49]. A more general analysis of the problem in the context of the breakdown of adia-

baticity for gapless systems has been presented in Ref. [117]. A numerical analysis of the raising of defects in a quenched spin chain model exhibiting a BKT transition has been performed in Ref. [110]; in that case defect formation is dominated by an isolated critical point, so that a LZ treatment based on the finite-size closure of the dynamical gap at that point is still possible. On the other hand, one can also devise a KZ scaling argument, which relies on the closing behavior of the gap as a function of the distance from the critical point [115, 36]. In some circumstances this problem can be quite subtle, since it is possible that the gap depends differently on the inverse size of the system and on the parameter driving the transition, so that the two approaches give different results: this seems to be the case for the system considered in the present chapter. The results presented in this chapter further investigate the dynamical defect formation after an adiabatic crossing of the BKT transition line; the major obstacle in understanding this type of dynamics raises from the fact that here the scaling of defects is generally due to multiple level crossings within the whole gapless phase. The chapter is organized as follows. In Sec. 2.2 the model is introduced and the main features of its phase diagram are recalled. In Sec. 2.3 the linear quenching scheme adopted in this work is discussed, and the excess energy of the system with respect to the adiabatic limit is defined: this quantity captures the essential physics of the defect formation in the system. All the numerical results of this chapter are concentrated in Sec. 2.4.

2.2 The Model

The Bose Hubbard (BH) model [73], well suited for describing interacting bosons in optical lattices [88], is defined by the following Hamiltonian

$$\mathcal{H}_{\mathrm{BH}} = -J \sum_i (a_i^\dagger a_{i+1} + \mathrm{h.c.}) + \frac{U}{2} \sum_i n_i(n_i - 1)\,. \tag{2.2.1}$$

Here $a_i^\dagger$ (a_i) are the boson creation (annihilation) operators on site i (we assumed that the lattice is one-dimensional), and $n_i = a_i^\dagger a_i$ is the corresponding occupation number. The parameters J and U respectively denote the tunneling between nearest neighbor lattice sites and the on-site interaction strength. At integer fillings $1, 2, \ldots$, when the ratio t/U is gradually increased, the BH chain undergoes a QPT of the BKT type from a Mott insulating state, where bosons are localized in an incompressible phase, to a superfluid, with long range phase order.

The BH model in equation 2.2.1 can be mapped into an effective spin-1 Hamiltonian in the limit of a large filling and for small particle number

fluctuations [1, 83]. When number fluctuations are not large it is possible to truncate the local Hilbert space to three states with particle numbers n_0, $n_0 \pm 1$ (n_0 being the average lattice filling per site). The reduced Hilbert space of site i can then be represented by three commuting bosons $t_{\alpha,i}$ ($\alpha = -1, 0, 1$), which obey the constraint $\sum_{\alpha=-1}^{1} t_{\alpha,i}^\dagger t_{\alpha,i} = \mathbb{I}$. In this way, the bosons of equation 2.2.1 are represented by $a_i^\dagger = \sqrt{n_0+1}\, t_{1,i}^\dagger t_{0,i} + \sqrt{n_0}\, t_{0,i}^\dagger t_{-1,i}$. In the limit $n_0 \gg 1$ the effective Hamiltonian becomes the Hamiltonian of a one-dimensional spin-1 XY chain with single ion anisotropy [138, 44],

$$\mathcal{H}_{\text{spin}} = -\frac{J_\perp}{2} \sum_i \left(S_i^+ S_{i+1}^- + \text{h.c.} \right) + D \sum_i (S_i^z)^2 \,, \tag{2.2.2}$$

where $S_i^+ = \sqrt{2}(t_{1,i}^\dagger t_{0,i} + t_{0,i}^\dagger t_{-1,i})$, $S_z^+ = t_{1,i}^\dagger t_{1,i} - t_{-1,i}^\dagger t_{-1,i}$ and with the identification

$$\frac{J n_0}{2} \to J_\perp \,, \qquad U \to D \tag{2.2.3}$$

(we chose to use the conventional notation for the spin-1 model). In the previous equations S_i^α are spin-1 operators on site i and $S_i^\pm = S_i^x \pm i S_i^y$; $J_\perp$ and D respectively characterize the nearest neighbor coupling strength in the xy plane and an uniaxial single-ion anisotropy along the transverse z direction. This system is invariant under rotations around the z axis, therefore the total magnetization $S_{\text{tot}}^z = \sum_i S_i^z$ is conserved. From now on all the quantities are expressed in units of the exchange coupling $J_\perp = 1$.

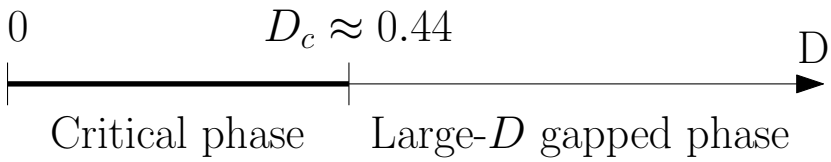

Figure 2.1: Phase diagram of the spin Hamiltonian 2.2.2 for $J_\perp = 1$ and $D \geq 0$.

The phase diagram associated to the Hamiltonian in 2.2.2 is sketched in figure 2.1. For $D > 0$ it consists in a large-D phase for $D > D_c$, that is characterized by zero total magnetization (in the limit $D \to \infty$ each spin has zero magnetization), and a BKT transition line for $D \leq D_c$; the critical point has been numerically estimated to be $D_c \simeq 0.44$ [29, 113, 11, 12, 147]. In the rest of the chapter we will only concentrate on the adiabatic dynamics of the Hamiltonian 2.2.2.

2.3 Adiabatic dynamics

The adiabatic quench is realized by slowly changing the anisotropy parameter D through the critical point D_c. We suppose to vary D linearly in time:

$$D(t) = D_{\text{in}} - \frac{t}{\tau}, \quad \text{with} \quad t \in [0, \tau(D_{\text{in}} - D_{\text{fin}})] \; ; \tag{2.3.1}$$

here τ is the quenching time-scale, D_{in} and D_{fin} respectively denote the initial and the final value of D. In all the cases that will be analyzed we consider $D_{\text{in}} > D_c$, and suppose to initialize the system in its ground state; on the other hand we take $D_{\text{fin}} < D_c$, so that during the quench the system crosses the BKT transition. Since the initial ground state has zero total magnetization, and this is conserved by the dynamics dictated by equation 2.2.2, only the excited states carrying zero magnetization will be accessible throughout the quench.

In order to quantify the loss of adiabaticity of the system following the quench, we study the behavior of the excess energy with respect to the actual adiabatic ground state, after a proper rescaling:

$$E_{\text{exc}}(t) = \frac{\langle \psi(t)|\mathcal{H}(t)|\psi(t)\rangle - \langle \psi_{GS}(t)|\mathcal{H}(t)|\psi_{GS}(t)\rangle}{\langle \psi_0|\mathcal{H}(t)|\psi_0\rangle - \langle \psi_{GS}(t)|\mathcal{H}(t)|\psi_{GS}(t)\rangle} \tag{2.3.2}$$

where $|\psi_0\rangle$ is the initial state of the system, that is the ground state of Hamiltonian $\mathcal{H}(0)$; $|\psi_{GS}(t)\rangle$ is the instantaneous ground state of $\mathcal{H}(t)$, and $|\psi(t)\rangle$ is the instantaneous wave function of the system. Strictly speaking, the quantity $E_{\text{exc}}(t)$ is not defined at the initial time $t = 0$, but one has $E_{\text{exc}}(t \to 0^+) = 1$; on the other hand at $t_f \equiv (D_{\text{in}} - D_{\text{fin}})/\tau$, the excess energy gives, apart from a constant factor, the final energy cost of defects in the system. The final excess energy ranges from $E_{\text{exc}}(t_f) = 1$ (totally impulsive case) to $E_{\text{exc}}(t_f) = 0$, for a fully adiabatic evolution.

An exact solution for the spin model in equation 2.2.2 is not available, not even for the static case, therefore one has to resort to numerical techniques. In order to investigate both static properties and the dynamics after the quench, we used the time-dependent Density Matrix Renormalization Group (t-DMRG) algorithm with open boundary conditions [137, 38]. For the dynamics at small sizes $L \leq 10$, we checked our t-DMRG results with an exact numerical algorithm which does not truncate the Hilbert space of the system. For static computations we were able to reach sizes of $L = 200$, while for dynamics simulations we considered systems of up to $L = 80$ sites. The time evolution has been performed with a second order Trotter expansion of $\mathcal{H}(t)$; in most simulations we chose a discretization time step $\delta t = 10^{-3}$, while the truncated Hilbert space dimension has been set up to $m = 200$.

2.4 Results

In this section we describe our results for the adiabatic dynamics of the spin-1 Hamiltonian. We first analyze the behavior of the excitation gaps which are relevant for the quenched dynamics. Then we focus on the dynamics, and discuss the behavior of the excess energy 2.3.2 as a function of the quenching rate τ. We first consider the slow-quench region for small system sizes and then concentrate on the scaling regime for larger sizes.

2.4.1 Dynamical gap

A great deal of understanding on the adiabatic dynamics derives from the knowledge of the finite-size scaling of the first excitations gaps. As stated before, since the dynamics of the system conserves the total z magnetization, if we suppose to start from the zero-magnetization ground state, only excited states with $S^z_{\rm tot} = 0$ will be involved during the dynamics. Therefore, the *dynamical gap* is defined as the first relevant gap for the dynamics, that is the energy difference between the ground state and the first excited state compatible with the integrals of motion.

As shown in figure 2.2, in the critical region $D < D_c$ the dynamical gap Δ scales approximately linearly as a function of the inverse system size L^{-1}. The same behavior also holds for relatively small values of $D - D_c$ within the gapped phase, as those considered in figure 2.2, so that the correlation length is still larger than the size of the system, and a quasi-critical regime is found [11, 12, 147]. On the other hand, we numerically checked that the leading term in finite-size corrections scale as L^{-2} for $D \gtrsim 2$, when the system is far from criticality. We extrapolated the value of $\Delta_0 = \Delta(L \to \infty)$ in the thermodynamic limit by performing a fit of numerical data for $L \geq 50$ which includes both the leading linear behavior and smaller quadratic corrections. Results are plotted in the inset of figure 2.2, as a function of D. According to the phase diagram of the system, which predicts a closure of the gap for $D < D_c \approx 0.44$, the asymptotic value of the gap is found to be constant and equal to zero for $0 \leq D \lesssim 0.45$ (up to values $\sim 2 \times 10^{-4}$), while it suddenly raises up as $\Delta_0 \sim \exp(-c/\sqrt{D - D_c})$ in the gapped phase close to criticality. Thus the dynamical gap closes analogously to the gap between the ground state and the first excited state with unconstrained magnetization, which is called *thermodynamical gap*, in a BKT transition [28].

The excitation energies of the first three dynamical excited levels in the subspace of zero magnetization and for a system of $L = 100$ sites are displayed in figure 2.3, as a function of the anisotropy D. In the large-D

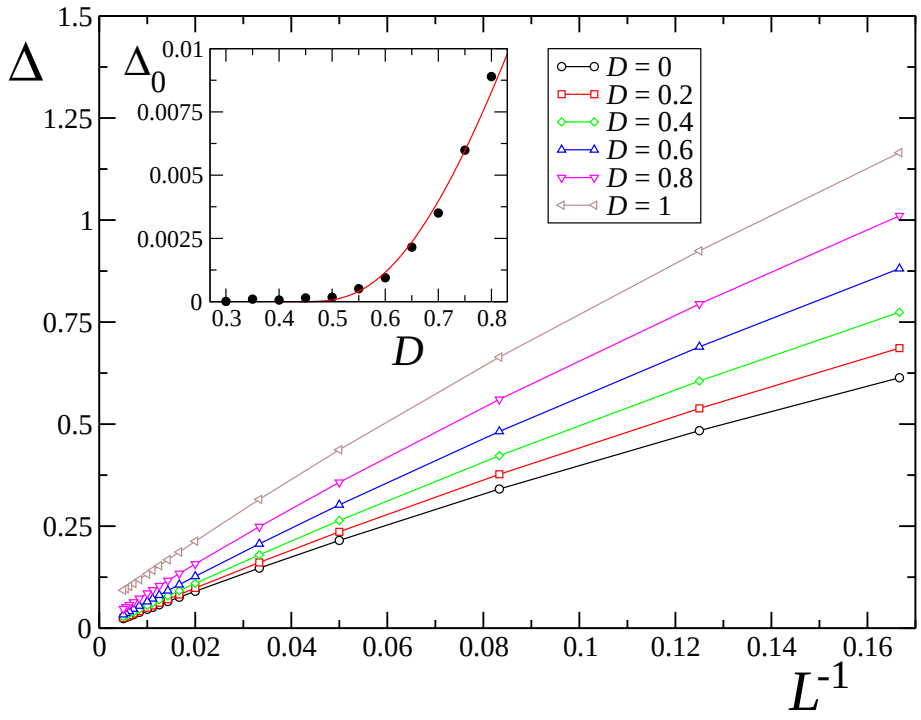

Figure 2.2: Ground state excitation energy Δ in the zero magnetization sector as a function of the inverse system size L^{-1} (we show data ranging from $L = 6$ to $L = 200$). The various curves are for different values of the single-ion anisotropy D. In the inset we plot the asymptotic value Δ_0 in the thermodynamic limit, as extracted from a quadratic fit of the data in main panel for $L \geq 50$ (black circles); the red line displays a fit $\Delta_0 \propto \exp(-c/\sqrt{D-0.44})$ of data with $c \approx 2.977$.

phase the dynamical gap $\Delta^{(1)} \equiv \Delta$ is well above the zero; when decreasing D it closes approximately linearly until $D \sim 2$, then it continues closing as far as it approaches a region for $D \lesssim 0.5$, where it becomes almost constant and very small, as shown in the inset.

We point out that this type of behavior is quite different from the scenario elucidated in the spin-1/2 Heisenberg model of Ref. [110]. In that case two types of quenches involving the antiferromagnetic BKT isotropic point were considered. While in the second quenching scheme the system started from the critical region and advanced in the opposite direction with respect to our case, the first quench started from the antiferromagnetic region and crossed both the BKT point and the ferromagnetic isotropic point. Remarkably, the excess energy was found to be essentially characterized by

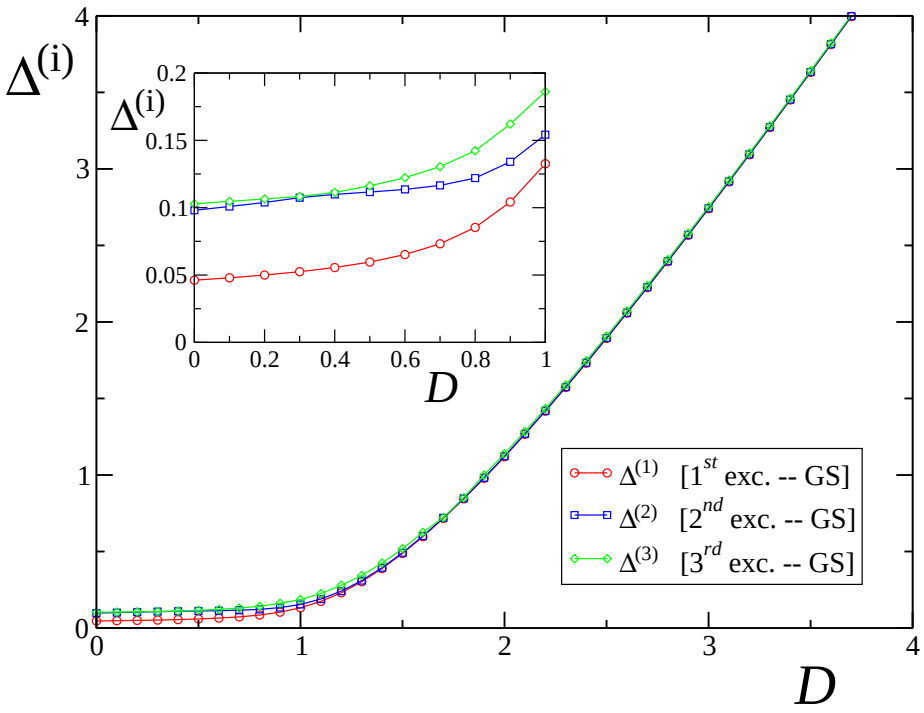

Figure 2.3: Excitation energy $\Delta^{(i)}$ of the three lowest excited dynamical levels for $L = 100$ spins in the subspace $S^z_{\rm tot} = 0$, as a function of D; the first excitation energy coincides with the dynamical gap: $\Delta^{(1)} \equiv \Delta$. The inset shows a zoom for $0 \leq D \leq 1$ of the same plot.

the features of the ferromagnetic critical point, where the gap closes faster than in all the other points along the critical line. Therefore it was possible to identify a dominant critical point which allowed for the applicability of a LZ scaling argument in determining the defect density. On the other hand, our quench involves the BKT transition line close to the antiferromagnetic isotropic point, and there are no dominant critical points, thus leading to a more complex scenario, as explained in the following.

2.4.2 Oscillations in the excess energy for slow quenches

Let us first consider systems of small sizes, as shown in figure 2.4 for $L = 6$ and $L = 8$ sites. We have evaluated the excess energy both with the t-DMRG algorithm (filled circles), and with an exact diagonalization which does not truncate the system's Hilbert space (empty squares). As the figure shows, data agree well.

On increasing the rate τ, we can recognize two different regimes. For very small values of τ the excess energy is close to its maximum, and the dependence on the size and on τ is very small. These points correspond to very fast quenches, where the system dynamics is strongly non-adiabatic and the initial state is substantially frozen. As a consequence, the state after the quench is found to be in a superposition of many excited states of the final Hamiltonian. A second region is characterized by a dominant power-law decay, according to $E_{\rm exc} \sim \tau^{-2}$ (see the straight lines in the two insets of figure 2.4), that is superimposed to an oscillatory behavior. This can be explained within a LZ approximation: for small values of D and L the gap is large and proportional to $1/L$, therefore at very small sizes only the ground state and the first excited state participate to the evolution of the system, while all the other excited states are not accessible. The power-law decay, as well as the oscillations naturally arise when effects of finite duration time are taken into account [150, 149]. Following the closing of the gap, the frequency of the oscillations decreases at increasing sizes, as it can be seen in the figure. The red curve displays a fit of numerical data obtained by an effective LZ model in which the initial coupling time $t_i < 0$ is finite, and the final time is $t_f = 0$ (see A for details on the fitting formula).

The oscillatory behavior can be drastically suppressed starting from a larger value of $D_{\rm in}$, which corresponds, in the LZ model, to decreasing the initial coupling time t_i; for $t_f \leq 0$ and in the limit of $t_i \to -\infty$ the oscillations disappear and a pure power-law $\sim \tau^{-2}$ decay survives [150, 149]. This is seen to emerge from numerical data of figure 2.5, where we started quenching from $D_{\rm in} = 4$. Notice also the substantial independence of $E_{\rm exc}$ on the system size in the fast quenching limit.

2.4.3 Scaling regime

The analysis of the effects of the quantum phase transitions on the adiabatic quench dynamics demands sufficiently large system sizes. We now concentrate on this aspect and study the excess energy as a function of τ for considerably larger values of L. Due to the increasing computational difficulty in simulating large systems, we restrict ourselves to quenching schemes in which $D_{\rm in} = 1$.

In figure 2.6 we plot the final excess energy of the system after a quench from $D_{\rm in} = 1$ to $D_{\rm fin} = 0$ of time duration τ. Starting from fast quenches and going towards slower ones, we can now distinguish three different regimes: the first strongly non-adiabatic regime at small τ is analogous to the one previously discussed for small sizes. In the opposite limit of very slow quenches

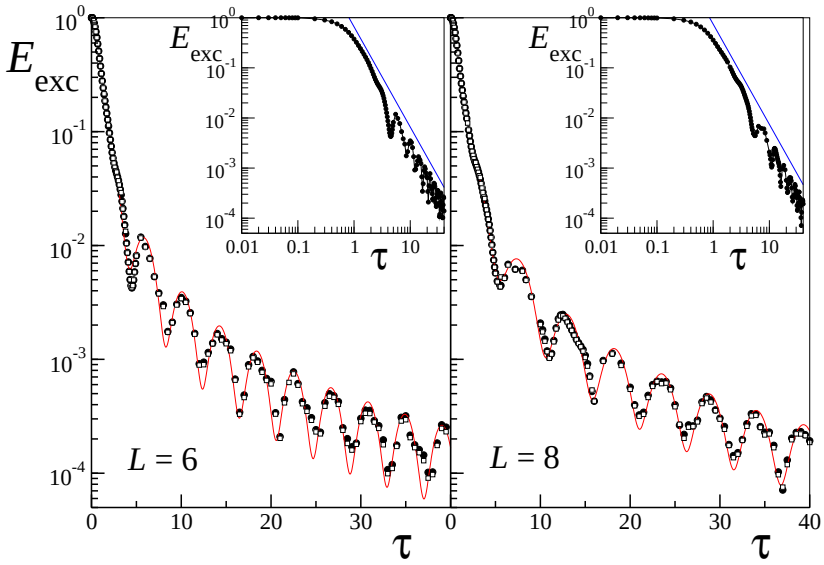

Figure 2.4: Final excess energy after an adiabatic quench of D from $D_{\rm in} = 1$ to $D_{\rm fin} = 0$, as a function of the quench velocity τ. Filled circles denote t-DMRG data, empty squares are obtained with exact diagonalization, while the continuous line is a numerical fit with the formula predicted by a LZ model for finite initial and final coupling times. The left panel shows data for $L = 6$ sites, while the right one is for $L = 8$. The insets show the same data in a log-log scale (straight blue lines denote a $\sim \tau^{-2}$ behavior). Note the smaller frequency of the oscillations for $L = 8$.

$\tau \gg 1$, we also recover the power-law τ^{-2} behavior superimposed to oscillations coming from an effective LZ description with finite coupling duration. Most interestingly, in between these two opposite situations, a characteristic power-law regime emerges, where:

$$E_{\rm exc} \sim \tau^{-\alpha} \quad \text{with} \quad \alpha \in [1, 2]\,. \tag{2.4.1}$$

This is dominated by transitions to the lowest dynamically accessible gap, and it is crucially affected by the critical properties of the system. The crossover time τ^* at which this regime ends typically increases with the size, as it can be qualitatively seen from the figure (arrows denote a rough estimate of τ^* for the different sizes), and diverges in the thermodynamic limit; unfortunately we were not able to analyze the scaling with L, because of the intrinsic difficulty in estimating the ending point of the $\tau^{-\alpha}$ behavior. Nonetheless, even at asymptotically small quenching velocities, for very large sizes the scaling of defects 2.4.1 ruled by criticality persists, thus meaning

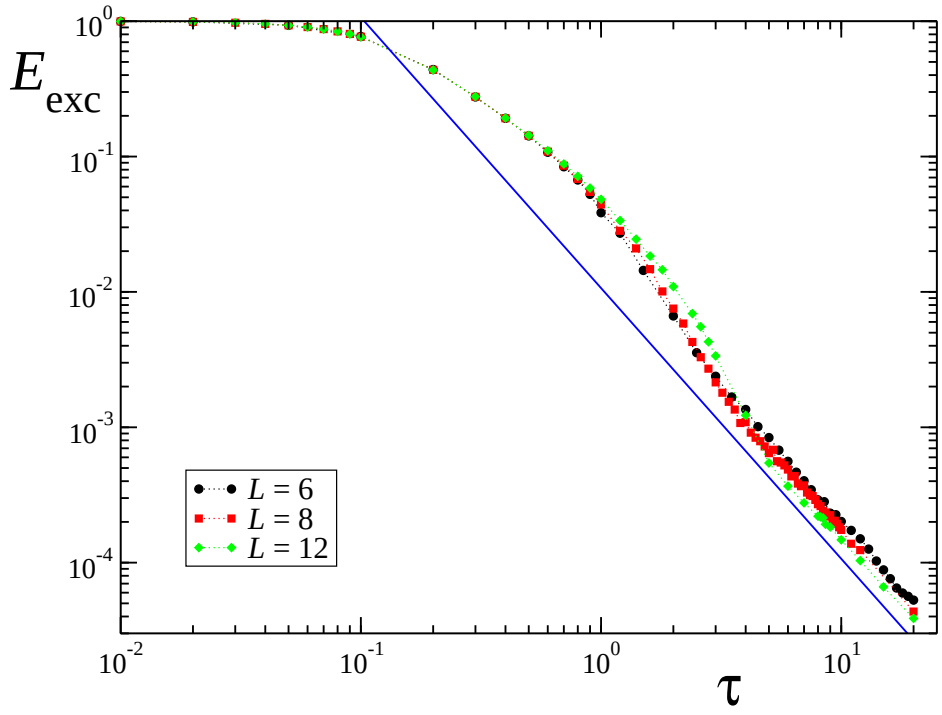

Figure 2.5: Excess energy after an adiabatic quench of D from $D_{\text{in}} = 4$ to $D_{\text{fin}} = 0$, as a function of τ. The various data are for different system sizes $L = 6$ (black circles), 8 (red squares), 12 (green diamonds). The straight blue line indicates a behavior $E_{\text{exc}} \sim \tau^{-2}$ and is plotted as a guideline.

that the system dynamics cannot be strictly adiabatic.

The scaling of the decay rate α with the size has been analyzed numerically, for data corresponding to L ranging from 10 to 60 spins; at $L < 10$ this regime was not identifiable. Some representative cases are shown in figure 2.6, where each of the four panels stands for a given system size, while straight continuous lines indicate the best power-law fits of the scaling regions. In the case of $L = 10$ sites (upper left panel), we cannot give a reliable estimate of α, since the width of the scaling region is narrow and the fit is very sensitive to its actual starting and ending points. The straight line in the plot corresponds to $\alpha \approx 1.798$ and has been obtained from a power-law fit of numerical data from $\tau = 1$ to $\tau^* = 3$. As one can see, this is hardly distinguishable from the τ^{-2} power-law behavior of the slow-quench regime (straight dashed line), thus meaning that the existence of the scaling region itself is here in doubt. This is not the case for the other panels, where a power-law behavior of the type in equation 2.4.1 is clearly visible. Namely,

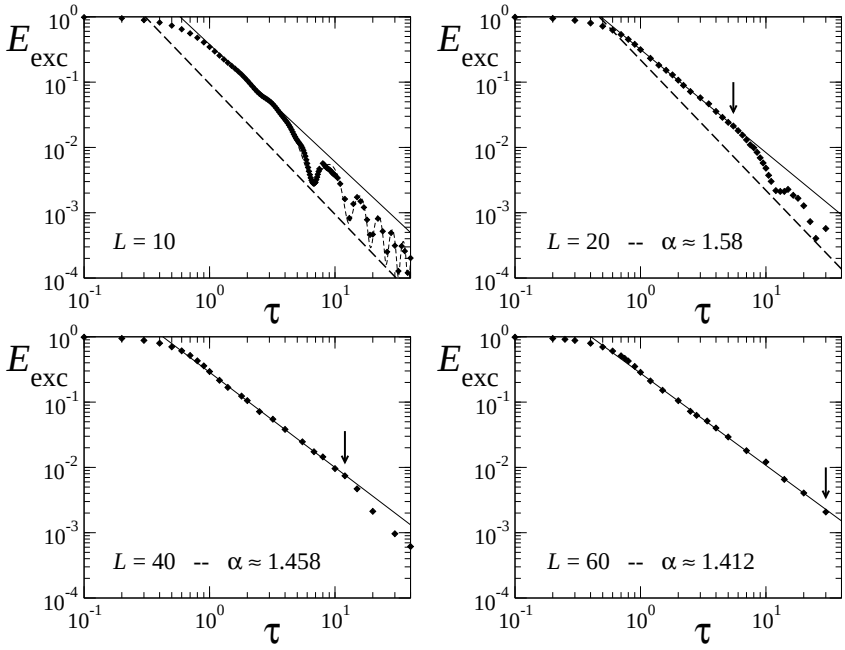

Figure 2.6: Final excess energy as a function of the quench rate τ. The various panels stand for different system sizes. Symbols denote numerical t-DMRG data, while the straight line is a power-law fit that has been performed for $\tau < \tau^*$ (τ^* is indicated by the vertical arrow). The two straight dashed lines in the upper panels denote a τ^{-2} behavior, and are plotted as guidelines. The oscillating dashed line at $L = 10$ is a fit of data with big τ, according to the LZ model for a finite coupling duration. The values of α corresponding to the power-law fits are quoted in each panel. Here we set $D_{\rm in} = 1$ and $D_{\rm fin} = 0$.

we fitted our data until the τ^* value, that is labeled in figure 2.6 by a vertical arrow: as we could expect, the size of the scaling region increases with L.

Summarizing the results obtained for the various sizes, in figure 2.7 we report the behavior of α as a function of L (in the inset we plot the same data with $1/L$ on the x-axis). The uncertainty affecting the value of α extracted from the power-law fits of numerical t-DMRG data is mostly due to the inaccurate knowledge of the extremes of the scaling region. For each value of L, we identified a trial power-law region and then computed several values of α by progressively sweeping out the points from that region, starting from the borders. We then evaluated error bars, that are displayed in the plot, by performing a statistical analysis of the values of α thus obtained. In order to give an estimate of the power-law decay rate in the thermodynamic

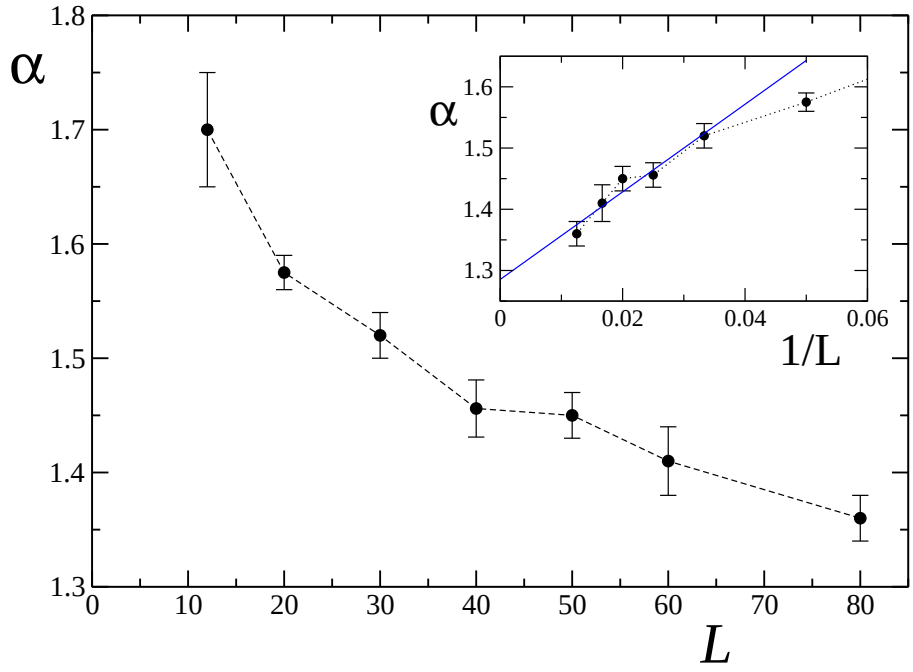

Figure 2.7: Power-law decay rate α in the intermediate scaling region for the excess energy, as a function of the system size L. The quench is performed from $D_{\text{in}} = 1$ to $D_{\text{fin}} = 0$. In the inset we plot the same quantity as a function of $1/L$. The blue line is a linear fit of data with $L \geq 30$, and predicts an asymptotic value of $\alpha_\infty \approx 1.28$ in the thermodynamic limit.

limit, we supposed that, at large L, α scales inversely proportional with the system size. In this way, performing a linear fit of data with $L \geq 30$, we extracted the asymptotic value $\alpha_\infty \approx 1.28$ in the thermodynamic limit (see straight blue line in the inset).

We would like to stress that, in this context, our numerical results seem not to find a straightforward explanation with LZ or KZ arguments. One could, for example, try to follow a standard LZ argument, that is based on the assumptions that the dynamical gap scales linearly with the inverse size, nearby and inside the critical region, and that the adiabaticity loss is essentially due to the presence of a dominant critical point, where the gap closes faster than elsewhere [157, 110]. In the LZ approximation, the probability of exciting the ground state is a global function of the product $\tau\Delta_{\text{m}}^2$, where Δ_{m} is the minimum gap achieved by the system during the quench. Assuming a critical scaling of the gap $\Delta_{\text{m}} \sim L^{-1}$, as shown in figure 2.2, the density of defects can be estimated by evaluating the typical

length L_ε of a defect-free region, once the probability for this to occur is ε. As a consequence, this would give $E_{\rm exc} \sim 1/L_\varepsilon \propto \tau^{-1/2}$, exactly as in the Ising case, in contrast with numerical evidence. On the other hand, a scaling argument based on the KZ mechanism can be adopted [157, 115]; this relies on the fact that the dynamical gap Δ_0 seems to close with $D-D_C$ as the thermodynamical gap in a BKT transition, that is, it depends on the anisotropy parameter as $\Delta_0 \propto \exp(-c/\sqrt{D-D_C})$ [28], so that the critical exponent for the correlation length ν diverges. In this case, the KZ scaling argument predicts a power-law scaling exponent $\alpha = (d+z)\nu/(z\nu+1)$, d being the dimension of the system and z, ν critical exponents; in our specific case $d = z = 1, \nu \to \infty$ thus leading to $\alpha = 2$ (plus some logarithmic corrections) [115, 36]. This again contrasts with our numerical evidence, thus revealing that the presence of a critical line in which the gap closes always in the same way seems to indicate that all the low-lying excitation spectrum becomes necessary to predict the actual behavior. We notice that the two above mentioned different dependencies of the dynamical gap on the inverse size, like $\sim 1/L$ for $L \to \infty$, and on the distance from the critical point, as $\sim e^{-c/\sqrt{D-D_c}}$, are confirmed quite precisely by our data.

We checked the dependence of α on the final point of the quench: in figure 2.8 we varied the ending point $D_{\rm fin}$, while keeping $D_{\rm in}$ and the system size fixed (explicit data for the excess energy $E_{\rm exc}$ as a function of τ are presented in the inset, at $L = 60$). For values of $D_{\rm fin}$ outside the critical region we find that α depends on $D_{\rm fin}$ at finite sizes. Nevertheless, the range of the scaling region shrinks with L and eventually disappears in the thermodynamic limit, so we argue that the dependence of α on $D_{\rm fin} > D_{\rm c}$ should be entirely due to finite size effects. For $D_{\rm fin} < D_{\rm c}$ we observe that the dependence of α on $D_{\rm fin}$ weakens as the system size is increased. In this case the scaling region is valid until a quench rate $\tau^* \overset{L\to\infty}{\longrightarrow} +\infty$; the power-law decay rate tends to a value that is independent of $D_{\rm fin} < D_c$ and has been extrapolated from numerical data of figure 2.7 to be $\alpha_\infty \approx 1.28$.

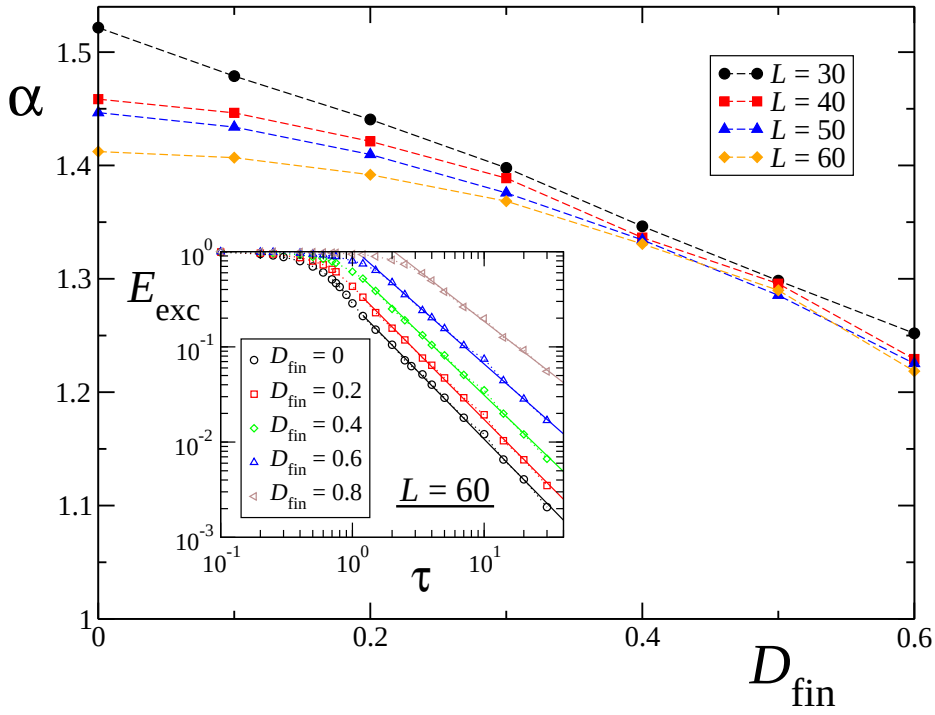

Figure 2.8: Power-law decay rate α as a function of the ending value for the quench $D_{\rm fin} < D_{\rm c}$ and for fixed $D_{\rm in} = 1$. Data are for different system sizes, as explained in the caption. In the inset we display the excess energy for a quench ending at various $D_{\rm fin}$, and for a system size $L = 60$. straight lines are power-law fits in the scaling regime.

Chapter 3

Quantum quenches, Thermalization and Many-Body Localization

3.1 Introduction

We turn our attention to the possibility of thermalization following a sudden quench and to its interplay with integrability. In this chapter we will show that a natural framework to characterize the effects of integrability on thermalization is that of *many-body localization* [2, 6, 77], which we briefly review in Sec. 3.4. A relation between integrability breaking and many-body localization was hinted in a recent interesting work by Pal and Huse [109], building on a series of seminal papers in disordered electron systems [2, 6]. In this chapter localization will be intended in the space of quasi-particles (and not necessarily in real space, as in Ref. [109]). More specifically, in analogy to a construction originally conceived for disordered electron systems [2, 6, 77], the quasi-particle space can be thought of as a multidimensional lattice where each point is identified by the occupations $n(k)$ of the various quasi-particle modes $|\Psi_\alpha\rangle = |\{n_\alpha(k)\}\rangle$ (see Fig. 3.1).

As long as states are localized in quasi-particle space, the system behaves as integrable: any initial condition spreads into few sites maintaining strong memory of the initial state. Thermalization will not occur. At the same time, the qualitative behavior of local and non-local operators in the quasi-particles is naturally going to be different: locality in quasi-particle space implies sensitivity to the localization/delocalization of states, while non-local operators always display an effective asymptotic thermal behavior. Once a strong enough integrability-breaking perturbation hybridizing the various

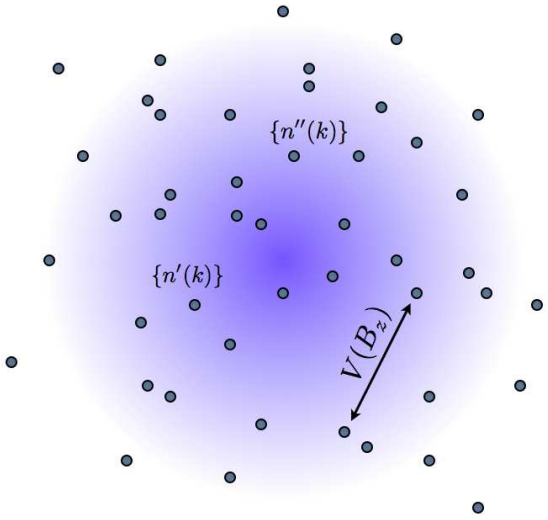

Figure 3.1: (color online). A cartoon of the quasi-particle space, where integrability breaking leads to a localization/delocalization transition. For an integrable model all states, represented by the occupations of quasi-particles $\{n(k)\}$, are localized. An integrability breaking perturbation introduces hopping matrix elements V among different sites, which hybridize provided $|E(\{n'(k)\} - E(\{n''(k)\}| \leq V$. For strong enough perturbations, this may lead to the delocalization of wave functions among all points in quasi-particle space in a microcanonical energy shell.

states $|n_\alpha(k)\rangle$ is applied, the consequent *delocalization in quasi-particle space* will lead to thermalization. An initial state is allowed to diffuse into all states in a micro-canonical energy shell generating a cascade of all possible lower energy excitations[1]. We investigate the validity of this scenario by studying the dynamics of a quantum XXZ spin-1/2 chain after a sudden quench of the anisotropy, in the presence of an integrability breaking term.

The chapter is organized as follows. First of all, in Section 3.2 we qualitatively recall the ideas of many-body localization transition, emphasizing the concept of inverse participation ratio. After introducing a specific model in Sec. 3.3, we characterize the deviations from integrability and the correspondent delocalization in quasi-particle space by means of the level statistics and of the properties of the many-body eigenstates in Sec. 3.4. We show that a well defined transition from Poisson (integrable) to Wigner-Dyson statistics (non-integrable) is closely associated to the localized/diffusive character of

[1]Notice that in general it is possible to have non-ergodic, but extended states (see Ref. [2] and refs. therein).

eigenstates in quasi-particle space. In Sec. 3.5 we turn to the study of the dynamics after a sudden quench, defining and discussing the behavior of the effective temperature. Keeping in mind the results of Sec. 3.4 characterizing the integrability breaking crossover, we show in Sec. 3.6 that the transition from non-thermal to thermal behavior in the dynamics of observables is directly connected to the localization/delocalization transition in quasi-particle space. In particular, by looking at the asymptotics of spin-spin correlation functions, we discuss how the emergence of thermalization is linked to the emergence of diffusive eigenstates in quasi-particle space. Finally, we study the sensitivity to integrability breaking of spin correlators in different directions and discuss the relation between the locality of observables in quasi-particle space and the corresponding behavior. In Appendix B we support the main findings of this Chapter performing the same numerical analysis for models with different integrability breaking terms.

3.2 Many-body localization transition

We now sketch very qualitatively the concept of many-body localization, originally introduced in the Refs. [2, 6], studying transport properties of electrons in random potentials. Although here we are not dealing with such kind of systems, it is nevertheless useful to recall them in order to understand the role of quantities such as the inverse participation ratio, discussed below.

In absence of electron-electron interaction in a disordered potential, all the physics is described by the phenomenon of Anderson localization: if one-particle wave functions are spatially extended then the dc electrical conductivity has a finite zero-temperature limit, if instead they are localized the conductivity vanishes for $T \to 0$. So Anderson localization of electronic states leads to the metal-to-insulator transition at zero temperature. Localized and extended states in a random potential can not be mixed in the one electron spectrum, so the latter is a combination of bands with extended states and bands with localized states. The border between a localized and an extended band is called mobility edge.

The presence of inelastic electron-electron interaction, i.e. collisions which create or annihilate real electron-hole pairs, has deep consequences on conductivity: Altshuler *et al.* [2, 6] show that electron-electron interaction alone is not enough to give a finite conductivity under a certain critical temperature T_c, but the conductivity is finite for $T > T_c$. Hence there exists a phase transition that manifests itself by the emerging of a finite conductivity. This transition can be thought of as a many-body localization transition, because it applies to the many-body eigenstates of the whole system: it does

not occur in real space, but rather in Fock space.

Depending on the strength of the disorder potential, a one-particle wave function $\phi_\alpha(\mathbf{r})$ of an eigenstate α can be classified as localized if $|\phi_\alpha(\mathbf{r})|^2 \propto \exp(|\mathbf{r}-\boldsymbol{\rho}_\alpha|/\zeta_{\rm loc})$ or extended in the volume V of the system if $|\phi_\alpha(\mathbf{r})|^2 \propto 1/V$. This asymptotic behavior can be translated into a property of the matrix elements of given operator, whose spatial correlation funtion decays exponentially if it is localized. In the situation in which all single-particle states are localized, assumed here, and without many-body effects, the conductivity is zero at any temperature.

If we now turn to the many-body system, its wave function $\Psi_k(\{\mathbf{r}_j\}_{j=1}^N)$ in coordinate representation depends on all the coordinates of the N particles, so a definition of localized state as for the one-particle functions is not possible. Nevertheless, a definition of many body localization is feasible by shifting the attention on observables: if the spatial correlation function of the matrix elements of a local operator computed on some many-body wave function falls exponentially with the distance, then those wave functions describe many-body localized states.
It can be shown that insulating or *localized* many-body states are found when electron-electron interaction mixes a finite number of many-body eigenstates. In this case, considering the creation of an electron-hole pair on top of some eigenstate Ψ_k with eigenvalue E_k and expanding on the other eigenstates:

$$c_\alpha^\dagger c_\beta|\Psi_k\rangle = \sum_{k'} C_{\alpha\beta}^{kk'}|\Psi_{k'}\rangle; \qquad \sum_{k'}|C_{\alpha\beta}^{kk'}|^2 = 1 \tag{3.2.1}$$

the number of terms contributing to the sum is large but finite:

$$\lim_{V\to\infty}\left[\sum_{k'}|C_{\alpha\beta}^{kk'}|^4\right]^{-1} < \infty. \tag{3.2.2}$$

Conductivity can be different from zero only if the wavefunctions of the excitations can be broken onto an infinite number of eigenstates:

$$\lim_{V\to\infty}\left[\sum_{k'}|C_{\alpha\beta}^{kk'}|^4\right]^{-1} = \infty. \tag{3.2.3}$$

which corresponds to the metallic or *extended* many-body state. The metallic states correspond to the case when electron-electron interaction mixes the excited state with all the eigenstates in the system with close enough energy $|C_{\alpha\beta}^{kk'}|^2 \propto$ "$\delta(E_k - E_{k'} + \omega_{\alpha\beta})$", where the δ-function is understood in a thermodynamic sense: its width, although large enough to include many

states, vanishes for $V \to \infty$.
The crucial quantity is thus $\left[\sum_{k'} |C_{\alpha\beta}^{kk'}|^4\right]^{-1}$, which is found in many different contexts and is known as *inverse participation ratio* (IPR). We will study the IPR for our finite systems in Section 3.4.
The presence of the many-body localization transition inplies that there exists an extensive many-body mobility edge, which separates localized states at sufficiently small energies from extended states at sufficiently high energies. The proof of the existence of the localized states goes through establishing a correspondence between the many-electron interacting system and the Anderson model on a certain graph. For example, in the case of quantum dots with a finite number of electrons, the Hamiltonian can be mapped into the one-particle Hamiltonian on a lattice with the topology of a Cayley tree and on-site disorder [2]. This problem has an exact solution that contains the localization transition. The many-body localization transition in the general $d-$dimensional case has been proved in Ref. [6].

3.3 The model

We consider the spin 1/2 anisotropic Heisenberg model with a random magnetic field, defined by:

$$\mathcal{H} = \sum_{i=1}^{L-1} \left[\left(\sigma_i^x \sigma_{i+1}^x + \sigma_i^y \sigma_{i+1}^y \right) + J_z \sigma_i^z \sigma_{i+1}^z \right] + B_z \sum_{i=1}^{L} h_i \sigma_i^z. \tag{3.3.1}$$

Here $\sigma_i^\alpha (\alpha = x, y, z)$ are the Pauli matrices, J_z is the anisotropy parameter, while B_z controls the strength of a random on-site magnetic field and h_i are random numbers uniformly distributed in $[-1, 1]$.

3.3.1 Relevant symmetries

In order to study the energy level statistics, we need to study the quantities of interest for the statistical properties separately in each symmetry sector of the Hamiltonian 3.3.1. For generic values of B_z, the model shows two symmetries. First, the system is invariant under rotations in the xy plane, so the z-component of the total spin $S^z = \sum_i \sigma_i^z/2$ is a conserved quantity. If the number of sites L is even, the largest subspace corresponds to $S^z = 0$, which has dimension $n \equiv \binom{L}{L/2}$. In the remainder of this chapter we will restrict to this sector, whose simplest basis is the computational basis at zero magnetization, given by the tensor products over the lattice sites of the eigenstates of σ_i^z.

Second, although the Hamiltonian 3.3.1 does not commute with the time reversal operator, it can be shown [3] that there exists an antiunitary operator, often related to as the non-standard time reversal operator, under whose action the Hamiltonian is invariant. This makes it possible to describe the statistical properties of the energy levels of 3.3.1 through the Gaussian Orthogonal Ensemble (GOE) and more precisely, since the model involves only two-body interactions, through the two-body random ensemble [13], embedded in the GOE.

3.3.2 Phase diagram

For $B_z = 0$ the model (3.3.1) is integrable by Bethe Ansatz [107], and exhibits two gapped phases, ferromagnetic ($J_z < -1$) and antiferromagnetic ($J_z > 1$). These phases are separated by a critical region $-1 \leq J_z \leq 1$, with J_z-dependent critical exponents [82] and quasi-long-range-order in the xy spin-plane.

The addition of the random term ($B_z \neq 0$) makes the system non-integrable [2]. The zero temperature phase diagram in presence of disorder has been studied in Ref. [54]: it shows a transition from quasi-long range order, typical of the pure XXZ model, on the line $-1 < J_z < 1$ with $B_z = 0$ and in a region with small B_z and $-1 \leq J_z \leq -1/2$, to a phase with a disordered ground state, rapidly decaying correlation functions and localized excitations.

At infinite temperature, the onset of many-body localization and the phase diagram have been studied in Refs. [108, 84, 103, 109]. In the first of these works [108], Oganesyan *et al.* considered the model of Eq.3.3.1 with a small next-nearest neighbor term and conjectured the existence of a localized phase at high magnetic fields from the exact diagonalization study of the spectral properties, the uncertainty coming from the impossibility of a finite-size scaling of the transition. Taking a different perspective, the onset of localization for the same model of [108] has been confirmed by Monthus *et al.* [103] with an exact renormalization procedure in configuration space. Further confirmations of the many-body localization transition at strong disorder for the model Eq. 3.3.1 came both from the emergence in real space of the asymptotic exponential localization of correlation functions [84], and recently from Ref. [109]. In the latter work the critical value $B_z^{\rm crit}$ of the magnetic field separating the non-ergodic many-body localized phase (in real space) at $B_z > B_z^{\rm crit}$, from the ergodic one at $B < B_z^{\rm crit}$, has been estimated to be at $B_z^{\rm crit} \sim 6 \div 8$ for $J_z = 1$ (in our units). The results

[2] The effect of other integrability breaking terms is shown in Appendix B.

presented below indicate the presence of a second non-ergodic localized phase (in quasi-particle space) for B_z close to zero that crosses over to the ergodic phase upon increasing B_z beyond B_z^*. The fate of this crossover in the thermodynamic limit and the eventual value of the critical B_z^* are yet to be determined [3].

3.4 Integrability and many-body localization

Having in mind the scenario sketched in Section 3.2, we now describe the effect of the integrability breaking perturbation in terms of many-body localization in the space of quasi-particles. We start characterizing quantitatively the crossover from integrability to nonintegrability through the level statistics indicator (LSI), in order to identify the range of magnetic fields B_z suitable for observing the onset of delocalization. The LSI is a quantity related to quantum chaos which depends on the energy spectrum, in particular on the energy spacing between neighboring levels.
Then we move to the study of the inverse participation ratio, properly defined in this context, motivated by the fact discussed in Section 3.2 that the many-body localization transition is in correspondence with a change in the behavior of the IPR. The many-body localization transition can be captured comparing the IPR in a given energy shell and the number of eigenstates in the same energy range, as we show at the end of this section.
It should be mentioned that several numerical works can be found in literature on the spectral properties of both isotropic and anisotropic Heisenberg chains [3, 13, 55, 92, 119, 136]: here we show the behavior of the LSI and the IPR in our model as a function of the energy eigenvalues, obtained numerically by exactly diagonalizing finite-size systems with up to 16 sites, and draw special attention on the relation between statistical quantities and many-body localization.

3.4.1 Level statistics indicator

We characterize the states involved in a quench by studying their spectral properties, which allow to distinguish quantum integrable from fully chaotic, non-integrable systems. Namely, defining $P(s)$ as the probability distribution of the spacing between neighboring levels $s \sim |E_{i+1} - E_i| > 0$ (modulo a normalization factor), it has been known for a long time [81] that integrable

[3] While for the parameters used in this chapter the low lying eigenstates are localized in the thermodynamic limit, in the following we will consider systems sizes smaller than the localization length.

systems show a Poisson (P) distribution:

$$P_P(s) = \exp(-s), \tag{3.4.1}$$

while non-integrable systems with the same symmetries of Eq.3.3.1 have a Wigner-Dyson (WD) distribution:

$$P_{WD}(s) = \frac{\pi s}{2} \exp(-\frac{\pi s^2}{4}). \tag{3.4.2}$$

The effect of an integrability-breaking perturbation with increasing weight can be quantified by means of the level statistics indicator (LSI) η, introduced in [87] and here specialized to a given energy shell:

$$\eta(E) \equiv \frac{\int_0^\infty |P_{[E,E+W]}(s) - P_{\rm P}(s)|ds}{\int_0^\infty |P_{\rm WD}(s) - P_{\rm P}(s)|ds} \ , \tag{3.4.3}$$

where $P_{[E,E+W]}(s)$ is the probability distribution of the level spacing computed for the eigenvalues in the window $[E, E+W]$. The LSI varies from zero in the integrable case, to unity for a WD distribution of the spacings.[4] A remark about the numerical calculation of η is in order. The most "natural" way to construct $P(s)$ is to compute all the differences between neighboring energies $\delta_i = E_{i+1} - E_i$, where E_i is the i-th eigenvalue, renormalize them to the average value buiding the quantities s_i and then build a normalized histogram. Although correct, this procedure gives large fluctuations in the extreme regions of the energy spectrum. The usual solution of this problem is to work with *unfolded* eigenvalues [81, 92]: they are renormalized values whose local density of states is equal to unity everywhere in the spectrum. In Fig. 3.2 we show $\eta(E)$ for several B_z values: while at low energies the statistics is always closely Poisson, in the center of the spectrum the statistics is Poisson for very small B_z, while it approaches Wigner-Dyson for $B_z \simeq 1$ [48]. For $B_z \geq 1$, η decreases again towards small values, since for $B_z \gg J_z$ the system turns into a trivial integrable model. This last result is coherent with those of Ref. [108] about the level statistics. We also studied the cumulative behavior of the LSI, computing η on states within a given excitation energy cutoff $E_{\leq}$, see Fig. 3.3. With increasing cutoff energy, the LSI approximately satures to a constant value, strongly dependent on the magnetic field. The curve in the inset further confirms that for large magnetic field the level spacing departs from the WD distribution.

[4] The definition used here for the level statistics indicator slightly differs from the standard one, which is $\eta = \frac{\int_0^{s_0}[P(s)-P_{\rm WD}(s)]ds}{\int_0^{s_0}[P_{\rm P}(s)-P_{\rm WD}(s)]ds}$ where $s_0 \approx 0.4729$ is the first intersection point of $P_{\rm P}(s)$ and $P_{\rm WD}(s)$. We cheked that the two definitions agree very well, our choice is due to numerical convenience.

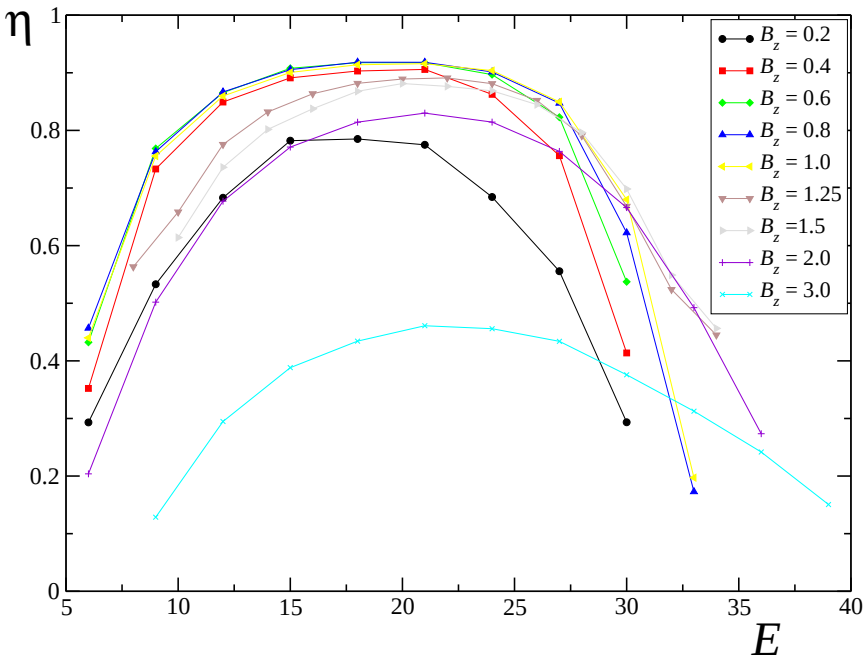

Figure 3.2: (color online). LSI η for a system of $L = 14$ sites in adjacent microcanonical shells of width W. Data are obtained by taking $W = 2$ for η; averages over 10^3 for η are taken. Here and in the following figures we consider $J_z = 0.5$; we also shift energies so that the ground state corresponds to $E = 0$. Units of $\hbar = k_B = 1$ are used throughout this chapter.

3.4.2 Inverse participation ratio

Besides the crossover in level statistics, on increasing disorder the eigenstates delocalize in the quasi-particle space. A suitable indicator of this delocalization is the Inverse Participation Ratio (IPR) [2, 86, 154]. We considered the IPR on two specific bases: the *Integrable* (I) basis consisting of the eigenstates $\{|n_I\rangle\}$ of the model in absence of randomness ($B_z = 0$), and the *Site* (S) basis $|n_S\rangle = |\sigma_1 \cdots \sigma_L\rangle$ ($\sigma_i = \pm 1$) composed of the eigenstates of σ_i^z. In these cases the energy-resolved IPR is defined as

$$\xi_{I/S}(E) = \frac{1}{N_{[E,E+W]}} \sum_{|\tilde{\psi}\rangle} \left(\sum_n |\langle n_{I/S}|\tilde{\psi}\rangle|^4 \right)^{-1}, \tag{3.4.4}$$

where $N_{[E,E+W]}$ is the total number of eigenstates $|\tilde{\psi}\rangle$ in the energy window $[E, E + W]$. Trivial particular cases of Eq.(3.4.4) happen when $|\psi\rangle$ is a state of the basis $\{|n\rangle\}$ or when it is a uniform superposition of exactly m basis states: the inverse participation ratio is $\xi = 1$ and $\xi = m$ respectively.

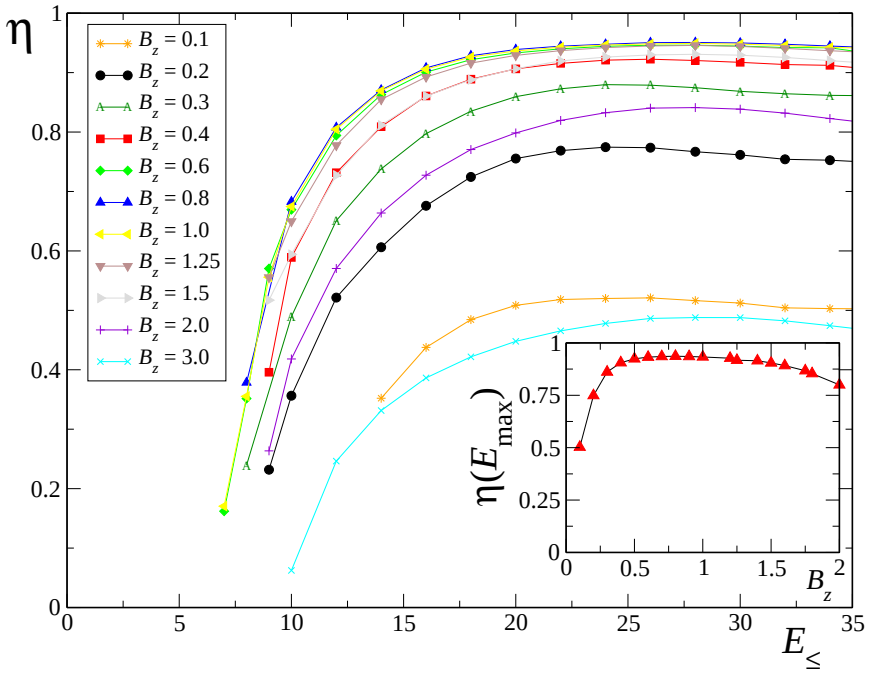

Figure 3.3: (color online). Main panel: cumulative LSI η for the same systems of Fig. 3.2 as a function of the energy cutoff. Inset: LSI of the full spectrum as a function of the magnetic field.

It can be shown [7, 13, 80] that for a N-dimensional state vector, whose components are randomly distributed according to a GOE, the expected IPR is $\xi_{\mathrm{GOE}} = \frac{N+2}{3}$.

In Fig. 3.4 we show our numerical results for a system of $L = 14$ sites as a function of energy, for different magnetic fields; at this size the zero magnetization sector of the Hilbert space is composed of $n = 3432$ states. As for the LSI, also here the extreme low and high energy regions of the spectrum are almost not sensitive to the breaking of integrability and to different magnetic fields. On the contrary, in the central part of the spectrum, the loss of integrability upon increasing B_z shows up as a progressive delocalization of the eigenstates with respect to the I-basis, as witnessed by the peak at $\xi_I \sim 800 \sim N/3$ in Fig. 3.4. Analogously to the LSI, also the cumulative IPR has been analyzed: in Fig. 3.5 we show the IPR both in the integrable and in the site basis. We see that in correspondence with the delocalization in the integrable basis, a concomitant localization happens with respect to the computational basis.

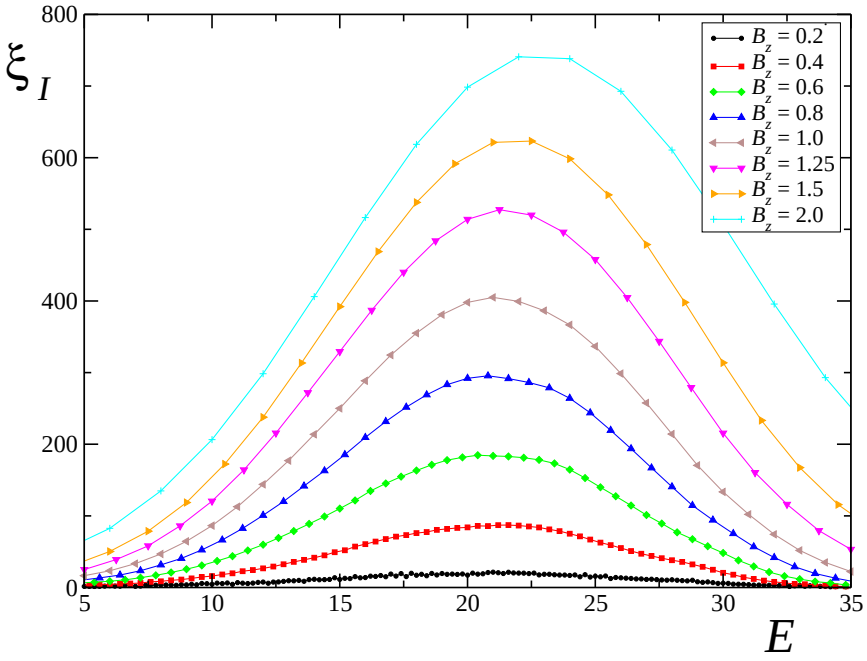

Figure 3.4: (color online). IPR for the integrable basis ξ_I. for a system of $L = 14$ sites, as a function of the energy window of the eigenstates. Data are obtained by taking $W = B_z$ for ξ_I; averages over 10^2 disorder realizations are taken.
5

3.4.3 Delocalizion in Fock space

Let us now study in more depth the qualitative difference between localized and delocalized states in quasi-particle space. We compare the inverse participation ratio $\xi_I(E)$ with the number of quasi-particle states $N(E)$ hybridized in a delocalized wave function. The quantity $N(E)$ can be roughly estimated by the number of states in the microcanonical energy shell $[E, E + V]$, where $V \approx 2B_z$ is the typical matrix element of the integrability-breaking perturbation. This comparison clearly elucidates the difference between quasi-integrable and non-integrable systems: in the first case $\xi_I \ll N(E)$ (Fig. 3.6, left panel), indicating that eigenstates are still close to those of the integrable system, while in the second case $\xi_I \approx N(E)$, thus meaning that all quasi-particle states within the microcanonical energy shell do hybridize (Fig. 3.6, right panel). Notice that in this context the low-lying eigenstates are rather peculiar: this part of the spectrum, which contains very few states as compared to the center (Fig. 3.6, upper left panel), has closely Poissonian statistics and is characterized by large

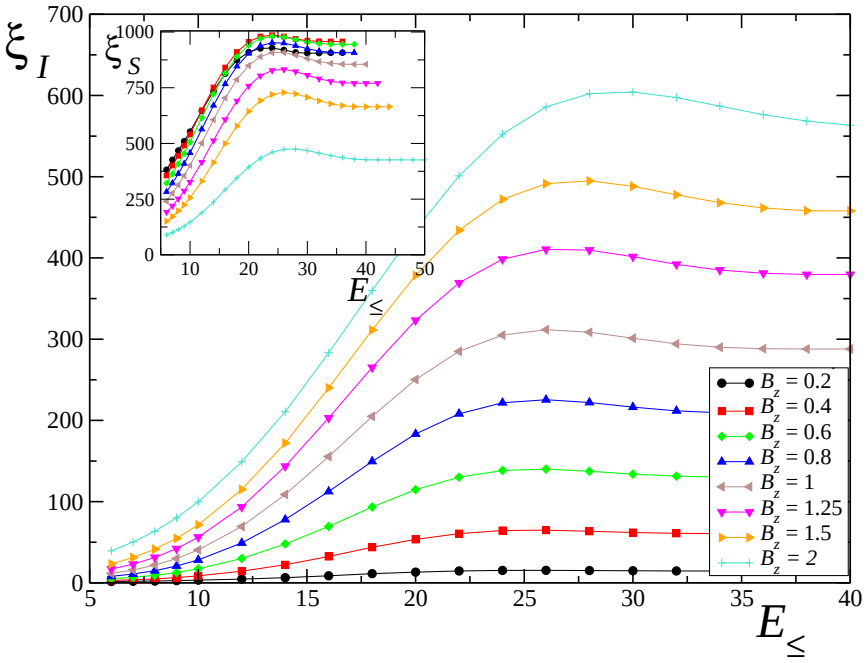

Figure 3.5: (color online) Cumulative IPR for the integrable basis ξ_I (main panel) and the site basis ξ_S (inset) for the same system of Fig. 3.4, as a function of the cutoff energy of the eigenstates.

fluctuations of statistical quantities.

3.5 Quench dynamics

In order to relate many-body localization to thermalization we will present, here and in the following section, some results for the dynamics following a sudden quench of the anisotropy parameter according to:

$$\begin{cases} J_{z0}, & t < 0 \\ J_z \neq J_{z0}, & t \geq 0. \end{cases} \tag{3.5.1}$$

We set the final value of $J_z = 0.5$ [6] and restrict $J_{z0} > -1$ (critical or antiferromagnetic region, for $B_z = 0$), while the B_z and random fields are kept constant throughout the evolution. The system is initially prepared in the ground state $|\psi_0\rangle$ of $\mathcal{H}(J_{z0})$, so that its (conserved) energy with respect to the final Hamiltonian $\mathcal{H}(J_z)$ is $E_0 = \langle\psi_0|\mathcal{H}(J_z)|\psi_0\rangle$. For growing values of J_{z0}, the state $|\psi_0\rangle$ tends towards the classical antiferromagnetic Néel state,

[6] We have checked explicitly that changing J_z to a different value within the critical region does not qualitatively affect our conclusions.

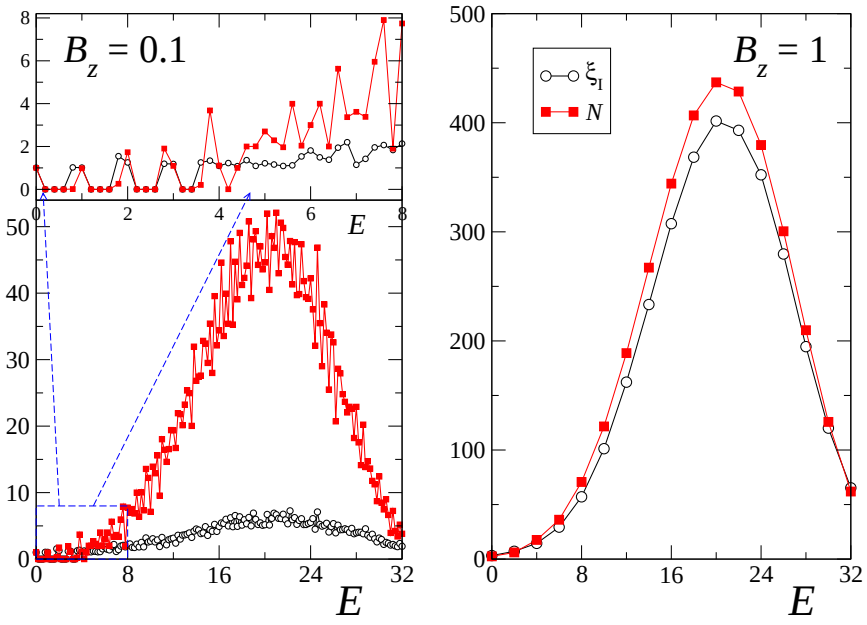

Figure 3.6: (color online). IPR in the integrable basis ξ_I at $B_z = 0.1$ (left panels), $B_z = 1$ (right panel), compared to the number of states N in an energy window of width $W = 2B_z$.

independent of J_{z0}. E_0/L saturates to a constant value, see Fig. 3.7, thus implying that a quench generally involves only a fraction of the eigenstates of the final Hamiltonian.

Contrary to local quenches, the work done on the system by changing the anisotropy from J_{z0} to J_z is extensive. It is then interesting to ask, after a quench involving an extensive injection of energy $E_0 - E_{\rm gs} \propto L$ ($E_{\rm gs}$ being the ground state energy of $\mathcal{H}(J_z)$), if the subsequent long-time evolution of the system is effectively described by an *equilibrium* dynamics governed by $\mathcal{H}(J_z)$. In view of a plausible equivalence between a microcanonical (fixed E_0) and a canonical equilibrium description of such a long-time dynamics, it is meaningful to define, as in previous instances [129, 130], an effective temperature $T_{\rm eff}$ by equating E_0 to the canonical average through the equation:

$$E_0 = \frac{{\rm Tr}[e^{-\mathcal{H}(J_z)/T_{\rm eff}}\mathcal{H}(J_z)]}{{\rm Tr}[e^{-\mathcal{H}(J_z)/T_{\rm eff}}]}. \qquad (3.5.2)$$

For the quenches considered here, the effective temperature can reach at most values of the order $T_{\rm eff} \sim 5$ for large J_{z0}, see Fig. 3.8. For these effective temperatures the states probed are located in the lower central part of the band.

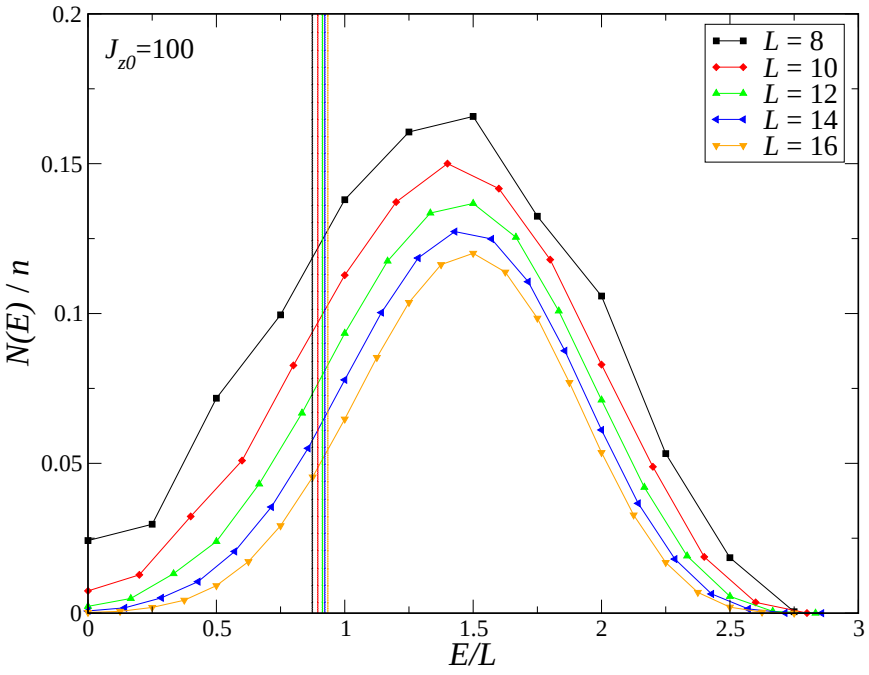

Figure 3.7: (color online) Curves with symbols: average fraction of states in microcanonical shells of width $W = 2B_z$ as a function of the energy per particle, with $J_z = 0.5$ and magnetic field amplitude $B_z = 1$. For sizes from $L = 8$ to $L = 14$ we average over $\sim 10^3$ realizations, for $L = 16$ over 100. Vertical lines: intensive initial energies for a quench from $J_{z0} = 100$ to $J_z = 0.5$ and $B_z = 1$. The data are obtained averaging on 1000 disorder realizations for each size, same color code as the curves.

3.6 Thermalization of observables

In this section we enlight the relation between thermalization and delocalization in quasi-particle space on the grounds of our numerical results.

Recalling the discussion in Chap.1, by thermalization we mean that the long-time expectation value of an observable, given by the diagonal ensemble average, equals the canonical expectation value. A word of caution about the ensemble equivalence: in this context of very small sizes, it is not necessarily true that the microcanonical expectation value corresponds with the canonical one.

We study the behavior of the Fourier transform of two-spin correlators:

$$n_k^\alpha \equiv \frac{1}{L}\sum_{j,l=1}^{L} e^{i(j-l)k/L}\sigma_j^\alpha\sigma_l^\alpha \qquad \alpha = x, z\ . \tag{3.6.1}$$

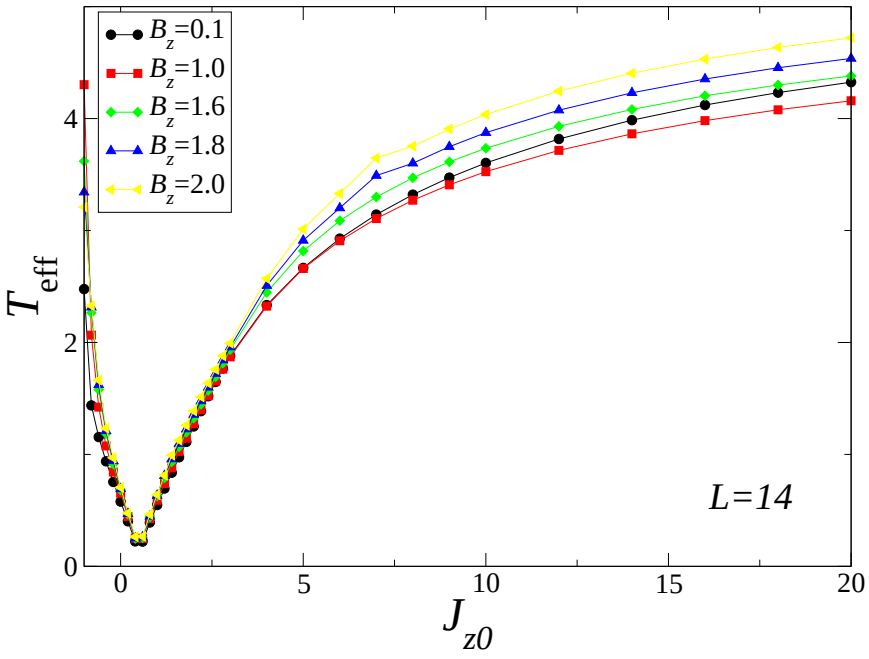

Figure 3.8: (color online). Effective temperatures as a function of the initial value of the anisotropy parameter J_{z0}, for a system of $L = 14$ sites. Averages on 100 disorder realizations, different curves correspond to different magnetic fields.

and compare the expectation value $n^{\alpha}_{T_{\rm eff}}(k) \equiv \langle n^{\alpha}_k \rangle_{T_{\rm eff}}$ in the canonical ensemble at the corresponding $T_{\rm eff}$, with the asymptotic value that is reached after the quench, calculated from the diagonal ensemble [123, 124, 126]:

$$n^{\alpha}_{Q}(k) \equiv \lim_{t\to\infty} \langle \psi(t)|n^{\alpha}_k|\psi(t)\rangle = \sum_i |c_i|^2 \langle \phi_i|n^{\alpha}_k|\phi_i\rangle, \qquad (3.6.2)$$

where $c_i \equiv \langle \phi_i|\psi_0\rangle$ and $|\psi(t)\rangle = e^{-i\mathcal{H}(J_z)t}|\psi_0\rangle$ is the state at time t. While correlators in the x-direction are always well reproduced by an effective thermal ensemble, correlators in the z-direction appear to be more sensitive to integrability and its breaking. This difference is already evident at a qualitative level by looking at $n^{\alpha}_{Q}(k)$ and $n^{\alpha}_{T_{\rm eff}}(k)$ for $\alpha = x, z$ (insets of Fig. 3.9). The discrepancies between thermal and diagonal ensemble x- and z-correlators are best seen at $k = \pi$: defining $\delta n^{\alpha}_{\pi} = |n^{\alpha}_{\rm Q}(\pi) - n^{\alpha}_{\rm T_{eff}}(\pi)|$, we observe that δn^{x}_{π} is more than an order of magnitude smaller, indicating a closely thermal behavior, while δn^{z}_{π} shows a sharp decrease as integrability is progressively broken by increasing B_z, towards a minimum value at $B_z = 1$, which corresponds to fully delocalized states in quasi-particle space. Notice that for $B_z > 1$, δn^{z}_{π} increases again, in agreement with the fact that $B_z \simeq 1$

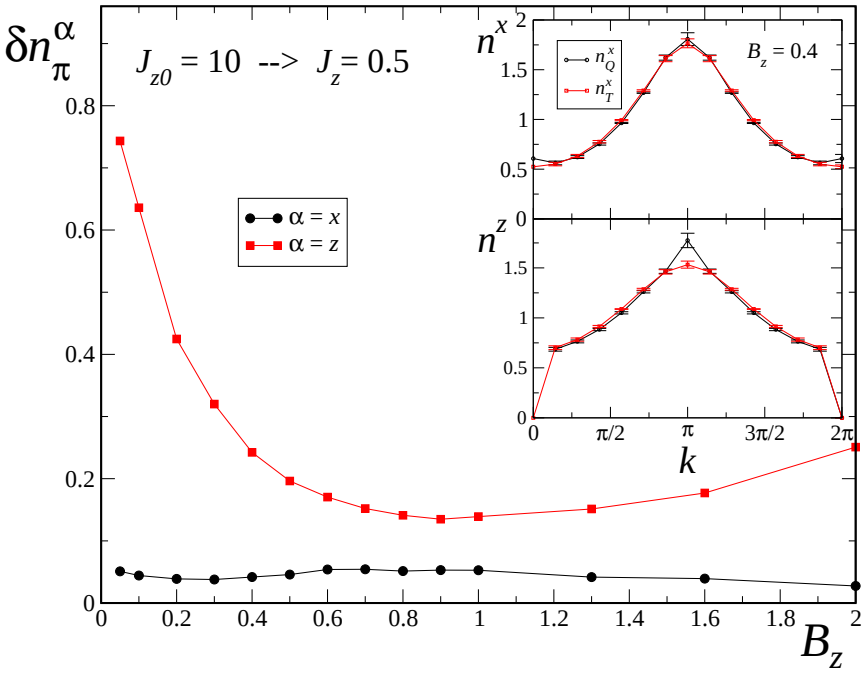

Figure 3.9: (color online). Differences δn_π^z and δn_π^x as a function of the random term B_z for a quench of the anisotropy parameter from $J_{z0} = 10$ to $J_z = 0.5$. Data are for $L = 14$ sites, averaged over 10^2 disorder realizations. Insets: momentum dependence of $n^\alpha_{Q/T_{\rm eff}}(k)$, for a given value of $B_z = 0.4$.

is the point where non-integrable behavior is most pronounced and that for large magnetic fields the system tends towards another integrable limit. In analogy with previous studies, the different sensitivity to integrability of correlators in different spin directions can be understood qualitatively as a consequence of the fact that σ^z is a local operator in quasi-particle space while σ^x is a non-local one [129, 130]. However we stress that this identification is here subtler than in the Ising chain, and is evident only in the XX limit ($J_z = 0$) and/or at low energies in the critical phase [107].

Chapter 4

Quench dynamics in the random Ising model.

4.1 Introduction

In this Chapter we present preliminary results [21] on the study of a random Ising chain and its dynamics after a quantum quench.
The random Ising model has been widely studied: the phase diagram, the critical exponents and the static properties are addressed in Refs. [98, 71, 72, 142, 153], while the dynamical correlations in imaginary time are numerically investigated in Refs. [152, 85]. The slow dynamics of the random Ising model crossing its quantum critical point through a linear time modulation of the transverse field has been studied in Ref. [22], where the density of defects and the residual energy are found to scale logarithmically with the time scale of the quench. Here we concentrate on a *sudden* quench of the transverse field, trying to elucidate the role of disorder in the asymptotic behavior of integrable systems and in particular on the thermalization of observables which have a non-local representation in terms of quasi-particles.
The numerical results presented below, although at a very preliminary stage, should be the extension to the disordered case of the results of Refs. [129, 130], concerning the dynamics of the ordered Ising model. In the latter papers it is shown that the autocorrelation function of the order parameter, $\rho^{xx}(t)$, undergoes thermalization after a quantum quench, while the transverse magnetization does not. As we discussed in Chapter 1 and 3, at the roots of this different behavior there is the different content of quasi-particles of the two operators: the order parameter and the transverse magnetization are characterized by a non-local and local expression in terms of quasi-particles respectively. In particular Rossini *et al.* [129, 130] find that

at long times $\rho^{xx}_Q(t) \sim e^{-t/\tau^{\varphi}_Q}$ decays exponentially with a time scale τ^{φ}_Q, which is shown to agree very well with τ^{φ}_T, setting the exponential decay of $\rho^{xx}_T(t)$ at thermal equilibrium. The decay rate after the quench is shown to depend only on the effective temperature of the quench and on the gap of the final Hamiltonian. Since both the ordered and random Ising models are integrable, it is interesting to verify whether the generalized Gibbs ensemble is able to predict the decay of ρ^{xx}, since the latter is a not an additive quantity [118]. We try to address this issue presenting some numerical findings limited to the ordered case, which turn out to be not completly conclusive and compare our results to those of Ref. [130] where a semiclassical analysis [132] is adopted.
This Chapter is organized as follows: in Section 4.2 we define the model and describe the exact solution of the statics and the dynamics in terms of fermions. Then in Section 4.3 we show the detailed calculation of the autocorrelation function in the various cases of interest. In Section 4.4 we show our numerical results for the autocorrelation function at equilibrium in real time, emphasizing the relation with the imaginary time dynamics. In Section 4.5 we show our numerical findings, starting from the ordered case, where we investigate the predictions of the GGE, and then moving to the disordered situation.

4.2 The model

We consider a quantum random Ising spin chain in one dimension, defined by the Hamiltonian:

$$\mathcal{H}(\Gamma) = -\sum_i J_i \sigma^x_i \sigma^x_{i+1} - \Gamma \sum_i h_i \sigma^z_i \,, \tag{4.2.1}$$

where σ^α_i ($\alpha = x, y, z$) are the Pauli matrices for the ith spin of the chain, J_i are random couplings between neighboring spins, h_i are random transverse fields, while Γ is a parameter setting the amplitude of the transverse magnetic fields. Hereafter we use units of $\hbar = k_B = 1$. We will consider finite chains of length L, with open boundary conditions (so that the first sum in Eq. (4.2.1) runs over $i = 1, \ldots, L-1$ and the second over $i = 1, \ldots, L$).

We drive the system out of equilibrium with a quantum quench of the transverse field, described by:

$$\Gamma(t) = \begin{cases} \Gamma_0 & t \leq 0 \\ \Gamma & t > 0 \,. \end{cases} \tag{4.2.2}$$

We initialize the system in the ground state $|\psi_0\rangle$ of $\mathcal{H}(\Gamma_0)$. At time $t > 0$ the system evolves with the new Hamiltonian $\mathcal{H}(\Gamma)$, according to:

$$|\psi_t\rangle = e^{-i\mathcal{H}(\Gamma)t}|\psi_0\rangle\,. \tag{4.2.3}$$

In one dimension and for nearest-neighbor couplings, there is no frustration associated to the random nature of the couplings J_i: by appropriately performing spin rotations of π along the x-spin axis, we can always change the desired σ_i^z into $-\sigma_i^z$ and invert accordingly the signs of the couplings in such a way that all J_i's turn out to be non-negative. As the distributions for the random J_i's and h_i's, we assume the same as in Ref. [22]: the J_i's are randomly distributed in the interval $[0, 1]$ with a flat distribution $\pi[J] = \theta(J)\theta(1 - J)$, where θ is the Heaviside function; we analogously assume the distribution $\pi[h] = \theta(h)\theta(1 - h)$ for the random magnetic fields. This choice for the random distributions implies, by duality arguments [72], that the critical point separating the large-Γ quantum paramagnetic from the low-Γ ferromagnetic phase is known to be located at $\Gamma_c = 1$.

4.2.1 Fermion representation and Bogoliubov-de Gennes equations

The model in Eq. (4.2.1) is integrable and can be exactly solved in terms of free fermionic quasiparticles [95]. The first step is mapping the spins into hard-core bosons $(a_j^\dagger, a_j)$:

$$\begin{cases} \sigma_j^x = & a_j^\dagger + a_j \\ \sigma_j^z = & 2a_j^\dagger a_j - 1 \end{cases} \tag{4.2.4}$$

which commute on different sites and satisfy the hard-core constraint $(a_i^\dagger)^2 = 0$. Then one applies the Jordan-Wigner transformation of the hard-core bosons into fermions $(c_j^\dagger, c_j)$:

$$a_j \equiv e^{i\pi \sum_{l<j} n_l} c_j = \left[\prod_{l=1}^{j-1}(1 - 2n_l)\right] c_j, \tag{4.2.5}$$

where $n_j = c_j^\dagger c_j$ is the fermionic number operator. With this transformation, Hamiltonian (4.2.1) with open boundary conditions is mapped into a quadratic form:

$$\mathcal{H} = -\sum_{i=1}^{L-1} J_i \left(c_i^\dagger c_i^\dagger + c_i^\dagger c_{i+1} + \text{h.c.}\right) - 2\Gamma \sum_{i=1}^{L} h_i c_i^\dagger c_i\,. \tag{4.2.6}$$

The system is then diagonalized by means of a Bogoliubov rotation [95, 112, 153], introducing the new fermionic operators $(\gamma_\mu^\dagger, \gamma_\mu)$:

$$\gamma_\mu = \sum_{j=1}^{L} (u_{j\mu}^* c_j + v_{j\mu}^* c_j^\dagger) \,; \tag{4.2.7}$$

[conversely one has $c_i = \sum_{\mu=1}^{L} (u_{i\mu}\gamma_\mu + v_{i\mu}^* \gamma_\mu^\dagger)$]. The L-dimensional vectors $\mathbf{u}_\mu^T = (u_{1\mu}, u_{2\mu}, \ldots, u_{L\mu})$ and $\mathbf{v}_\mu^T = (v_{1\mu}, v_{2\mu}, \ldots, v_{L\mu})$, for $\mu = 1, \ldots, L$, satisfy the Bogoliubov-de Gennes coupled equations:

$$\tilde{H} \begin{pmatrix} \mathbf{u}_\mu \\ \mathbf{v}_\mu \end{pmatrix} = \epsilon_\mu \begin{pmatrix} \mathbf{u}_\mu \\ \mathbf{v}_\mu \end{pmatrix} , \tag{4.2.8}$$

where $\tilde{H}$ is a $2L \times 2L$ real symmetric matrix of the form

$$\tilde{H} = \begin{pmatrix} A & B \\ -B & -A \end{pmatrix} \tag{4.2.9}$$

and A, B are $L \times L$ real matrices whose nonzero elements are given by $A_{i,i} = -\Gamma h_i$, $A_{i,i+1} = A_{i+1,i} = -J_i/2$, $B_{i,i+1} = -B_{i+1,i} = -J_i/2$. In the general disordered case it is necessary to diagonalize this $2L \times 2L$ eigenvalue problem numerically; the vectors $\mathbf{u}_\mu$ and $\mathbf{v}_\mu$ can be always chosen to be real. The spectrum of Eqs. (4.2.8) is given by $\pm\epsilon_\mu$, with $\epsilon_\mu \geq 0$ and, in terms of the new fermion operators $(\gamma_\mu^\dagger, \gamma_\mu)$, $\mathcal{H}$ becomes diagonal:

$$\mathcal{H} = \sum_{\mu=1}^{L} 2\epsilon_\mu \left(\gamma_\mu^\dagger \gamma_\mu - \frac{1}{2} \right) . \tag{4.2.10}$$

The ground state of $\mathcal{H}$ is the Bogoliubov vacuum state $|\psi_0\rangle$ annihilated by all the γ_μ's: $\gamma_\mu |\psi_0\rangle = 0$, with an energy $E_0 = -\sum_{\mu=1}^{L} \epsilon_\mu$.

4.2.2 Dynamics at $T = 0$: Heisenberg equations

The dynamics of model (4.2.1) can be suitably described within the Heisenberg formalism. Due to the particularly simple quadratic form of Eq. (4.2.6) in terms of the c-fermions, the Heisenberg equations of motion for the c operators are linear and are given by:

$$i\frac{d}{dt} c_{i,H}(t) = 2 \sum_{i=1}^{L} [A_{i,j}(t) c_{j,H}(t) + B_{i,j}(t) c_{j,H}^\dagger(t)] \tag{4.2.11}$$

(the subscript $_H$ stands for Heisenberg representation). These can be solved with a time-dependent Bogoliubov theory, obtained as follows. If we denote

with $\gamma_{\mu,0}$ the Bogoliubov operators that diagonalize $\mathcal{H}(t=0)$ at the initial time, and $\mathbf{u}^0_\mu, \mathbf{v}^0_\mu$ the corresponding initial eigenvectors, it is simple to verify that the Ansatz:

$$c_{i,H}(t) = \sum_{\mu=1}^{L} (u_{i\mu}(t)\gamma_{\mu,0} + v^*_{i\mu}(t)\gamma^\dagger_{\mu,0}) \tag{4.2.12}$$

does indeed solve the Eqs. (4.2.11), provided the time-dependent coefficients $u_{i,\mu}$ and $v_{i,\mu}$ satisfy the following system of first order differential equations:

$$i\frac{d}{dt}\begin{pmatrix} \mathbf{u}_\mu \\ \mathbf{v}_\mu \end{pmatrix} = 2\tilde{H}(t)\begin{pmatrix} \mathbf{u}_\mu \\ \mathbf{v}_\mu \end{pmatrix}. \tag{4.2.13}$$

Equations (4.2.13) can be easily solved in our specific case, where the time dependence of the model is given by Eq. 4.2.2. Indeed the evolution at $t \geq 0$ can be thought of as the time-independent evolution of $\tilde{H}(\Gamma)$ but with non trivial initial conditions. More precisely one can define U^Γ as the matrix of the eigenvectors of $\tilde{H}(\Gamma)$:

$$U^\Gamma = \begin{pmatrix} \mathbf{u}^\Gamma_1 & \cdots & \mathbf{u}^\Gamma_L & (\mathbf{v}^\Gamma_1)^* & \cdots & (\mathbf{v}^\Gamma_L)^* \\ \mathbf{v}^\Gamma_1 & \cdots & \mathbf{v}^\Gamma_L & (\mathbf{u}^\Gamma_1)^* & \cdots & (\mathbf{u}^\Gamma_L)^* \end{pmatrix} \tag{4.2.14}$$

and U^{Γ_0} as the matrix of the eigenvectors of $\tilde{H}_0$:

$$U^{\Gamma_0} = \begin{pmatrix} \mathbf{u}^{\Gamma_0}_1 & \cdots & \mathbf{u}^{\Gamma_0}_L & (\mathbf{v}^{\Gamma_0}_1)^* & \cdots & (\mathbf{v}^{\Gamma_0}_L)^* \\ \mathbf{v}^{\Gamma_0}_1 & \cdots & \mathbf{v}^{\Gamma_0}_L & (\mathbf{u}^{\Gamma_0}_1)^* & \cdots & (\mathbf{u}^{\Gamma_0}_L)^* \end{pmatrix} \tag{4.2.15}$$

Since both U^Γ and U^{Γ_0} are unitary real matrices, one has the simple relation:

$$U^\Gamma (U^\Gamma)^T = U^{\Gamma_0}(U^{\Gamma_0})^T \tag{4.2.16}$$

where T stands for transpose matrix. By defining[1] $M \equiv (U^{\Gamma_0})^T U^\Gamma$ the relation at time $t=0$ between U^Γ and U^{Γ_0} is simply $U^{\Gamma_0} = U^\Gamma M^T$. So the solution of the Heisenberg equations of motion is given by:

$$U^{\Gamma_0}_{jl}(t) = \sum_{m=1}^{2L} U^\Gamma_{jm} M_{lm} e^{-2i\epsilon_m t}, \tag{4.2.17}$$

which can be easily evaluated numerically. Notice that solving the system's dynamics in this way has a computational cost which increases only linearly with the size L, thus sensibly reducing the a-priori exponential complexity of a generic many-body quantum system; this makes it feasible to study quite large Ising chains.

[1] This is the definition we implement numerically

4.3 Autocorrelation function of the order parameter

The order parameter of the transverse field Ising model is given by σ^x. In what follows we are interested in the autocorrelation function of the order parameter in real time, i.e. the expectation value of $\sigma^x_{L/2}(t)\sigma^x_{L/2}(0)$ on the central site of the chain. We will now show the detailed evaluation in three cases:

1. evolution starting from the ground state $|\psi_0\rangle$ of a given $\mathcal{H}(\Gamma_0)$ at $T = 0$,

2. equilibrium, in the canonical ensemble,

3. equilibrium, in the generalized Gibbs ensemble (GGE).

for which we have implemented the numerical computation.

4.3.1 Evolution starting from the ground state

Let us consider the case in which at time $t = 0$ the system is initialized in the ground state $|\psi_0\rangle$ of an initial Hamiltonian $\mathcal{H}(\Gamma_0)$ and evolves at $t > 0$ according to a constant Hamiltonian $\mathcal{H}(\Gamma)$. The autocorrelation function of the order parameter on site j given by:

$$\begin{aligned} \rho^{xx}_j(t) &\equiv \langle\psi_0|\sigma^x_{j,H}(t)\sigma^x_{j,H}(0)|\psi_0\rangle \\ &= \langle\psi_0|e^{i\mathcal{H}(\Gamma)t}\sigma^x_j e^{-i\mathcal{H}(\Gamma)t}\sigma^x_j|\psi_0\rangle \end{aligned} \tag{4.3.1}$$

In particular we study the average value $[\rho^{xx}]_{\rm av}$ over many disorder realizations of the Hamiltonian in Eq. 4.2.1. Since the quantity in Eq. 4.3.1 is in general a complex number, we separately perform the average of its real and imaginary part:

$$[\rho^{xx}_j(t)]_{\rm av} \equiv [\Re(\rho^{xx}_j(t))]_{\rm av} + i\,[\Im(\rho^{xx}_j(t))]_{\rm av}\,. \tag{4.3.2}$$

The correlation function in Eq. (4.3.1) on a generic site j can be computed taking advantage of the analytical solution of the random Ising model described above. The first step is to write the time dependent x-spin operator on site j, $\sigma^x_j(t)$, in terms of Jordan-Wigner c-fermions, according to Eqs. (4.2.4)-(4.2.5) (hereafter time dependent operators are always meant

to be in Heisenberg representation), so that

$$\rho_j^{xx}(t) = \langle\psi_0| \prod_{l=1}^{j-1} \Big[1 - 2n_l(t)\Big] (c_j^\dagger(t) + c_j(t)) \prod_{l=1}^{j-1} \Big[1 - 2n_l(0)\Big] (c_j^\dagger(0) + c_j(0))|\psi_0\rangle \tag{4.3.3}$$

By introducing the operators $A_j = c_j^\dagger + c_j$ and $B_j = c_j^\dagger - c_j$, and using the identity $A_j B_j = e^{-i\pi c_j^\dagger c_j}$, we can rewrite the autocorrelation function as:

$$\rho_j^{xx}(t) = \langle\psi_0| \prod_{l=1}^{j-1} \Big[A_l(t)B_l(t)\Big] A_j(t) \prod_{l=1}^{j-1} \Big[A_l(0)B_l(0)\Big] A_j(0)|\psi_0\rangle\,. \tag{4.3.4}$$

Wick's theorem allows to evaluate the above expression. If $\Gamma_0 = \Gamma$ it is trivial. When $\Gamma_0 \neq \Gamma$ at $t = 0$ the Hamiltonian $\mathcal{H}(\Gamma_0)$ is diagonalized in terms of some $\gamma_\mu^{\Gamma_0}$ and $\gamma_\mu^{\dagger\Gamma_0}$, $|\psi_0\rangle$ being the vacuum state of such operators. At $t > 0$ the evolution is simply given in terms of the eigenvectors of $\mathcal{H}(\Gamma)$, but the state $|\psi_0\rangle$, constant in the Heisenberg picture, is *not* the instantaneous vacuum state of the operators γ_μ^Γ and $\gamma_\mu^{\dagger\Gamma}$ which diagonalize $\mathcal{H}(\Gamma)$. So, in order to apply Wick's theorem, one must rewrite the operators $A(t)$ and $B(t)$ in Eq. 4.3.4 in terms of the operators $\gamma_\mu^{\Gamma_0}$ and $\gamma_\mu^{\dagger\Gamma_0}$ and their evolution. Wick's theorem for fermions requires the sum over all possible products of pair averages, with a sign 1 or -1 depending on whether an even or odd permutation of the operators is necessary to get the operators in the product back to the original order. This is called a Pfaffian, see i.e. the book [98]. If the number of operators $2n$ is too large (here $n = 2j - 1$), evaluation of the Pfaffian is intractable because the number of terms $(2n-1)!!$ grows too fast. However, the Pfaffian is also the square root of the determinant of an antisymmetric matrix (of order $2n$) formed by pair averages. If $A, B, \ldots, Z$ are Fermi operators one has:

$$\langle ABC\ldots Z\rangle = \begin{vmatrix} 0 & \langle AB\rangle & \langle AC\rangle & \cdots & \langle AZ\rangle \\ -\langle AB\rangle & 0 & \langle BC\rangle & \cdots & \langle BZ\rangle \\ -\langle AC\rangle & -\langle BC\rangle & 0 & \cdots & \langle CZ\rangle \\ \vdots & \vdots & \vdots & \ddots & \vdots \\ -\langle AZ\rangle & -\langle BZ\rangle & -\langle CZ\rangle & \cdots & 0 \end{vmatrix}^{1/2} \tag{4.3.5}$$

Let us write explicitly the determinant for a chain of $L = 3$ sites and $j = 2$. For lightening the notation we use the notation $\langle\ldots\rangle \equiv \langle\psi_0|\ldots|\psi_0\rangle$. The autocorrelation function is given by:

$$\rho_2^{xx}(t) = \langle A_1(t)B_1(t)A_2(t)A_1(0)B_1(0)A_2(0)\rangle \tag{4.3.6}$$

which as a determinant looks like:

$$\rho_2^{xx}(t) = \begin{vmatrix} 0 & \langle A_1(t)B_1(t)\rangle & \langle A_1(t)A_2(t)\rangle & \langle A_1(t)A_1(0)\rangle & \langle A_1(t)B_1(0)\rangle & \langle A_1(t)A_2(0)\rangle \\ -\langle A_1(t)B_1(t)\rangle & 0 & \langle B_1(t)A_2(t)\rangle & \langle B_1(t)A_1(0)\rangle & \langle B_1(t)B_1(0)\rangle & \langle B_1(t)A_2(0)\rangle \\ -\langle A_1(t)A_2(t)\rangle & -\langle B_1(t)A_2(t)\rangle & 0 & \langle A_2(t)A_1(0)\rangle & \langle A_2(t)B_1(0)\rangle & \langle A_2(t)A_2(0)\rangle \\ \vdots & \vdots & \vdots & \vdots & \ddots & \vdots \\ -\langle A_1(t)A_2(0)\rangle & -\langle B_1(t)A_2(0)\rangle & -\langle A_2(t)A_2(0)\rangle & -\langle A_1(0)A_2(0)\rangle & -\langle B_1(0)A_2(0)\rangle & 0 \end{vmatrix}^{1/2} \tag{4.3.7}$$

Let us compute explicilty one of matrix elements in Eq. 4.3.7, for example $\langle B_j(t)A_l(0)\rangle$.

$$\langle B_j(t)A_l(0)\rangle = \langle c_j^\dagger(t)c_l^\dagger(0)\rangle + \langle c_j^\dagger(t)c_l(0)\rangle - \langle c_j(t)c_l^\dagger(0)\rangle - \langle c_j(t)c_l(0)\rangle. \tag{4.3.8}$$

It is now necessary to write the c_i operators in terms of the $\gamma_\mu^{\Gamma_0}$:

$$\begin{aligned} c_i(t) = & \sum_{\mu=1}^{L}\left(u_{i\mu}^{\Gamma_0}(t)\gamma_\mu^{\Gamma_0} + v_{i\mu}^{*\Gamma_0}(t)\gamma_\mu^{\dagger\Gamma_0}\right) \\ = & \sum_{\mu=1}^{L}\left(\left[\sum_{\nu=1}^{2L} U_{i\nu}^{\Gamma} M_{\mu\nu} e^{-2i\epsilon_\nu t}\right]\gamma_\mu^{\Gamma_0} + \left[\sum_{\nu=1}^{2L} U_{i\nu}^{\Gamma} M_{\mu+L,\nu} e^{2i\epsilon_\nu t}\right]\gamma_\mu^{\dagger\Gamma_0}\right) \end{aligned} \tag{4.3.9}$$

where we used Eq. 4.2.17. An equation analogous to Eq. 4.3.9 can be written for $c_i^\dagger(t)$. It is worth noting that the above equation is valid generically for $|\psi_0\rangle$ ground state $\mathcal{H}(\Gamma_0)$ with an arbitrary Γ_0. The situation $\Gamma_0 = \Gamma$ is a trivial particular case, M being the identity matrix. With these expressions we can evaluate for example the last term in the sum taking into account that only terms of the form $\langle\gamma_\mu\gamma_\mu^\dagger\rangle$ are nonzero:

$$\langle\psi_0|c_j(t)c_l(0)|\psi_0\rangle = \sum_\mu u_{j\mu}^{\Gamma_0}(t)v_{l\mu}^{*\Gamma_0}(0) \tag{4.3.10}$$

and putting all the terms together one finds:

$$\begin{aligned} \langle\psi_0|B_j(t)A_l(0)|\psi_0\rangle = & \sum_{\mu=1}^{L}\Big(u_{l\mu}^{*\Gamma_0}(t)v_{j\mu}^{\Gamma_0}(0) + v_{l\mu}^{*\Gamma_0}(t)v_{j\mu}^{\Gamma_0}(0) \\ & - u_{j\mu}^{\Gamma_0}(t)u_{l\mu}^{*\Gamma_0}(0) - u_{j\mu}^{\Gamma_0}(t)v_{l\mu}^{*\Gamma_0}(0)\Big) \end{aligned} \tag{4.3.11}$$

In a similar fashion one can build up the whole matrix of Eq. 4.3.7. It is composed of four blocks:

$$\begin{pmatrix} B^{t,t} & B^{t,0} \\ B^{0,t} & B^{0,0} \end{pmatrix} \tag{4.3.12}$$

where B^{t_1,t_2} is a square matrix composed of correlators of the kind $\langle A_k(t_1)B_l(t_2)\rangle$, $\langle A_k(t_1)A_l(t_2)\rangle$, $\langle B_k(t_1)B_l(t_2)\rangle$. The off-diagonal blocks $B^{t,0}$ and $B^{0,t}$ are not antisymmetrical individually.

4.3.2 Autocorrelation function in the canonical ensemble

In Refs. [129, 130] for the ordered Ising model, the evolution of ρ_{Q}^{xx} after a quantum quench from Γ_0 to Γ is compared to the canonical expectation value $\rho_{T_{\mathrm{eff}}}^{xx} = \langle \sigma_{L/2}^x(t)\sigma_{L/2}^x(0)\rangle_{T_{\mathrm{eff}}}$, where T_{eff} is the effective temperature. It is obtained from the equation:

$$\langle \mathcal{H}(\Gamma)\rangle_{T_{\mathrm{eff}}} = E_0\,, \tag{4.3.13}$$

where $E_0 = \langle\psi_0|\mathcal{H}(\Gamma)|\psi_0\rangle$ is the initial energy of the system given a quench. We perform the same calculation in the presence of disorder. So given a temperature T, the system is described by a density matrix $Z^{-1}e^{-\mathcal{H}/T}$ constant in time, $Z = \mathrm{Tr}(e^{-\mathcal{H}(\Gamma)/T})$ being the partition function. The canonical expectation value of the autocorrelation function is defined by:

$$\langle \rho_j^{xx}(t)\rangle_T \equiv Z^{-1}\,\mathrm{Tr}\left(e^{-\mathcal{H}(\Gamma)/T}\rho_j^{xx}(t)\right)\,. \tag{4.3.14}$$

Using the same expressions as in the $T = 0$ case we can write:

$$\langle \rho_j^{xx}(t)\rangle_T = \frac{\mathrm{Tr}\left(e^{-\mathcal{H}(\Gamma)/T}\prod_{l=1}^{j-1}\Big[A_l(t)B_l(t)\Big]A_j(t)\prod_{l=1}^{j-1}\Big[A_l(0)B_l(0)\Big]A_j(0)\right)}{\mathrm{Tr}(e^{-\mathcal{H}(\Gamma)/T})} \tag{4.3.15}$$

The quantity in Eq. 4.3.15 can be evaluated by means of the Wick's theorem generalized to the canonical ensemble [69]. The basic contraction $\gamma_\mu^{\cdot}\gamma_\nu^{\dagger\cdot}$ is not unity but instead related to the Fermi function n_μ:

$$\gamma_\mu^{\cdot}\gamma_\nu^{\dagger\cdot} \equiv \langle\gamma_\mu\gamma_\nu^\dagger\rangle_T = \delta_{\mu\nu}(1-n_\mu)\,, \qquad n_\mu = \frac{1}{1+\exp(2\epsilon_\mu/T)} \tag{4.3.16}$$

After applying the Wick's theorem, we obtain the same matrix as in the case $T = 0$, but with the contractions defined as above. So the same arguments bring us to write the determinant in Eq. 4.3.5. Let us write explicitly one matrix element, for example $\langle B_j(t)A_l(0)\rangle_T$:

$$\langle B_j(t)A_l(0)\rangle_T = \langle c_j^\dagger(t)c_l^\dagger(0)\rangle_T + \langle c_j^\dagger(t)c_l(0)\rangle_T - \langle c_j(t)c_l^\dagger(0)\rangle_T - \langle c_j(t)c_l(0)\rangle_T. \tag{4.3.17}$$

Since the Hamiltonian is constant each instantaneous eigenvector of the Hamiltonian is constant up to a trivial phase and thus we have a simple expression for the time evolution of c_i and $c_i^\dagger$:

$$\begin{aligned} c_i(t) &= \sum_{\mu=1}^{L}\left(u_{i\mu}^\Gamma(t)\gamma_\mu^\Gamma + v_{i\mu}^{*\Gamma}(t)\gamma_\mu^{\dagger\Gamma}\right) \\ &= \sum_{\mu=1}^{L}\left(u_{i\mu}^\Gamma e^{-2i\epsilon_\mu t}\gamma_\mu^\Gamma + v_{i\mu}^{*\Gamma}e^{2i\epsilon_\mu t}\gamma_\mu^{\dagger\Gamma}\right) \end{aligned} \tag{4.3.18}$$

So we can evaluate all the terms:

$$\begin{aligned}
\langle c_j^\dagger(t)c_k^\dagger(0)\rangle_T &= \textstyle\sum_\mu \left(v_{j\mu}(t)u_{k\mu}^*(0)(1-n_\mu) + u_{j\mu}^*(t)v_{k\mu}(0)n_\mu\right)\\
\langle c_j^\dagger(t)c_k(0)\rangle_T &= \textstyle\sum_\mu \left(v_{j\mu}(t)v_{k\mu}^*(0)(1-n_\mu) + u_{j\mu}^*(t)u_{k\mu}(0)n_\mu\right)\\
\langle c_j(t)c_k^\dagger(0)\rangle_T &= \textstyle\sum_\mu \left(u_{j\mu}(t)u_{k\mu}^*(0)(1-n_\mu) + v_{j\mu}^*(t)v_{k\mu}(0)n_\mu\right)\\
\langle c_j(t)c_k(0)\rangle_T &= \textstyle\sum_\mu \left(u_{j\mu}(t)v_{k\mu}^*(0)(1-n_\mu) + v_{j\mu}^*(t)u_{k\mu}(0)n_\mu\right)
\end{aligned} \tag{4.3.19}$$

and, for example, we find:

$$\begin{aligned}
\langle B_j(t)A_l(0)\rangle_T = \;& \textstyle\sum_\mu \Big(\Big[v_{j\mu}(t)u_{l\mu}^*(0) + v_{j\mu}(t)v_{l\mu}^*(0)\\
- \;& u_{j\mu}(t)u_{l\mu}^*(0) - u_{j\mu}(t)v_{l\mu}^*(0)\Big](1-n_\mu)\\
+ \;& \Big[u_{j\mu}^*(t)v_{l\mu}(0) + u_{j\mu}^*(t)u_{l\mu}(0)\\
- \;& v_{j\mu}^*(t)v_{l\mu}(0) - v_{j\mu}^*(t)u_{l\mu}(0)\Big]n_\mu\Big)
\end{aligned} \tag{4.3.20}$$

4.3.3 Autocorrelation function in the GGE

As we discussed in Chapter 1, the asymptotic state of integrable systems after a quantum quench may often be described by means of the generalized Gibbs ensemble. For the model considered here the conserved quantities are the populations of quasi-particles, i.e. the number of excitations in each mode:

$$p_\mu \equiv \langle\psi_0|\gamma_\mu^{\dagger\Gamma}\gamma_\mu^\Gamma|\psi_0\rangle\,, \quad \text{for} \quad \mu = 1, L\,. \tag{4.3.21}$$

The density matrix of the generalized ensemble is:

$$\rho_{\rm G} \equiv \frac{\exp\left(-\sum_\mu \beta_\mu \gamma_\mu^{\dagger\Gamma}\gamma_\mu^\Gamma\right)}{\mathrm{Tr}\,\exp\left(-\sum_\mu \beta_\mu \gamma_\mu^{\dagger\Gamma}\gamma_\mu^\Gamma\right)} \tag{4.3.22}$$

where β_μ is a Lagrangian multiplier. The ensemble average is taken analogously to the more familiar the canonical ensemble, tracing over $\rho_{\rm G}$. Fixing the number of excitations for each μ at a given value p_μ amounts to fixing a set of *effective* $\beta_{\mu,\rm eff}$ according to:

$$\langle\gamma_\mu^{\dagger\Gamma}\gamma_\mu^\Gamma\rangle_{\rm G} \equiv \mathrm{Tr}\left(\rho_{\rm G}\gamma_\mu^{\dagger\Gamma}\gamma_\mu^\Gamma\right) = \frac{1}{(e^{\beta_{\mu,\rm eff}}+1)} = p_\mu \tag{4.3.23}$$

which must be solved to extract the $\{\beta_{\mu,\rm eff}\}$. The population p_μ is simply computed expressing the operators γ_μ^Γ and $\gamma_\mu^{\dagger\Gamma}$ in terms of the operators $\gamma_\mu^{\Gamma_0}$ and $\gamma_\mu^{\dagger\Gamma_0}$, for which $|\psi_0\rangle$ is the vacuum state. Indeed both the expressions are true:

$$\left\{\begin{array}{ll} c_i = & \sum_\mu(u_{i\mu}^\Gamma\gamma_\mu^\Gamma + v_{i\mu}^{*\Gamma}\gamma_\mu^{\dagger\Gamma})\\ c_i^\dagger = & \sum_\mu(v_{i\mu}^\Gamma\gamma_\mu^\Gamma + u_{i\mu}^{*\Gamma}\gamma_\mu^{\dagger\Gamma})\end{array}\right. \quad \left\{\begin{array}{ll} c_i = & \sum_\mu(u_{i\mu}^{\Gamma_0}\gamma_\mu^{\Gamma_0} + v_{i\mu}^{*\Gamma_0}\gamma_\mu^{\dagger\Gamma_0})\\ c_i^\dagger = & \sum_\mu(v_{i\mu}^{\Gamma_0}\gamma_\mu^{\Gamma_0} + u_{i\mu}^{*\Gamma_0}\gamma_\mu^{\dagger\Gamma_0})\end{array}\right. \tag{4.3.24}$$

Inverting the first pair of equations, see Eq. 4.2.7, and inserting the second pair we find:

$$\begin{aligned} p_\mu = & \langle\psi_0|\gamma_\mu^{\dagger\Gamma}\gamma_\mu^{\Gamma}|\psi_0\rangle \\ = & \sum_{jl\nu}\Big(v_{j\mu}^{\Gamma}u_{l\mu}^{*\Gamma}u_{j\nu}^{\Gamma_0}v_{l\nu}^{*\Gamma_0}+v_{j\mu}^{\Gamma}v_{l\mu}^{*\Gamma}u_{j\nu}^{\Gamma_0}u_{l\nu}^{*\Gamma_0} \\ & +u_{j\mu}^{\Gamma}u_{l\mu}^{*\Gamma}v_{j\nu}^{\Gamma_0}v_{l\nu}^{*\Gamma_0}+u_{j\mu}^{\Gamma}v_{l\mu}^{*\Gamma}v_{j\nu}^{\Gamma_0}u_{l\nu}^{*\Gamma_0}\Big) \end{aligned} \tag{4.3.25}$$

Let us now consider the ensemble average of the autocorrelation function (in order to avoid confusion with the density matrix ρ_{G} we write $\rho^{xx}(t)$ in terms of the Pauli matrices):

$$\begin{aligned} \langle\sigma_{L/2}^x(t)\sigma_{L/2}^x(0)\rangle_{\mathrm{G}} \equiv & \ \mathrm{Tr}\left(\rho_{\mathrm{G}}\sigma_{L/2}^x(t)\sigma_{L/2}^x(0)\right) \\ = & \ \mathrm{Tr}\left(\rho_{\mathrm{G}}\prod_{l=1}^{j-1}\Big[A_l(t)B_l(t)\Big]A_j(t)\prod_{l=1}^{j-1}\Big[A_l(0)B_l(0)\Big]A_j(0)\right) \end{aligned} \tag{4.3.26}$$

In order to evaluate this product we can still use a generalization of the Wick's theorem, which can be proven following exactly the same steps leading to the generalization to the canonical ensemble[69] defining the contraction as:

$$\hat{\mathcal{A}}^{\cdot}\hat{\mathcal{B}}^{\cdot} \equiv \langle\mathcal{A}\mathcal{B}\rangle_{\mathrm{G}} = \mathrm{Tr}\left(\rho_{\mathrm{G}}\mathcal{A}\mathcal{B}\right) \tag{4.3.27}$$

for two fermionic operators $\mathcal{A}$ and $\mathcal{B}$. The basic contractions in order to prove Wick's theorem are:

$$\gamma_\mu^{\dagger\Gamma\cdot}\gamma_\mu^{\Gamma\cdot} = \langle\gamma_\mu^{\dagger\Gamma}\gamma_\mu^{\Gamma}\rangle_{\mathrm{G}} = \frac{1}{1+e^{\beta_\mu}} \qquad \gamma_\mu^{\Gamma\cdot}\gamma_\mu^{\Gamma\dagger\cdot} = \langle\gamma_\mu^{\Gamma}\gamma_\mu^{\Gamma\dagger}\rangle_{\mathrm{G}} = \frac{1}{1+e^{-\beta_\mu}}\,. \tag{4.3.28}$$

Once we have the Wick's theorem properly generalized, as in the previous cases we can build up the block matrix whose determinant is the square of $\langle\sigma_{L/2}^x(t)\sigma_{L/2}^x(0)\rangle_{\mathrm{G}}$. Proceeding in a similar fashion as for $T>0$ we have:

$$\langle B_j(t)A_l(0)\rangle_{\mathrm{G}} = \langle c_j^\dagger(t)c_l^\dagger(0)\rangle_{\mathrm{G}} + \langle c_j^\dagger(t)c_l(0)\rangle_{\mathrm{G}} - \langle c_j(t)c_l^\dagger(0)\rangle_{\mathrm{G}} - \langle c_j(t)c_l(0)\rangle_{\mathrm{G}}. \tag{4.3.29}$$

Again the time evolution of the $c_i(t)$ and $c_i^\dagger(t)$ is trivial because, being the Hamiltonian constant, the eigenvectors evolve only with a phase according to:

$$u_{i\mu}^{\Gamma}(t) = u_{i\mu}^{\Gamma}e^{-2i\epsilon_\mu t} \qquad v_{i\mu}^{*\Gamma}(t) = v_{i\mu}^{*\Gamma}e^{2i\epsilon_\mu t}\,. \tag{4.3.30}$$

The only difference with the finite temperature case is that the ensemble averages are taken over ρ_{G}, so we find:

$$\begin{aligned}
\langle c_j^\dagger(t)c_k^\dagger(0)\rangle_{\mathrm{G}} &= \sum_\mu \Big(v_{j\mu}(t)u_{k\mu}^*(0)(1-p_\mu) + u_{j\mu}^*(t)v_{k\mu}(0)p_\mu \Big) \\
\langle c_j^\dagger(t)c_k(0)\rangle_{\mathrm{G}} &= \sum_\mu \Big(v_{j\mu}(t)v_{k\mu}^*(0)(1-p_\mu) + u_{j\mu}^*(t)u_{k\mu}(0)p_\mu \Big) \\
\langle c_j(t)c_k^\dagger(0)\rangle_{\mathrm{G}} &= \sum_\mu \Big(u_{j\mu}(t)u_{k\mu}^*(0)(1-p_\mu) + v_{j\mu}^*(t)v_{k\mu}(0)p_\mu \Big) \\
\langle c_j(t)c_k(0)\rangle_{\mathrm{G}} &= \sum_\mu \Big(u_{j\mu}(t)v_{k\mu}^*(0)(1-p_\mu) + v_{j\mu}^*(t)u_{k\mu}(0)p_\mu \Big)
\end{aligned} \tag{4.3.31}$$

and the effective populations associated to the quench are computed via Eq. 4.3.23.

4.4 Evolution in real time

We now concentrate on the autocorrelation function $\rho^{xx}(t)$ in the presence of disorder at $T = 0$ with a constant (i.e. without quench) Hamiltonian $\mathcal{H}(\Gamma)$, focussing on the *real* time evolution. This is different from what is found in literature [152, 85] where the *imaginary* time evolution for a constant Hamiltonian is considered. Nonetheless our choice is mandatory in order to study the non-equilibrium dynamics: a quench in imaginary time would cause the autocorrelation function to develop divergent terms, as one can see writing $\rho_Q^{xx}(\tau)$ in Lehmann representation.

Let us briefly recall the known results about the average autocorrelation function in imaginary time $[\rho_j^{xx}(\tau)]_{\mathrm{av}}$ for a constant Hamiltonian ($\Gamma = \Gamma_0$) in the off-critical case. The key advantage of computations in imaginary time is a smoother behavior of observables, where oscillating terms raising from imaginary phases are suppressed. A first observation is that $[\rho_j^{xx}(\tau)]_{\mathrm{av}}$ is always real. By scaling arguments [85] one can show that it behaves like:

$$[\rho_j^{xx}(\tau)]_{\mathrm{av}} \sim \tau^{-1/z(\delta)}, \tag{4.4.1}$$

where $\delta = |\ln\Gamma|/2$ (with the distributions $\pi[J]$ and $\pi[h]$ above) measures the distance from the critical point and $z(\delta)$ is the dynamical exponent [71, 72, 153]:

$$z(\delta) = \begin{cases} \frac{1}{2\delta} + \text{const.} & \text{for} \quad |\delta| \ll 1 \\ \to \infty & \text{for} \quad |\delta| \to 0 \end{cases} \tag{4.4.2}$$

The autocorrelation function at the critical point depends on the logarithm of the imaginary time [122].

Rigorously speaking, one should always consider the connected part of the autocorrelation function:

$$\rho_j^{xx}(\tau)_{\mathrm{conn}} = \rho_j^{xx}(\tau) - \langle\sigma_j^x\rangle^2, \tag{4.4.3}$$

that is the difference between the autocorrelation function and the square of the residual magnetization at the thermodynamic limit. Indeed in the ferromagnetic phase ($\Gamma < 1$) the longitudinal field magnetization $\langle \sigma^x \rangle$ is non-zero, while it vanishes in the paramagnetic phase ($\Gamma > 1$), so in the latter case $\rho_j^{xx}(\tau)_{\rm conn} = \rho_j^{xx}(\tau)$.

For a constant Hamiltonian, the behavior of the order-parameter autocorrelator in imaginary time can be of interest also for our purposes, since, in principle, one can switch to real time through an analytic continuation. Unfortunately this is not in general a trivial operation. In fact, defining the spectral function as:

$$A(\omega) = \sum_n \delta(\omega - (E_n - E_0)) |\langle \phi_0^\Gamma | \sigma_j^x | \phi_n^\Gamma \rangle|^2. \tag{4.4.4}$$

one can show that $\rho_j^{xx}(\tau)$ is the Laplace transform of $A(\omega)$, while $\rho_j^{xx}(t)$ is its Fourier transform. So formally one could perform an inverse Laplace transform from $\rho_j^{xx}(\tau)$ to get the spectral function $A(\omega)$, and then Fourier transform the result to get the autocorrelation function in real time $\rho_j^{xx}(t)$. Unfortunately the inverse Laplace transform requires the knowledge of the correlation function in a general complex time:

$$A(\omega) = \int_{\gamma - i\infty}^{\gamma + i\infty} ds\, e^{\omega s} \rho_j^{xx}(s)\,, \tag{4.4.5}$$

γ being a real number, which is not trivial at all.

We now show our numerical results in real time. In the following we will always compute ρ_j^{xx} on the central site of the chain $j = L/2$, in order to reduce boundary effects, therefore hereafter we drop the site index subscript $L/2$. Let us first consider the paramagnetic case. In the main panel of Fig. 4.1 we show our numerical findings for the modulus of $[\rho^{xx}(t)]_{\rm av}$ for several values of $\Gamma > \Gamma_c$. After an initial transient time $t \lesssim 1$, the autocorrelation function exhibits a power-law decay $[\rho^{xx}(t)]_{\rm av} \sim t^{-\alpha}$ that is superimposed to damped oscillations. An interpolation in the power-law regions leads to exponents α which are shown in the inset of Fig. 4.1. These rates are compatible with those found by Igloi and Rieger [85] after an analogous analysis in imaginary time. In their case the autocorrelation function is always real and has a smooth behavior instead of an oscillatory one.

For $\Gamma < \Gamma_c$ the chain develops a ferromagnetic order (in the limiting $\Gamma = 0$ case all the spins are aligned with each other, either in the $+\hat{x}$ or in the $-\hat{x}$ direction). Hence the residual magnetization in the $\hat{x}$ direction on each site is finite for $t \to \infty$. Therefore in this case we compute the *connected* autocorrelation function $\rho^{xx}_{\rm conn}$ in real time, that is defined according to the

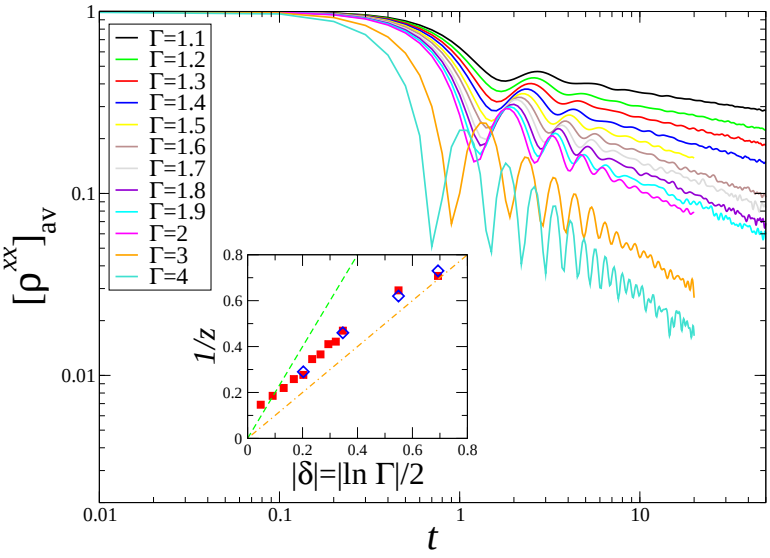

Figure 4.1: Modulus of the average autocorrelation function $[\rho^{xx}(t)]_{\rm av}$ on the central site, for different values of $\Gamma > 1$, for a chain of $L = 20$ sites. Averages are performed over 10^5 disorder realizations. In the inset red squares are the power law rates relative to the curves in the main panel, while blue diamonds are the rates extracted from the imaginary-time data, quoted from Fig.14 of Ref. [85].

formula in Eq. (4.4.3). The residual magnetization $m \equiv \langle \sigma^x \rangle$ in a chain with open boundary conditions is given by [85]:

$$m^{\rm obc} = \langle 1|\sigma^x|0\rangle\,, \tag{4.4.6}$$

where $|0\rangle$ is the ground state and $|1\rangle = \gamma_1^\dagger|0\rangle$. This quantity can be evaluated in an analogous way as $\rho^{xx}(t)$, by taking into account that the operator σ^x changes the parity of the γ_j fermion quasiparticles. In Fig. 4.2 we show the absolute value of $[\Re\,(\rho^{xx}_{\rm conn})]_{\rm av}$. Differently from the paramagnetic case, here it is much more difficult to observe a power law behavior at long times. We argue that more disorder instances are needed to get a smoother curve at $t \gtrsim 1$, since we are averaging much smaller quantities than in the paramagnetic phase. Nevertheless, with a large enough number of disorder realizations, we expect $\rho^{xx}_{\rm conn}$ to display a power law behavior at long times, in tight relation with what happens in imaginary time, superimposed to damped oscillations.

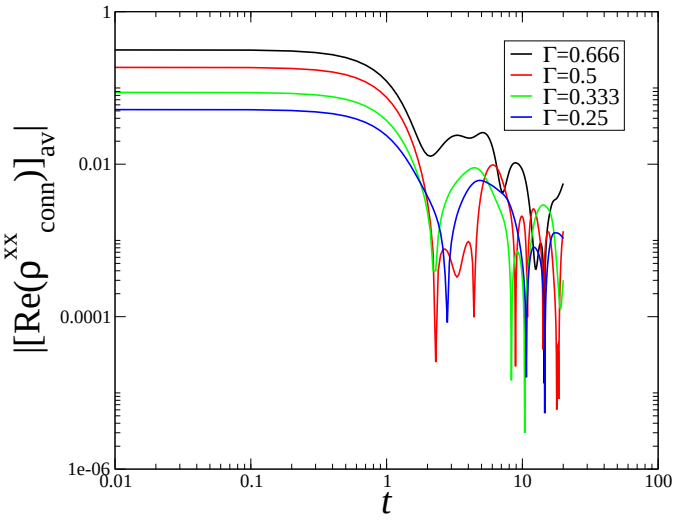

Figure 4.2: Real part of the connected part of the autocorrelation function $[\Re\rho^{xx}_{\rm conn}(t)]_{\rm av}$ for different values of $\Gamma < 1$ for a chain of $L = 20$ sites, averaged over 10^5 disorder realizations.

4.5 Quenches and thermalization

4.5.1 Numerical findings in the ordered case

As we discussed in Chapter 1 the generalized Gibbs ensemble (GGE) is expected to predict the asymptotic value of observables in several situations. An interesting question is whether the GGE gives correct predictions on the behavior of $\rho^{xx}(t)$. Some results concerning the validity of the GGE in the ordered Ising model are shown in Ref.[129, 130]. We briefly recall some results of those papers and then show our numerical findings.

In Refs. [129, 130] the autocorrelation function of the order parameter after a quench is shown to decay exponentially in time, according to $\rho^{xx}_Q(t) \sim e^{-t/\tau^\varphi_Q}$. Defining the effective temperature $T_{\rm eff}$ from Eq. 4.3.13, one can compare the behavior of ρ^{xx}_Q with that at thermal equilibrium at $T = T_{\rm eff}$, which is exponential too, with a time scale $\tau^\varphi_{T_{\rm eff}}$. Actually Rossini *et al.* do not perform the exact calculation of $\rho^{xx}_{T_{\rm eff}}$ but instead take advantage of the semiclassical analysis of Sachdev [132] , leading to $\tilde\tau^\varphi_{T_{\rm eff}}$. In particular $\tilde\tau^\varphi_T$ can be expressed as:

$$\tilde\tau^\varphi_T = \left(\int \frac{dk}{\pi} e^{-\epsilon_k/T} |v_k| \right)^{-1} \tag{4.5.1}$$

where $v_k = \partial_k \epsilon_k$ is the velocity of the thermally excited quasi-particles and $e^{-\epsilon_k/T}$ is their Boltzmann weight. In particular Eq. 4.5.1 gives $\tilde\tau^\varphi_T \approx$

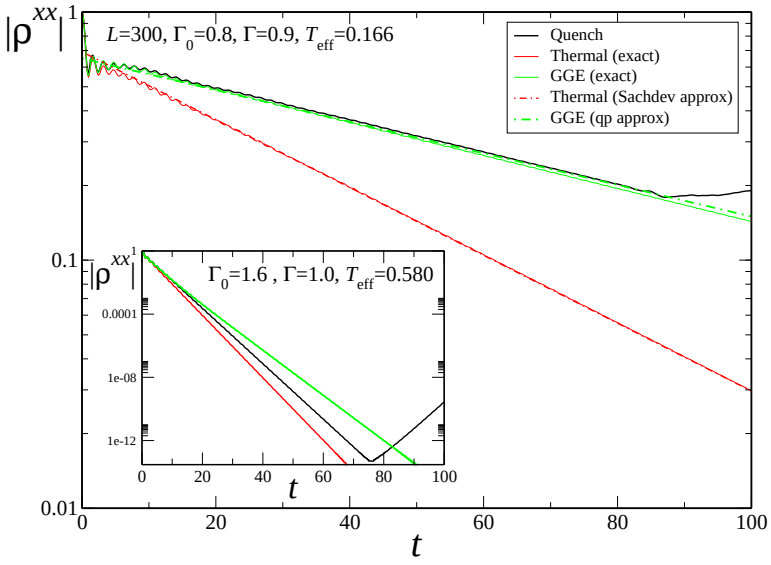

Figure 4.3: (color online). Ordered case. Comparison between ρ^{xx}_Q after the quench (black), exact thermal ρ^{xx}_T (red, continuous line), exact GGE ρ^{xx}_G (green, continuous line), Sachdev approximation $e^{-t/\tilde{\tau}^{\varphi}_T}$ (red, dash-dotted line) and $e^{-t/\tilde{\tau}^{\varphi}_{GGE}}$ (green, dashed line) expectation values. Main panel: quench from $\Gamma_0 = 0.8$ to $\Gamma = 0.9$, inset: $\Gamma_0 = 1.6$, $\Gamma = 1.0$. Data for $L = 300$.

$\frac{\pi}{2T}e^{\Delta/T}$ for $T \ll \Delta$, while at criticality $\tilde{\tau}^{\varphi}_T = \frac{8}{\pi T}$ for $T \ll J$, where J is the ordered nearest neighbor coupling in Eq. 4.2.1. The comparison of τ^{φ}_Q and $\tilde{\tau}^{\varphi}_T$ gives a satisfactory agreement. Nevertheless the decay rates τ^{φ}_Q are better reproduced modifying Equation 4.5.1 substituting the Boltzmann weight with the occupation numbers of quasi-particles f_k after the quench, namely:

$$\tilde{\tau}^{\varphi}_{GGE} = \left(\int \frac{dk}{\pi} f_k |v_k| \right)^{-1} \tag{4.5.2}$$

This is very reminescent of the GGE but we stress that it is an approximation. Here we would like to compare the approximated results coming from Eqs. 4.5.1 and 4.5.2 with the exact results of ρ^{xx}_T and $\rho^{xx}_G \sim e^{-t/\tau^{\varphi}_{GGE}}$. If we consider the main panel of Fig. 4.3 we find that the semiclassical approximations are excellent and in particular the GGE predicts correctly the decay of ρ^{xx}_Q. Nevertheless we find that for quenches ending at the critical point $\Gamma = 1$ the agreement is much worse, as shown in the inset of Fig. 4.3. Since finite-size effects are very relevant at criticality, we perform a finite-size scaling of $\tau^{\varphi}(L)$. In Fig. 4.4 we show ρ^{xx}_G in the GGE for different system sizes for a quench from $\Gamma_0 = 1.6$ to $\Gamma = 1.0$. The time scale τ^{φ}_{GGE} strongly

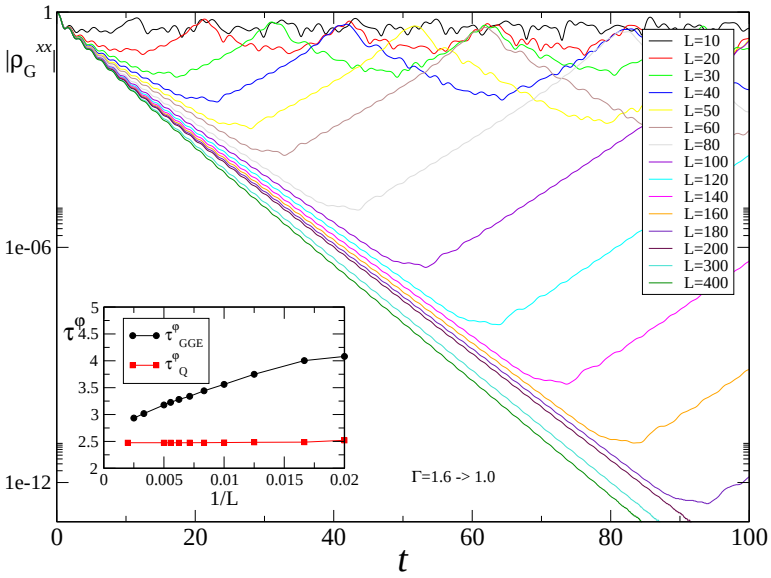

Figure 4.4: (color online). Main panel: autocorrelation function ρ_G^{xx} in the GGE for a quench from $\Gamma_0 = 1.6$ to $\Gamma = 1.0$ in the ordered case, for different system sizes. Inset: comparison between the time scales: τ^{φ}_{GGE} (black dots), found from the curves in the main panel, and τ^{φ}_{Q} (red squares), from the quench dynamics.

depends on the size of the system. This is more evident comparing the time scale τ^{φ}_{GGE} in the GGE with the one found from the quench dynamics, which is basically independent of the size. From the inset of Fig. 4.4 we are not able to draw a conclusive statement on the convergence of $\tau^{\varphi}_{GGE}(L)$ to $\tau^{\varphi}_{Q}(L)$ for $L \to \infty$. In Fig. 4.5 we try to change the initial value of Γ_0, with Γ fixed to the critical value. From the inset of Fig. 4.5 we see that the discrepancy between the decay rates found in the GGE and in the quench dynamics is significant if $\Gamma_0 > 1$.

4.5.2 Preliminary results about the disordered case

In Fig. 4.6 we show our results for the dynamics after a quench in the presence of disorder. The qualitative picture that emerges from the main panel of Fig. 4.6 is analogous to the one described in Fig. 4.1 in the time-independent case: after a short transient there is a power-law decay superimposed to oscillations. Nevertheless the power-law exponents α involved here are much smaller, as shown in the inset. We find that the algebraic decay is present for large times, independently of the width of the quench $|\Gamma - \Gamma_0|$. Due to the very large number of disorder instances on which we average ($\sim 10^5$),

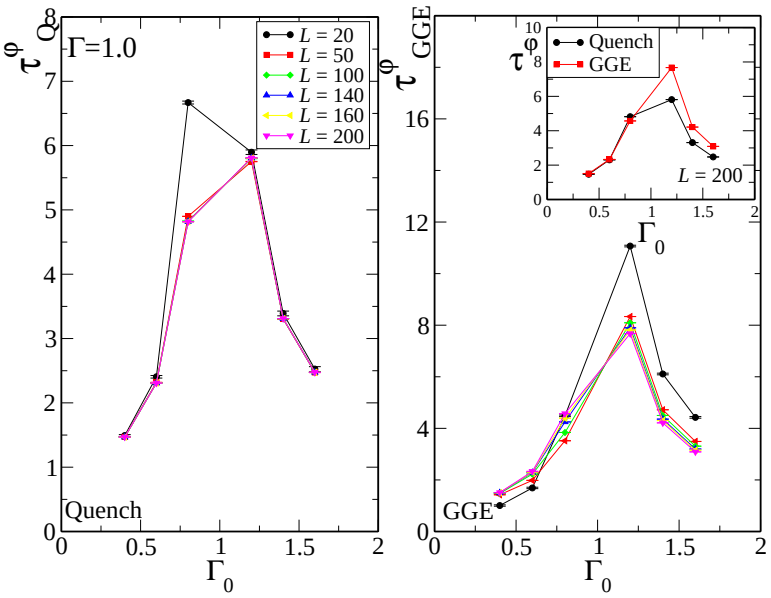

Figure 4.5: (color online) Ordered case. Time scale τ^{φ} (from the fit $\rho \sim e^{-t/\tau^{\varphi}}$) as a function of the initial value of the transverse field Γ_0 for different system sizes. Left panel: time scale $\tau^{\varphi}_{\rm Q}$ of $\rho^{xx}_{\rm Q}$ after a quench, right panel: time scale $\tau^{\varphi}_{\rm G}$ of $\rho^{xx}_{\rm G}$. Inset: comparison of $\tau^{\varphi}_{\rm Q}$ and $\tau^{\varphi}_{\rm G}$ for a system of $L = 200$.

we considered only times up to $t = 100$. Since at present we do not have analytical arguments explaining the algebraic decay, in principle we cannot rule out the possibility that a different decay establishes in the asymptotic regime. The comparison with what happens in the ordered case is very interesting, because there the decay is exponential and here the numerics suggests a power-law decay. If in the ordered case it is possible to identify a time-scale which depends on the quench, here we can only find an exponent α.

As for the ordered case, an effective temperature can be associated to each quench. In particular we compute the effective temperature from Eq. 4.3.13 for each disorder instance and then take the average. We find the curves of Fig. 4.7, which, despite the small number of disorder realizations, have a clear profile. For the random chain, the effective temperature does not seem to have a cusp for $\Gamma = \Gamma_0$, in close analogy to what happens for the critical case in the ordered chain (see for example the inset of Fig.2 in Ref. [129]).

The following step is verifying whether a finite temperature is able to destroy the power-law decay. In Fig. 4.8 we show the real part of ρ^{xx}_{T} evaluated

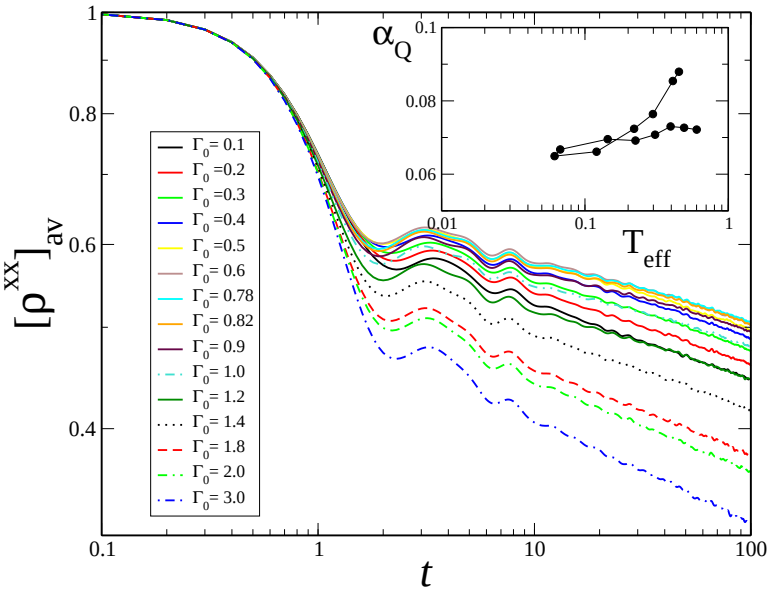

Figure 4.6: Modulus of the average autocorrelation function $|[\rho^{xx}(t)]_{\rm av}|$ for different values of Γ_0, and fixed $\Gamma = 0.8$ in the ferromagnetic phase, for a chain of $L = 20$ sites. Data are averaged over 10^5 disorder realizations. Inset, black dots: decay rates α of the real part of the curves in main panel extracted from a power law fit in the time interval $t \in [30, 100]$.

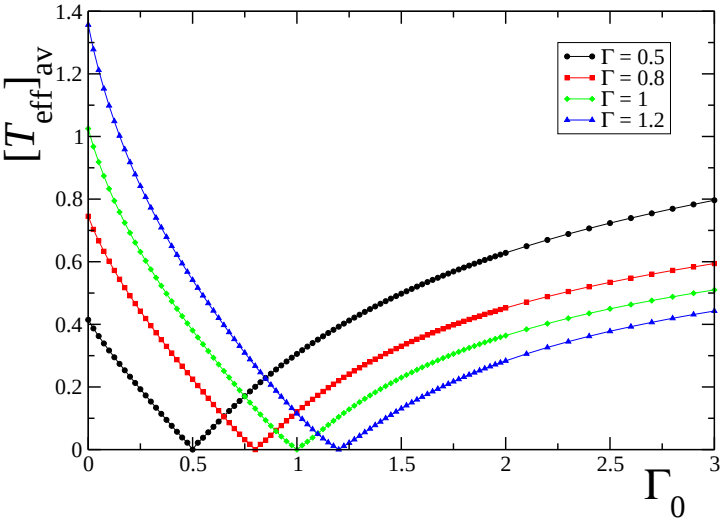

Figure 4.7: (color online). Effective temperature for quenched systems as a function of Γ_0, for different values of Γ. Data for a chain of $L = 20$ sites, averages are performed over 10^3 disorder realizations.

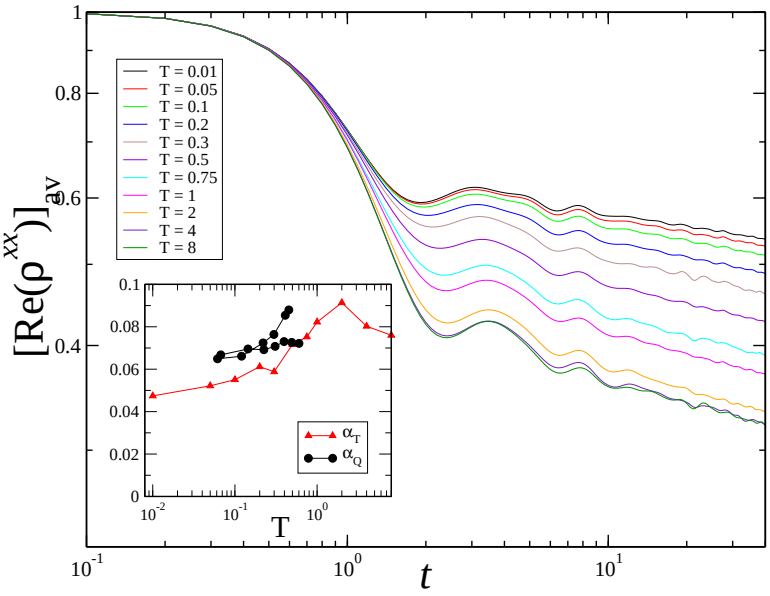

Figure 4.8: Real part of the autocorrelation function ρ^{xx} at thermal equilibrium with $\Gamma = 0.8$ for different values of the temperature for a chain of $L = 20$ sites and 10^5 disorder realizations. Inset: decay rates of the curves in main panel from a power law fit (red triangles), same decay rates of Fig. 4.6 (black dots).

at $\Gamma = 0.8$ for different temperatures. Also in this case we find power-law decays at long times, superimposed to oscillations. Apart from high temperature, where maybe some finite size effect is going on, the decay rates seem to increase with growing temperatures, which is reasonable.
As for the ordered case, we are not able at present to establish the validity of the predictions of the GGE in general, we can nevertheless show an example where it does seem to work, as in Fig. 4.9.

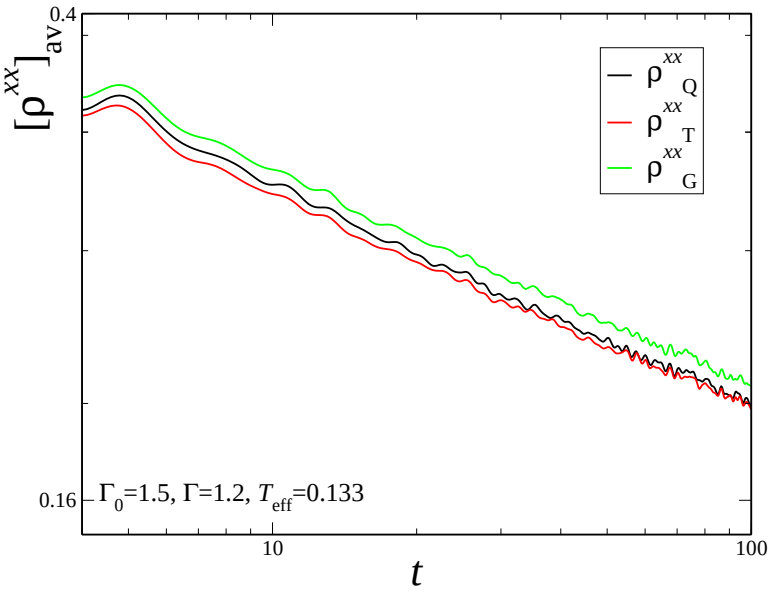

Figure 4.9: Modulus of the average ρ^{xx} for a system of $L = 30$ sites, 10^5 disorder instances. Comparison between the quench from $\Gamma_0 = 1.5$ to $\Gamma = 1.2$ (black), thermal with $T = 0.133$ (red) and the GGE (green) expectation values.

Conclusions

The quench dynamics of many-body systems has been the focus of this thesis. We tried to enlight some of the relations linking the various aspects of the problem, quantum phase transitions and the loss of adiabaticity on one side, integrability, thermalization and disorder on the other. In this conclusive section, the main results achieved are summerized chapter by chapter.

We first considered a case of slow quench, i.e. a situation in which the Hamiltonian of a quantum system has a parameter with a continuous time dependence. As we described in Chapter 1, this kind of problems becomes extremely interesting when, during its evolution, the system crosses a quantum critical point. In this case the evolution cannot be adiabatic. The precise characterization of the critical point in terms of critical exponents turns out to be fundamental to understand the out-of-equilibrium dynamics resulting from the quench in terms of scaling laws, as originally proposed in Refs. [157, 115]. As an example of slow quench, in Chapter 2 we have analyzed the quench dynamics of a quantum anisotropic spin-1 XY chain, when it crosses a Berezinskii-Kosterlitz-Thouless quantum phase transition. The quench has been performed on the uniaxial single-spin anisotropy, and has been chosen to vary linearly in time with a given velocity. We focused on the residual excess energy of the system after the quench, and studied its dependence on the velocity of the quench. For very slow quenches and finite system sizes we were able to describe the properties of the system in terms of an effective Landau Zener model, where the system can only get excited to its first excited state. Most interestingly, we pointed out the emergence of an intermediate region where the excess energy drops as a power-law with the quench rate, and exhibits a non trivial scaling behavior. At least for the finite sizes considered there, the decay rate depends on the size of the crossed critical region, and cannot be explained in terms of usual scaling arguments, such as the standard Kibble-Zurek mechanism and its generalization to critical surfaces [110, 141, 45, 49]. In the thermodynamic

limit the system obeys a non-trivial scaling behavior $E_{\text{exc}} \sim \tau^{-\alpha}$, with $1 < \alpha < 2$, even when $\tau \to \infty$ (i.e., for very slow quenches).

Then we turned our attention to the problem of sudden quenches. In particular in Chapter 3 we have discussed the relation between thermalization and integrability breaking. We considered the dynamics of a quantum XXZ Heisenberg spin chain following a quantum quench of the anisotropy parameter, in presence of a random on-site magnetic field which breaks integrability. We first studied in detail the breaking of integrability for different values of the disorder strength. To this aim we investigated the level spacing statistics and the inverse participation ratio as functions of the energy eigenvalues. The former is a spectral property capturing the crossover from a Poisson distrubition of the spacing, typical of integrable systems, to a Wigner-Dyson distribution, describing nonintegrable systems. The latter quantity characterizes the delocalization of the eigenstates in the presence of disorder with respect to an arbitrary basis, in particular we chose the integrable basis, composed of the eigenstates of the system in absence of disorder, and the computational basis. We found that at finite sizes there is a range of disorder in which the system shows a clear Wigner-Dyson distribution, while for small or very large magnetic fields the system tends to two integrable limits: the ordered XXZ and a classical spin system respectively. Then we suggested a way to trace the many-body (de)localization transition in Fock space [2, 6] by comparing the density of states with the inverse participation ratio in the integrable basis in a given microcanonical shell. We have shown that thermalization of observables happens in correspondence with the above transition and finally we have discussed the relation between the locality of observables in quasi-particle space and the corresponding behavior. Building on these results we have argued in general that if one wants to know when and how an interacting many-body system thermalizes, one should study the corresponding many-body localization/delocalization transition in quasi-particle space. Further numerical analyses of this scenario were shown in the Appendix B. We think that it would be very useful to find systems which allow to support our findings analitically.

In Chapter 4 we illustrated some preliminary results about the quantum Ising model in the presence of random couplings and random magnetic fields. This model is integrable, because it is equivalent to a system of free fermions. We focused on the dynamics following a quantum quench of the transverse fields. The idea behind the choice of this problem is understanding the effect of disorder on thermalization. For example, for the Ising model with no disorder, it has been shown [129, 130] that the autocorrelation function of the order parameter ρ^{xx} thermalizes after a quantum quench. Recalling

the discussion of Chapter 1 and the findings of Chapter 3, this result can be understood reminding that the order parameter in this case has a non-local expression in terms of quasi-particles. Does the presence of disorder change significantly the relaxation of ρ^{xx}? Although this work is at its initial stage, our numerical results suggest that the behavior of ρ^{xx} drastically changes if disorder is introduced. If in the ordered case ρ^{xx} decays exponentially and it is therefore possible to identify a time scale of the relaxation, in the disordered situation the decay is only algebraic. The autocorrelation ρ^{xx} evaluated at thermal equilibrium shows an analogous behaviour, passing from an exponential to a power-law decay. Another aim of the work in Chapter 4 would be to investigate the validity of the generalized Gibbs ensemble predictions for ρ^{xx} in the long-time limit, which is not a priori guaranteed, both with and without disorder. Unfortunately, on the grounds of our numerical results we are not able to draw a conclusive statement on this issue.

In this Thesis we addressed some problems concerning closed quantum systems out of equilibrium and tried to fit them into the theoretical frameworks developed in recent years. Nonetheless, the deep motivation moving this work lies in the amazing experimental possibilities offered by the rapidly growing field of cold atoms. The future perspective in the study of non-equilibrium systems, like the ones considered here, is having theory and experiment advancing hand in hand, with a direct comparison between theoretical predictions and *ad-hoc* engineered experiments.

Appendix A

Landau-Zener model for finite coupling times

The Landau-Zener (LZ) model consists in a two level system describing an avoided level crossing: two energy levels moving in time are widely separated at first, then they approach each other with time, and finally part away again [94, 155]. When the two levels are well separated, each eigenstate preserves an individual character; on the other hand, when levels are close together, they mix due to their interaction. The Hamiltonian is given by:

$$\mathcal{H}_{LZ} = \begin{pmatrix} -\Delta(t) & \Omega \\ \Omega & \Delta(t) \end{pmatrix}, \tag{A.0.1}$$

with a detuning $\Delta(t) = \beta^2 t$ (where $\beta^2 > 0$), and a time independent coupling Ω that, in the original LZ model, is supposed to last from $t_i = -\infty$ to $t_f = +\infty$ [94, 155]. Here we review the general case where the coupling is turned on at t_i and off at t_f [150, 149]. The equation A.0.1 is written in the basis of the two eigenstates of the Hamiltonian in absence of interaction Ω.

The probability amplitudes $\vec{C}(t_i) = [C_1(t_i),\, C_2(t_i)]^T$ for the two levels at the beginning are connected to the ones at the final time t_f by the unitary evolution matrix $U(t_f, t_i)$, so that: $\vec{C}(t_f) = U(t_f, t_i)\,\vec{C}(t_i)$. The elements of U are given by:

$$\begin{aligned} U_{11}(T_f, T_i) \quad &= \tfrac{\Gamma(1-\frac{1}{2}i\omega^2)}{\sqrt{2\pi}} [D_{i\omega^2/2}(T_f\sqrt{2}e^{-i\pi/4}) \\ &\times D_{-1+i\omega^2/2}(T_i\sqrt{2}e^{i3\pi/4}) + D_{i\omega^2/2}(T_f\sqrt{2}e^{i3\pi/4}) \\ &\times D_{-1+i\omega^2/2}(T_i\sqrt{2}e^{-i\pi/4})]\,, \end{aligned} \tag{A.0.2}$$

$$U_{12}(T_f,T_i) = \frac{\Gamma(1-\frac{1}{2}i\omega^2)}{\omega\sqrt{\pi}} e^{i\pi/4}[-D_{i\omega^2/2}(T_f\sqrt{2}e^{-i\pi/4}) \times D_{i\omega^2/2}(T_i\sqrt{2}e^{i3\pi/4}) + D_{i\omega^2/2}(T_f\sqrt{2}e^{i3\pi/4})\, D_{i\omega^2/2}(T_i\sqrt{2}e^{-i\pi/4})]\,, \tag{A.0.3}$$

where we have introduced the rescaled time $T = \beta t$ and the dimensionless coupling strength $\omega = \Omega/\beta$, while $D_\nu(z)$ denotes the parabolic cylinder functions. If we suppose that the system is initialized in its ground state, i.e., $\vec{C}(t_i) = [1,\, 0]^T$, the transition probability to the excited state at the final time is given by $P^{(d)}(t_f,t_i) = |U_{21}(t_f,t_i)|^2$.

It is useful to write the excitation probabilities also in the adiabatic basis, composed of the instantaneous system eigenstates. The basis used in the previous expression and the adiabatic basis are related by a unitary transformation. If $\vec{A}(t) = [A_1(t),\, A_2(t)]^T$ are the probability amplitudes for the two levels in the adiabatic basis, then $\vec{A}(t) = \mathbf{R}(t)\,\vec{C}(t)$, where $\mathbf{R}(t)$ is the rotation matrix

$$\mathbf{R}(T) = \begin{pmatrix} \cos\vartheta(t) & -\sin\vartheta(t) \\ \sin\vartheta(t) & \cos\vartheta(t) \end{pmatrix}, \tag{A.0.4}$$

with $\tan[2\vartheta(t)] = \Omega(t)/\Delta(t)$. Therefore, the evolution matrix in the adiabatic representation is given by $U_a(t_f,t_i) = \mathbf{R}^T(t_f)\,U(t_f,t_i)\,\mathbf{R}(t_i)$, and the adiabatic-following solution for the transition probability is $P^{(a)}(t_f,t_i) = |U_{21}^{(a)}(t_f,t_i)|^2$.

For the original LZ model, where the coupling is supposed to last from $t_i \to -\infty$ to $t_f \to +\infty$, the expression for the excitation probability at the end of the quench simplifies to an exponential form:

$$P^{(a)}(+\infty,-\infty) = e^{-\pi\omega^2}\,. \tag{A.0.5}$$

In the case of a *finite* coupling duration, that ends before or exactly at the crossing (i.e., $t_f \leq 0$), we have a much involved expression, which predicts a leading power-law behavior $P^{(a)} \sim \tau^{-2}$ superimposed to an oscillating behavior. Eventually oscillations are damped for long lasting couplings: in the limiting case where the quench ends at the critical point and is infinite lasting ($t_i = -\infty$, $t_f = 0$), the probability is given by

$$P^{(a)}(0,-\infty) = \frac{1}{16\,\omega^4} \sim \frac{1}{\tau^2}\,. \tag{A.0.6}$$

The scaling with the quench velocity τ follows from the fact that the times $t \propto \tau$, while $\beta^2 \propto 1/\tau$ (this implies that $\omega \propto \sqrt{\tau}$).

We used the explicit formula for the adiabatic transition probability $P^{(a)}(0,t_i<0)$ in order to fit t-DMRG data for the excess energy of our

system in the regime of large τ, where defects still do not form and the quench dynamics can be considered adiabatic. While it is clear that $t_i < 0$ in our case, it is not obvious a priori whether $t_f < 0$ or $t_f = 0$, since LZ relies on the assumption that there is only one point of closest approach of the energy levels; on the contrary, in our model we have a whole critical line. We actually chose $t_f = 0$ and used $t_i < 0$ as a fitting parameter, having not a rigorous criterion at our disposal, but following the qualitative picture suggested from figure 2.3: the gap closes monotonically during the quench, reaching the minimum at D_{fin}. The red curves in figure 2.4 have been obtained by fitting numerical data with the theoretical prediction given by $P^{(a)}$; we admitted a global rescaling prefactor ϕ and imposed the following constraints: $T_i = -T_0\sqrt{\tau}$, $T_f = 0$, $\omega = \omega_0\sqrt{\tau}$. The fitting parameters are T_0, ω_0, ϕ. For the left panel ($N = 6$) we chose $T_0 \approx 0.8$, $\omega_0 = 0.84$, $\phi = 1.72$, while for the right one ($N = 8$) $T_0 \approx 0.735$, $\omega_0 = 0.7$, $\phi = 0.9$.

Appendix B

Additional material on Many-Body Localization and Thermalization

B.1 Models and quantities of interest

We support the findings of Chapter 3 (and also Ref. [26]) with disordered XXZ models containing different integrability breaking terms, namely a random anisotropy R_z (defined below in Eq. B.1.4) or a random next-nearest neighbor hopping J_n (Eq. B.1.5). Although disorder is in general not strictly necessary to break integrability, we choose to use disordered models because they allow a better statistical analysis. In this section we define the models and the quantities of interest, the results are shown in Sec. B.2.
The general structure of the disordered Hamiltonians considered here is:

$$\mathcal{H} = \mathcal{H}_{\text{Int}}(J_z) + \Delta \sum_i \mathcal{O}_i h_i \tag{B.1.1}$$

where $\mathcal{H}_{\text{Int}}$ is integrable, Δ is the amplitude of disorder, $\mathcal{O}_i$ is a few-body term defined on site i, $\{h_i\}$ are random numbers uniformly distributed in $[-1, 1]$. The integrable part of the Hamiltonian is the anisotropic Heisenberg chain:

$$\mathcal{H}_{\text{Int}}(J_z) \equiv \mathcal{H}_{\text{H}} = \sum_{i=1}^{L-1} \left[J \left(\sigma_i^x \sigma_{i+1}^x + \sigma_i^y \sigma_{i+1}^y \right) + J_z \sigma_i^z \sigma_{i+1}^z \right] \tag{B.1.2}$$

Hereafter we will take $J = 1$ and express all the couplings in units of J. The non-integrable models [54, 48] are given by:

$$\mathcal{H}_{\mathrm{H,Z}} = \mathcal{H}_{\mathrm{H}} + \quad B_z \sum_{i=1}^{L} h_i \sigma_i^z \tag{B.1.3}$$

$$\mathcal{H}_{\mathrm{H,A}} = \mathcal{H}_{\mathrm{H}} + \quad R_z \sum_{i=1}^{L-1} h_i \sigma_i^z \sigma_{i+1}^z \tag{B.1.4}$$

$$\mathcal{H}_{\mathrm{H,N}} = \mathcal{H}_{\mathrm{H}} + \quad J_n \sum_{i=1}^{L-2} h_i \sigma_i^z \sigma_{i+2}^z \tag{B.1.5}$$

where $\{\sigma_i^\alpha\}$, $\alpha = x, y, z$ are Pauli matrices on site i. With the notation of Eq. B.1.1, we have for example $\Delta = B_z$, $\mathcal{O}_i = \sigma_i^z$ in Eq. B.1.3. We consider a sudden quench of J_z:

$$J_z(t) = \begin{cases} J_{z,i} & \text{for} \quad t < 0 \\ J_{z,f} & \text{for} \quad t \geq 0\,. \end{cases} \tag{B.1.6}$$

The results shown here are obtained numerically by means of exact diagonalization for systems with open boundary conditions.
For the models considered below we have performed the same analysis of Chapter 3 computing the same quantities, whose definition we now recall. We refer to Chapter 3 for a theoretical justification of their choice.
We study the level statistics by means of the level statistics indicator (LSI) η:

$$\eta \equiv \frac{\int_0^\infty |P(s) - P_{\mathrm{P}}(s)| ds}{\int_0^\infty |P_{\mathrm{WD}}(s) - P_{\mathrm{P}}(s)| ds}. \tag{B.1.7}$$

where $P(s)$ is the probability distribution function of the level spacing between neighboring levels.With this definition[1] the LSI is zero for systems with a Poisson distribution P_{P} of the spacings and is unity if the distribution is Wigner-Dyson P_{WD}. The LSI is characterized as a function of the energy eigenvalues in individual microcanonical shells according to:

$$\eta(E) \equiv \frac{\int_0^\infty |P_{[E,E+W]}(s) - P_{\mathrm{P}}(s)| ds}{\int_0^\infty |P_{\mathrm{WD}}(s) - P_{\mathrm{P}}(s)| ds}\,, \tag{B.1.8}$$

where $P_{[E,E+W]}(s)$ is the level statistics computed in the window $[E, E+W]$, and cumulatively:

$$\eta(E_{\leq}) \equiv \frac{\int_0^\infty |P_{[E_{\leq}]}(s) - P_{\mathrm{P}}(s)| ds}{\int_0^\infty |P_{\mathrm{WD}}(s) - P_{\mathrm{P}}(s)| ds}\,, \tag{B.1.9}$$

[1] The definition used here for the level statistics indicator slightly differs from the standard one, which is

$$\eta = \frac{\int_0^{s_0} [P(s) - P_{\mathrm{WD}}(s)] ds}{\int_0^{s_0} [P_{\mathrm{P}}(s) - P_{\mathrm{WD}}(s)] ds}$$

where $s_0 \approx 0.4729$ is the first intersection point of $P_{\mathrm{P}}(s)$ and $P_{\mathrm{WD}}(s)$. We cheked that the two definitions agree very well, our choice is due to numerical convenience.

where $P_{[E_\leq]}$ is the level statistics of eigenvalues with excitation energy less than $E_\leq$ with respect to the ground state energy.
We study the inverse participation ratio (IPR) ξ defined for a state $|\psi\rangle$ by:

$$\xi(|\psi\rangle) \equiv \left(\sum_n |\langle n|\psi\rangle|^4\right)^{-1} \tag{B.1.10}$$

where $\{|n\rangle\}$ is a basis of states whose choice is arbitrary. In our calculations $|\psi\rangle$ are the eigenstates of the disordered model Eq. B.1.1 and the basis $\{|n\rangle\}$ is the site (S) basis $|n_S\rangle = |\sigma_1 \cdots \sigma_L\rangle$ ($\sigma_i = \pm 1$), composed of the eigenstates of σ_i^z, and the integrable (I) basis, composed of the eigenstates $|n_I\rangle$ of the model in absence of randomness ($\Delta = 0$). Analogously to LSI, also the IPR is computed both in microcanonical shells and cumulatively, averaging on the eigenstates $|\psi\rangle$ and then on disorder.
Considering now the dynamics following the quantum quench, we first compute the effective temperature for each disorder realization from the equation:

$$E_0 \equiv \langle \mathcal{H}(J_{z,f})\rangle_{T_{\text{eff}}} = \text{Tr}\left(\rho(T_{\text{eff}})\mathcal{H}(J_{z,f})\right) \tag{B.1.11}$$

and then average over disorder. In Eq. B.1.11 $\rho(T_{\text{eff}})$ is the canonical density matrix of the final Hamiltonian at the effective temperature $\rho(T_{\text{eff}}) = 1/Z \exp(-\mathcal{H}(J_{z,f})/T_{\text{eff}})$.
We study the following observables:

$$n^\alpha(k) \equiv \frac{1}{L}\sum_{j,l=1}^{L} e^{i(j-l)k/L}\langle \sigma_j^\alpha \sigma_l^\alpha\rangle \qquad \alpha = x, z. \tag{B.1.12}$$

We compare their expectation value in the canonical ensemble at the effective temperature $n^\alpha_{T_{\text{eff}}}(k) \equiv \langle n^\alpha(k)\rangle_{T_{\text{eff}}}$ with the expectation value in the diagonal ensemble $n^\alpha_Q(k)$, see Eq. 3.6.2. We study the thermalization in terms of the absolute discrepancies:

$$\delta n^\alpha(k) \equiv |n^\alpha_Q(k) - n^\alpha_{T_{\text{eff}}}(k)| \tag{B.1.13}$$

B.2 Numerical results.

B.2.1 Level statistics

In Fig. B.1 we show the level statistics indicator η for a system of $L = 14$ sites. While for $\Delta = B_z$ a clear crossover from Poisson to Wigner-Dyson is visible, in the other two cases the statistics does not reach a Wigner-Dyson distribution, the maximum value of LSI being $\eta \sim 0.4$.

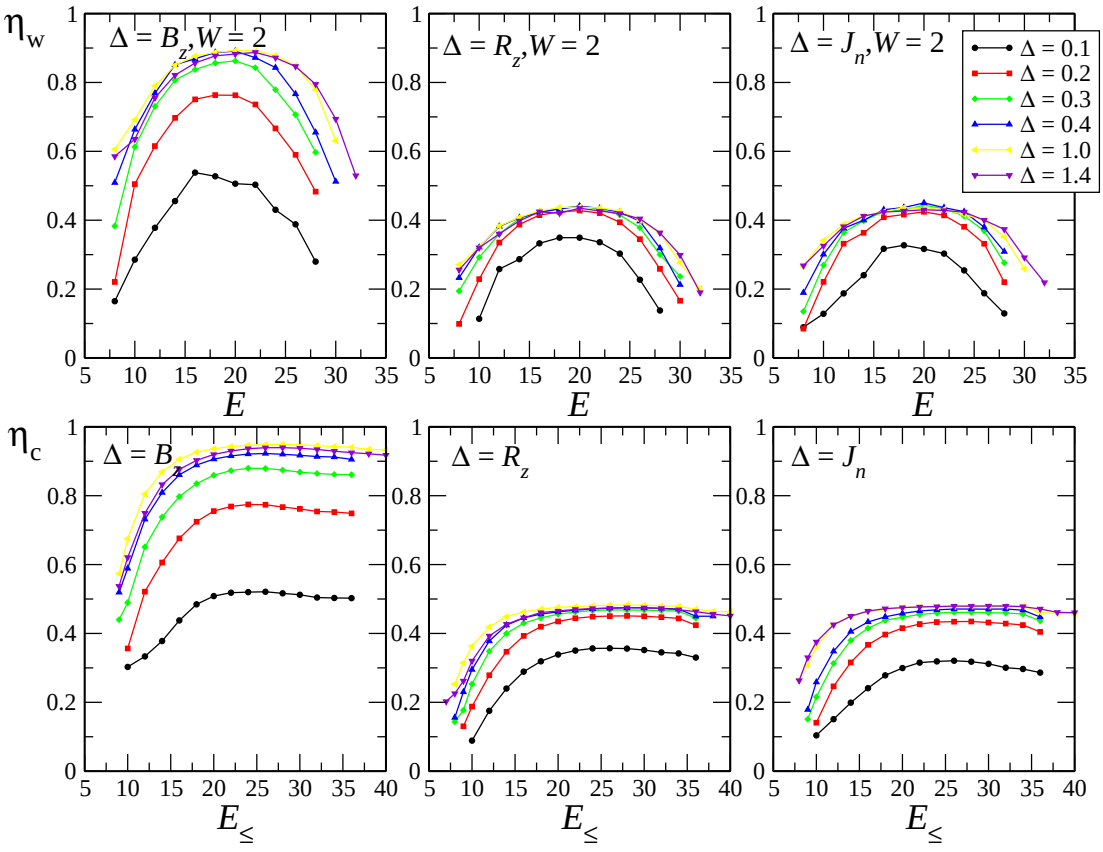

Figure B.1: Data for $L = 14$ with different values of the disorder Δ. Top panels: LSI in a microcanonical shells of width $W = 2$, lower panels: cumulative LSI. Average over 500 disorder instances for R_z and J_n, and ~ 1000 for B_z).

In Fig. B.2 we show the inverse participation ratio both in the integrable (top) and in the site basis (bottom). The IPR in the integrable basis in all the three cases shows that the eigenstates delocalize with increasing values of the disorder. This is more evident for the case $\Delta = B_z$, similarly to what happens for the LSI. The IPR in the computational basis has the opposite behavior, decreasing for larger values of the disorder. This is coherent with the fact that for all of the three cases the states of the computational basis are the eigenstates of the system for $\Delta \gg J_z$. In Fig. B.3 we quantify the delocalization in quasi-particle space induced by the integrability-breaking term. As expected from the study of the LSI and the IPR, in the cases

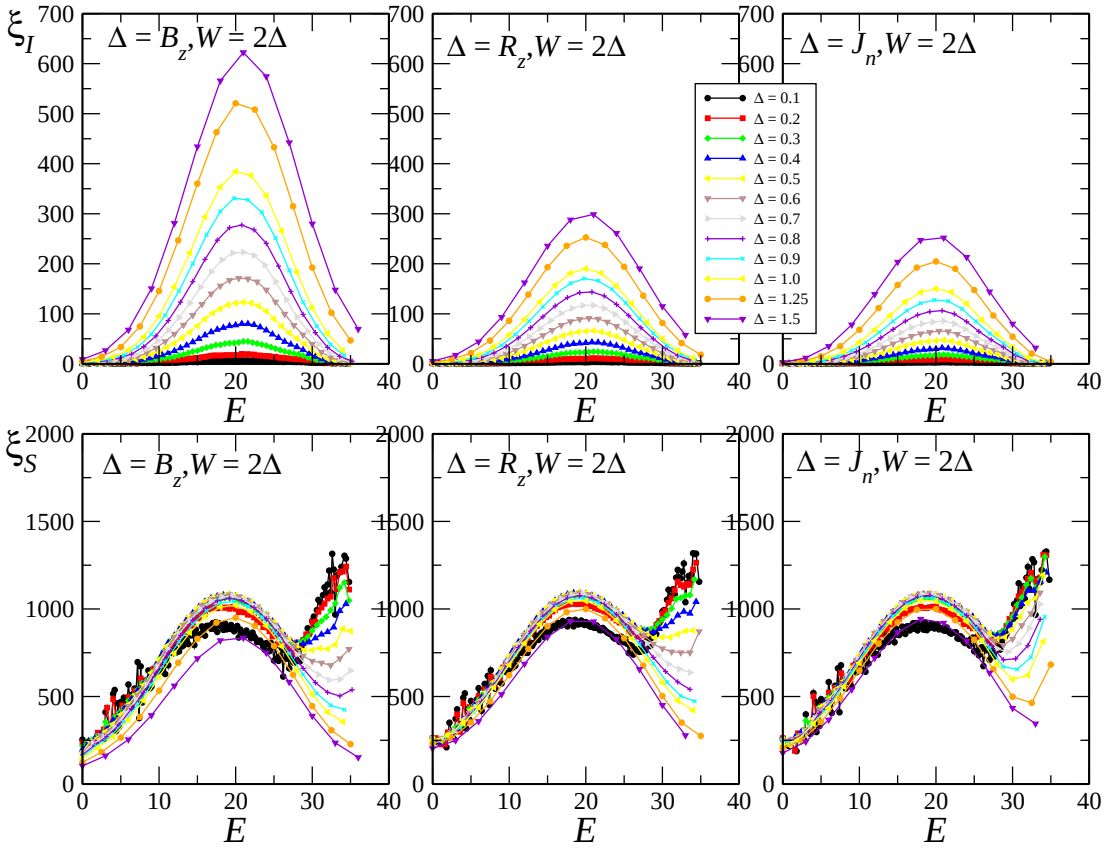

Figure B.2: Data for $L = 14$ with different values of the disorder Δ. Top panels: IPR in the integrable basis in a microcanonical shell of width $W = 2\Delta$, lower panels: IPR in the site basis. Average over 100 disorder instances.

$\Delta = R_z, J_n$ with $\Delta = 0.9$ the disorder term hybridized less states than the $\Delta = B_z$ term.

B.2.2 Effective temperature

In Fig. B.4 we show the effective temperature as a function of the initial value of the anisotropy for a system of $L = 12$ sites. In all the three cases the effective temperature satures for large values of J_z, because the ground state tends to the antiferromagnetic Néel state. For $J_z \gg 1$ and $\Delta \lesssim 1$ the effective temperature is $T_{\text{eff}} \sim 5$ in the three situations.

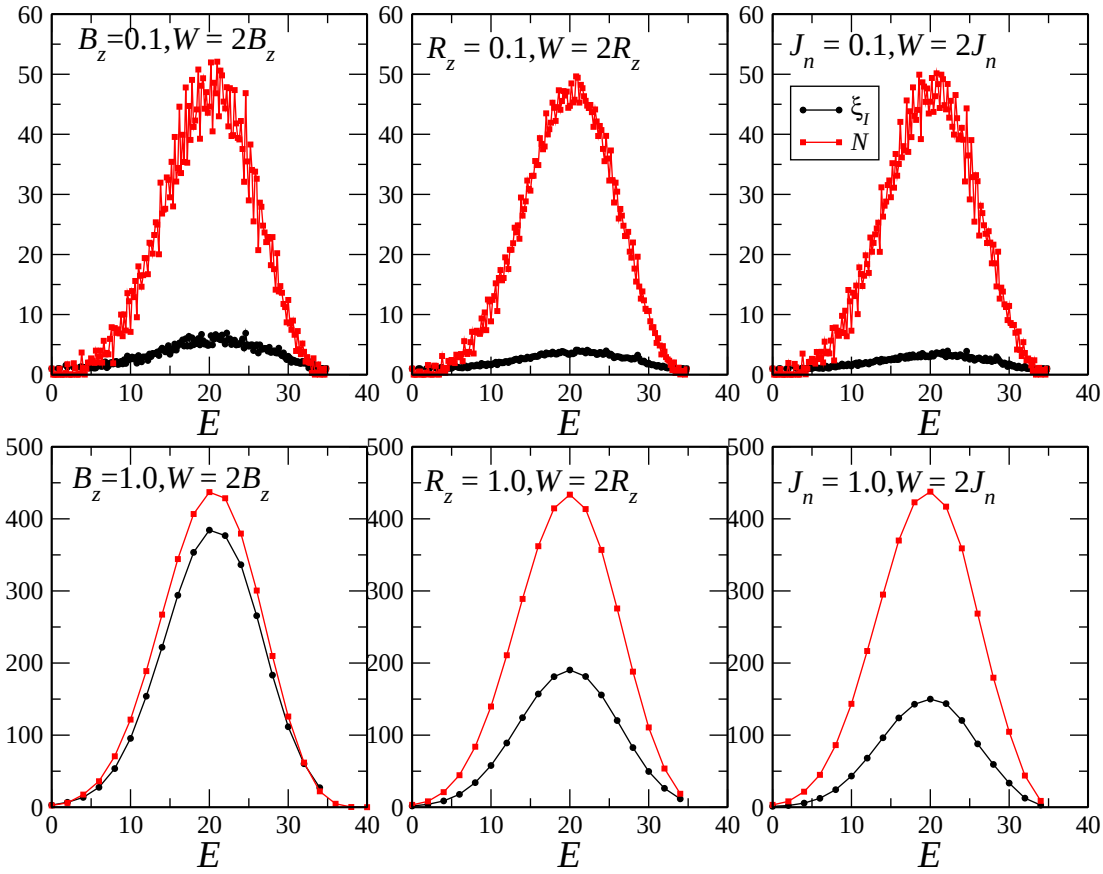

Figure B.3: Data for $L = 14$ with different values of the disorder Δ. Comparison between IPR in the integrable basis and number of states in microcanonical shells of width 2Δ. Upper panels $\Delta = 0.1$, lower panels $\Delta = 0.9$.

B.2.3 Thermalization of observables

An example of the different behavior of $n^x(k)$ and $n^z(k)$ is shown in Fig. B.5. The difference is best seen at $k = \pi$. The absolute discrepancy between the diagonal and the canonical ensemble prediction as a function of the initial value of the anisotropy are shown in Fig. B.6 for a system of $L = 12$ sites. The discrepancies between the diagonal and the canonical ensemble prediction as a function of the disorder amplitude are shown in Fig. B.7.

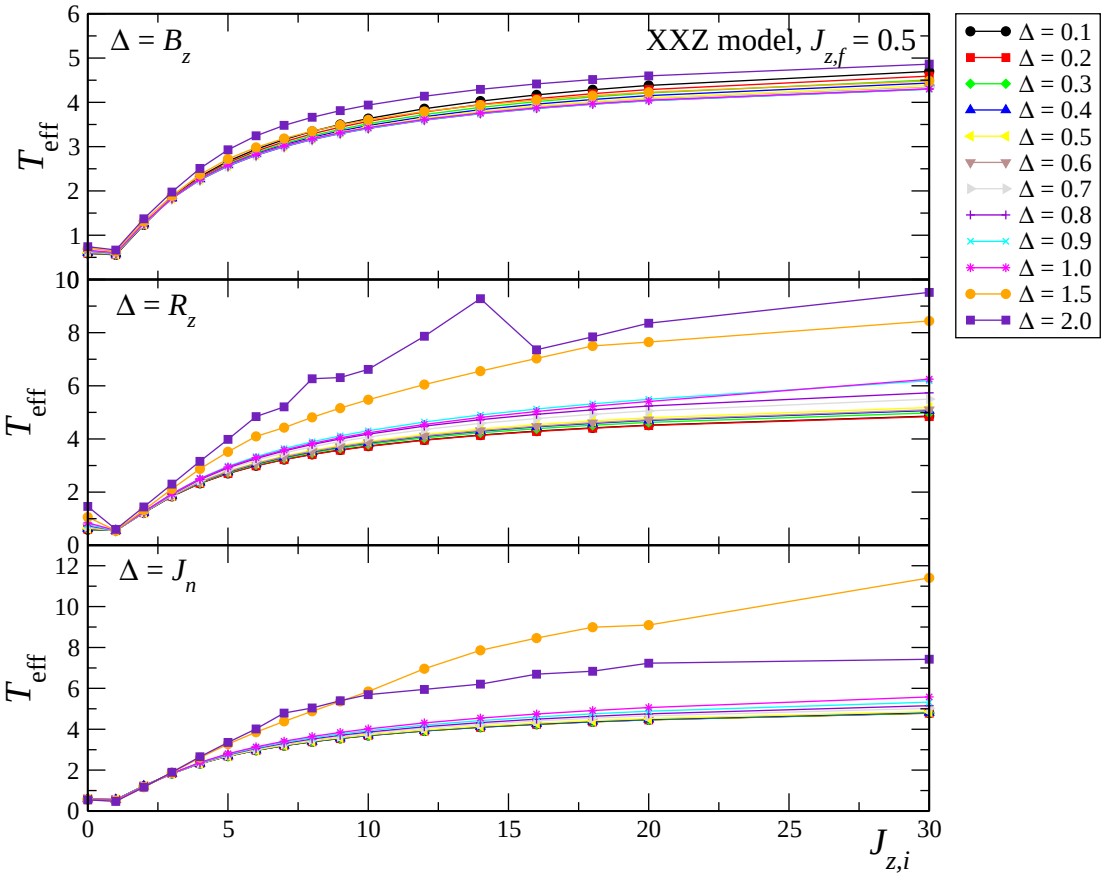

Figure B.4: Data for $L = 12$ with different values of the disorder. Average over 200 disorder instances.

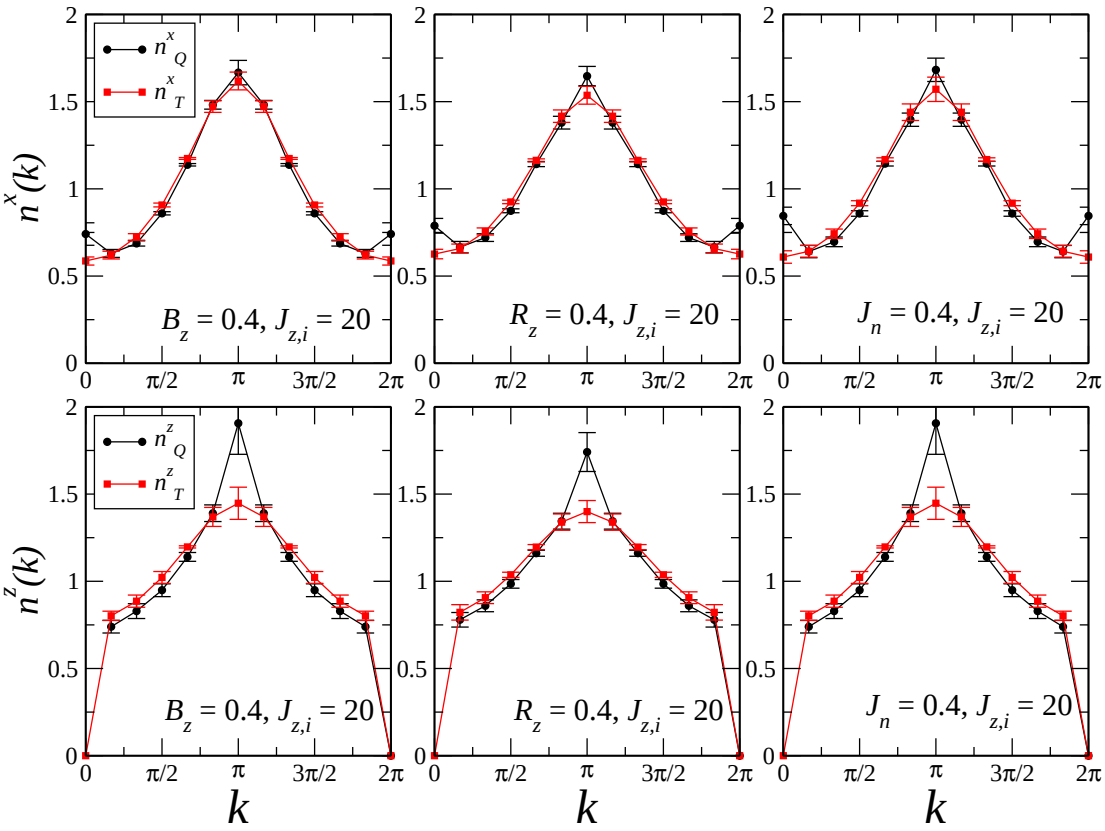

Figure B.5: Comparison between the diagonal and canonical expectation value of the momentum dependence n^α of the two-spin correlation function. Data for a quench from $J_{z,i} = 20$ to $J_{z,f} = 0.5$ and disorder intensity $\Delta = 0.4$. Upper panels: $n^x_Q(k)$ versus $n^x_T(k)$, lower panels $n^z_Q(k)$ versus $n^z_T(k)$. From left to right column: $\Delta = B_z$, $\Delta = R_z$, $\Delta = J_n$.

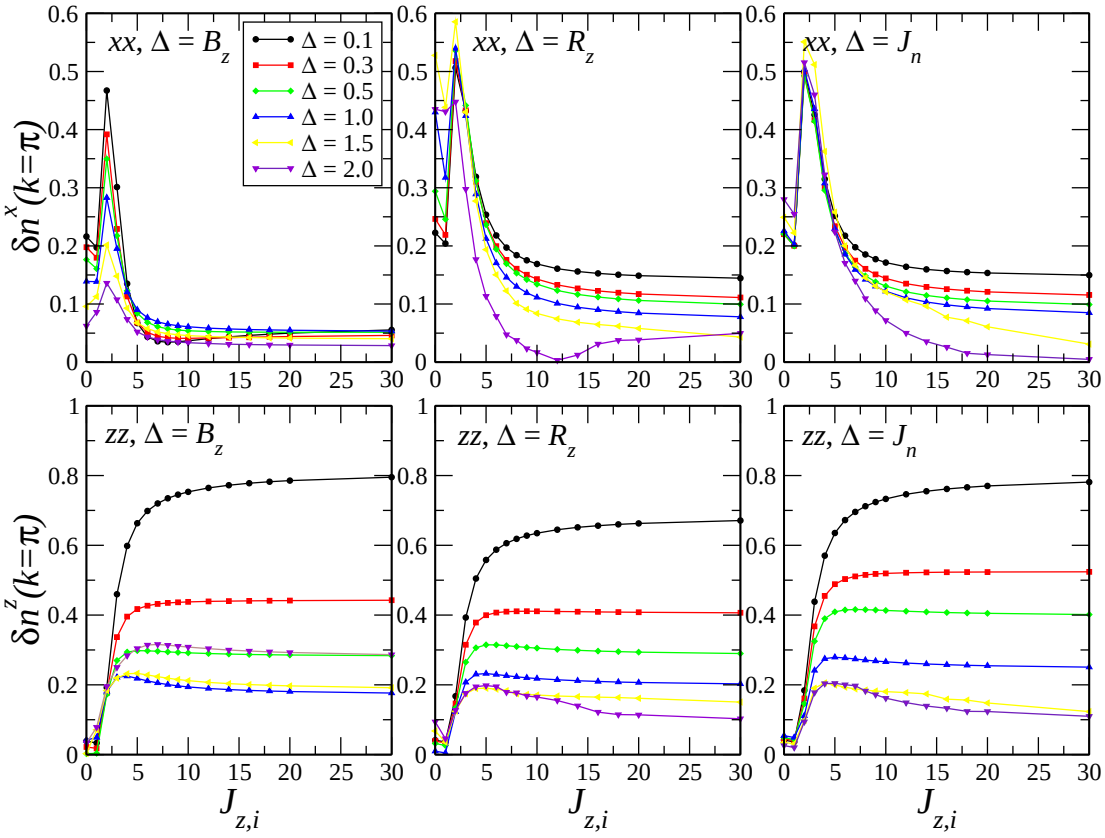

Figure B.6: Discrepancies $\delta n^x(\pi)$ (upper panels) and $\delta n^z(\pi)$ (lower panels) for a quench to $J_{z,f} = 0.5$ for different values of the disorder amplitude in the three cases. Data for $L = 12$, average on 200 disorder instances.

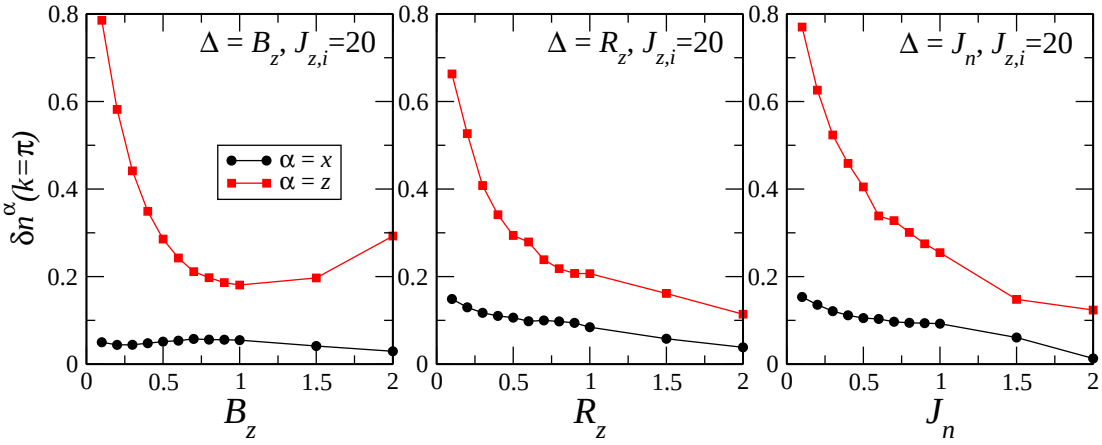

Figure B.7: Discrepancies $\delta n^x(\pi)$ (black circles) and $\delta n^z(\pi)$ (red squares) for a quench from $J_{z,i} = 20$ to $J_{z,f} = 0.5$. Data for $L = 12$, average on 200 disorder instances.

Bibliography

[1] E. Altman and A. Auerbach. Oscillating superfluidity of bosons in optical lattices. *Phys. Rev. Lett.*, 89(25):250404, 2002.

[2] B. L. Altshuler, Y. Gefen, A. Kamenev, and L. S. Levitov. Quasiparticle lifetime in a finite system: A nonperturbative approach. *Phys. Rev. Lett.*, 78(14):2803–2806, 1997.

[3] Y. Avishai, J. Richert, and R. Berkovits. Level statistics in a heisenberg chain with random magnetic field. *Phys. Rev. B*, 66(5):052416, 2002.

[4] R. Barankov and A. Polkovnikov. Optimal nonlinear passage through a quantum critical point. *Phys. Rev. Lett.*, 101:076801, 2008.

[5] T. Barthel and U. Schollwöck. Dephasing and the steady state in quantum many-particle systems. *Phys. Rev. Lett.*, 100(10):100601, 2008.

[6] D. Basko, I. Aleiner, and B. Altshuler. Metal-insulator transition in a weakly interacting many-electron system with localized single-particle states. *Annals of Physics*, 321(5):1126 – 1205, 2006.

[7] G. P. Berman, F. Borgonovi, F. M. Izrailev, and V. I. Tsifrinovich. Delocalization border and onset of chaos in a model of quantum computation. *Phys. Rev. E*, 64(5):056226, 2001.

[8] G. Biroli, L. F. Cugliandolo, and A. Sicilia. Kibble-zurek mechanism and infinitely slow annealing through critical points. *Phys. Rev. E*, 81(5):050101, 2010.

[9] G. Biroli, C. Kollath, and M. A. Laeuchli. Does thermalization occur in an isolated system after a global quantum quench? `arXiv:0907.3731`, 2009.

[10] I. Bloch, J. Dalibard, and W. Zwerger. Many-body physics with ultracold gases. *Rev. Mod. Phys.*, 80(3):885–964, 2008.

[11] C. D. E. Boschi, E. Ercolessi, F. Ortolani, and M. Roncaglia. On $c = 1$ critical phases in anisotropic spin-1 chains. *Eur. Phys. J. B*, 35(4):465–473, 2003.

[12] C. D. E. Boschi and F. Ortolani. Investigation of quantum phase transitions using multi-target dmrg methods. *Eur. Phys. J. B*, 41(4):14, 2004.

[13] W. G. Brown, L. F. Santos, D. J. Starling, and L. Viola. Quantum chaos, delocalization, and entanglement in disordered heisenberg models. *Phys. Rev. E*, 77(2):021106, 2008.

[14] P. Calabrese and J. Cardy. Entanglement entropy and quantum field theory. *JSTAT*, 2004(06):P06002, 2004.

[15] P. Calabrese and J. Cardy. Evolution of entanglement entropy in one-dimensional systems. *JSTAT*, 2005(04):P04010, 2005.

[16] P. Calabrese and J. Cardy. Time dependence of correlation functions following a quantum quench. *Phys. Rev. Lett.*, 96(13):136801, 2006.

[17] P. Calabrese and J. Cardy. Entanglement and correlation functions following a local quench: a conformal field theory approach. *JSTAT*, 2007(10):P10004, 2007.

[18] P. Calabrese and J. Cardy. Quantum quenches in extended systems. *JSTAT*, 2007(06):P06008, 2007.

[19] P. Calabrese and J. Cardy. Entanglement entropy and conformal field theory. *J.of Phys. A*, 42(50):504005, 2009.

[20] T. Caneva. *Adiabatic dynamics of many-body systems close to a quantum critical point.* PhD thesis, SISSA, 2009.

[21] T. Caneva, E. Canovi, D. Rossini, G. E. Santoro, and A. Silva. Quantum quenches in a random ising chain. In preparation, 2010.

[22] T. Caneva, R. Fazio, and G. E. Santoro. Adiabatic quantum dynamics of a random ising chain across its quantum critical point. *Phys. Rev. B*, 76:144427, 2007.

[23] T. Caneva, R. Fazio, and G. E. Santoro. Adiabatic quantum dynamics of the lipkin-meshkov-glick model. *Phys. Rev. B*, 78:104426, 2008.

[24] T. Caneva, M. Murphy, T. Calarco, R. Fazio, S. Montangero, V. Giovannetti, and G. E. Santoro. Optimal control at the quantum speed limit. *Phys. Rev. Lett.*, 103(24):240501, 2009.

[25] E. Canovi, D. Rossini, R. Fazio, and G. E. Santoro. Adiabatic dynamics of a spin-1 chain across the berezinskii-kosterlitz-thouless quantum phase transition. *J. Stat. Mech.*, page P03038, 2009.

[26] E. Canovi, D. Rossini, R. Fazio, G. E. Santoro, and A. Silva. Quantum quenches, thermalization and many-body localization. `arXiv:1006.1634`, 2010.

[27] M. A. Cazalilla. Effect of suddenly turning on interactions in the luttinger model. *Phys. Rev. Lett.*, 97(15):156403, 2006.

[28] M. Chaikin and T. Lubensky. *Principles of condensed matter physics*. Cambridge University Press, 1995.

[29] W. Chen, K. Hida, and B. C. Sanctuary. Ground-state phase diagram of $s = 1$ xxz chains with uniaxial single-ion-type anisotropy. *Phys. Rev. B*, 67(10):104401, 2003.

[30] R. W. Cherng and L. S. Levitov. Entropy and correlation functions of a driven quantum spin chain. *Phys. Rev. A*, 73(4):043614, 2006.

[31] G. D. Chiara, S. Montangero, P. Calabrese, and R. Fazio. Entanglement entropy dynamics of heisenberg chains. *JSTAT*, 2006(03):P03001, 2006.

[32] D. Chowdhury, U. Divakaran, and A. Dutta. Adiabatic dynamics in passage across quantum critical lines and gapless phases. *Phys. Rev. E*, 81(1):012101, 2010.

[33] L. Cincio, J. Dziarmaga, M. M. Rams, and W. H. Zurek. Entropy of entanglement and correlations induced by a quench: Dynamics of a quantum phase transition in the quantum ising model. *Phys. Rev. A*, 75:052321, 2007.

[34] S. R. Clark and D. Jaksch. Dynamics of the superfluid to mott-insulator transition in one dimension. *Phys. Rev. A*, 70(4):043612, 2004.

[35] M. Cramer, C. M. Dawson, J. Eisert, and T. J. Osborne. Exact relaxation in a class of nonequilibrium quantum lattice systems. *Phys. Rev. Lett.*, 100(3):030602, 2008.

[36] F. M. Cucchietti, B. Damski, J. Dziarmaga, and W. H. Zurek. Dynamics of the bose-hubbard model: Transition from a mott insulator to a superfluid. *Phys. Rev. A*, 75(2):023603, 2007.

[37] B. Damski. The simplest quantum model supporting the kibble-zurek mechanism of topological defect production: Landau-zener transitions from a new perspective. *Phys. Rev. Lett.*, 95:035701, 2005.

[38] G. De Chiara, M. Rizzi, D. Rossini, and S. Montangero. Density Matrix Renormalization Group for Dummies. *Journal of Computational and Theoretical Nanoscience*, 5(7):1277–1288, 2008.

[39] C. De Grandi, R. A. Barankov, and A. Polkovnikov. Adiabatic nonlinear probes of one-dimensional bose gases. *Phys. Rev. Lett.*, 101(23):230402, 2008.

[40] C. De Grandi, V. Gritsev, and A. Polkovnikov. Quench dynamics near a quantum critical point: Application to the sine-gordon model. *Phys. Rev. B*, 81(22):224301, 2010.

[41] C. De Grandi, V. Gritsev, and A. Polkovnikov. Quench dynamics near a quantum critical point: Application to the sine-gordon model. *Phys. Rev. B*, 81(22):224301, 2010.

[42] C. De Grandi and A. Polkovnikov. *Quantum Quenching, Annealing and Computation*, chapter Adiabatic perturbation theory: from Landau-Zener problem to quenching through a quantum critical point. Lecture Notes in Physics. Springer, Heidelberg, 2010.

[43] A. del Campo, G. D. Chiara, G. Morigi, M. B. Plenio, and A. Retzker. Structural defects in ion crystals by quenching the external potential: the inhomogeneous kibble-zurek mechanism. `arXiv:1002.2524`, 2010.

[44] M. den Nijs and K. Rommelse. Preroughening transitions in crystal surfaces and valence-bond phases in quantum spin chains. *Phys. Rev. B*, 40(7):4709–4734, 1989.

[45] S. Deng, G. Ortiz, and L. Viola. Dynamical non-ergodic scaling in continuous finite-order quantum phase transitions. *Europhys. Lett.*, 84:67008, 2008.

[46] S. Deng, G. Ortiz, and L. Viola. Anomalous nonergodic scaling in adiabatic multicritical quantum quenches. *Phys. Rev. B*, 80(24):241109, 2009.

[47] J. M. Deutsch. Quantum statistical mechanics in a closed system. *Phys. Rev. A*, 43(4):2046–2049, 1991.

[48] M. Di Stasio and X. Zotos. Connection between low energy effective hamiltonians and energy level statistics. *Phys. Rev. Lett.*, 74(11):2050–2053, 1995.

[49] U. Divakaran, A. Dutta, and D. Sen. Quenching along a gapless line: A different exponent for defect density. *Phys. Rev. B*, 78(14):144301, 2008.

[50] U. Divakaran, V. Mukherjee, A. Dutta, and D. Sen. Defect production due to quenching through a multicritical point. *J. Stat. Mech.*, page P02007, 2009.

[51] B. Dóra, E. V. Castro, and R. Moessner. Quantum quench dynamics and population inversion in bilayer graphene. `arXiv:1004.3757`, 2010.

[52] B. Dóra and R. Moessner. Nonlinear electric transport in graphene: Quantum quench dynamics and the schwinger mechanism. *Phys. Rev. B*, 81(16):165431, 2010.

[53] U. Dorner, P. Fedichev, D. Jaksch, M. Lewenstein, and P. Zoller. Entangling strings of neutral atoms in 1d atomic pipeline structures. *Phys. Rev. Lett.*, 91:073601, 2003.

[54] C. A. Doty and D. S. Fisher. Effects of quenched disorder on spin-1/2 quantum xxz chains. *Phys. Rev. B*, 45(5):2167–2179, 1992.

[55] F. Dukesz, M. Zilbergerts, and L. F. Santos. Interplay between interaction and (un)correlated disorder in one-dimensional many-particle systems: delocalization and global entanglement. *New J. of Phys.*, 11, 2009.

[56] J. Dziarmaga. Dynamics of a quantum phase transition: Exact solution of the quantum ising model. *Phys. Rev. Lett.*, 95(24):245701, 2005.

[57] J. Dziarmaga. Dynamics of a quantum phase transition in the random ising model: Logarithmic dependence of the defect density on the transition rate. *Phys. Rev. B*, 74:064416, 2006.

[58] J. Dziarmaga. Dynamics of a quantum phase transition and relaxation to a steady state. `arXiv:0912.4034`, 2009.

[59] J. Dziarmaga, J. Meisner, and W. H. Zurek. Winding up of the wavefunction phase by an insulator-to-superfluid transition in a ring of coupled bose-einstein condensates. *Phys. Rev. Lett.*, 101:115701, 2008.

[60] J. Dziarmaga and M. M. Rams. Dynamics of an inhomogeneous quantum phase transition. `arXiv:0904.0115`, 2009.

[61] M. Eckstein and M. Kollar. Nonthermal steady states after an interaction quench in the falicov-kimball model. *Phys. Rev. Lett.*, 100(12):120404, 2008.

[62] M. Eckstein, M. Kollar, and P. Werner. Thermalization after an interaction quench in the hubbard model. *Phys. Rev. Lett.*, 103(5):056403, 2009.

[63] M. Fagotti and P. Calabrese. Evolution of entanglement entropy following a quantum quench: Analytic results for the xy chain in a transverse magnetic field. *Phys. Rev. A*, 78(1):010306, 2008.

[64] M. Fagotti and P. Calabrese. Entanglement entropy of two disjoint blocks in xy chains. *JSTAT*, 2010(04):P04016, 2010.

[65] E. Farhi, J. Goldstone, S. Gutmann, J. Lapan, A. Lundgren, and D. Preda. A quantum adiabatic evolution algorithm applied to random instances of an NP-Complete problem. *Science*, 292:472, 2001.

[66] A. Faribault, P. Calabrese, and J.-S. Caux. Bethe ansatz approach to quench dynamics in the richardson model. *J.of Math. Phys.*, 50(9):095212, 2009.

[67] A. Faribault, P. Calabrese, and J.-S. Caux. Quantum quenches from integrability: the fermionic pairing model. *JSTAT*, 2009(03):P03018, 2009.

[68] E. Fermi, J. Pasta, and S. Ulam. Studies of nonlinear problems. Document LA-1940, 1955.

[69] A. Fetter and J. Walecka. *Quantum Theory of Many-particle Systems*. McGraw-Hill, New York, New York.

[70] D. Fioretto and G. Mussardo. Quantum quenches in integrable field theories. *New Journal of Physics*, 12(5):055015, 2010.

[71] D. S. Fisher. Random transverse field ising spin chains. *Phys. Rev. Lett.*, 69(3):534–537, 1992.

[72] D. S. Fisher. Critical behavior of random transverse-field ising spin chains. *Phys. Rev. B*, 51:6411, 1995.

[73] M. P. A. Fisher, P. B. Weichman, G. Grinstein, and D. S. Fisher. Boson localization and the superfluid-insulator transition. *Phys. Rev. B*, 40(1):546–570, 1989.

[74] G. Gallavotti. *Statistical Mechanics: A Short Treatise*. Springer, Berlin, 1999.

[75] D. M. Gangardt and M. Pustilnik. Correlations in an expanding gas of hard-core bosons. *Phys. Rev. A*, 77(4):041604, 2008.

[76] S. Goldstein, J. L. Lebowitz, R. Tumulka, and N. Zanghi. Long-time behavior of macroscopic quantum systems: Commentary accompanying the english translation of john von neumann's 1929 article on the quantum ergodic theorem. `ariXiv:1003.2129`, 2010.

[77] I. V. Gornyi, A. D. Mirlin, and D. G. Polyakov. Interacting electrons in disordered wires: Anderson localization and low-t transport. *Phys. Rev. Lett.*, 95(20):206603, 2005.

[78] M. Greiner, O. Mandel, T. Esslinger, T. Hansch, and I. Bloch. Quantum phase transition from a superfluid to a mott insulator in a gas of ultracold atoms. *Nature*, 415(6867):39–44, 2002.

[79] V. Gritsev and A. Polkovnikov. *Understanding Quantum Phase Transitions*, chapter Universal Dynamics Near Quantum Critical Points. Taylor & Francis, Boca Raton, 2010.

[80] T. Guhr, A. Muller-Groeling, and H. Weidenmuller. Random-matrix theories in quantum physics: Common concepts. *Phys. Rep.*, 299(4-6):190–425, 1998.

[81] F. Haake. *Quantum Signatures of Chaos*. Springer-Verlag, Berlin, 1991.

[82] F. D. M. Haldane. Effective harmonic-fluid approach to low-energy properties of one-dimensional quantum fluids. *Phys. Rev. Lett.*, 47(25):1840–1843, 1981.

[83] S. D. Huber, E. Altman, H. P. Büchler, and G. Blatter. Dynamical properties of ultracold bosons in an optical lattice. *Phys. Rev. B*, 75(8):085106, 2007.

[84] M. Žnidaric, T. c. v. Prosen, and P. Prelovšek. Many-body localization in the heisenberg xxz magnet in a random field. *Phys. Rev. B*, 77(6):064426, 2008.

[85] F. Iglói and H. Rieger. Random transverse ising spin chain and random walks. *Phys. Rev. B.*, 57:11404, 1998.

[86] F. Izrailev. Simple-models of quantum chaos - spectrum and eigenfunctions. *Phys. Rep.*, 196(5-6):299–392, 1990.

[87] P. Jacquod and D. L. Shepelyansky. Emergence of quantum chaos in finite interacting fermi systems. *Phys. Rev. Lett.*, 79(10):1837–1840, 1997.

[88] D. Jaksch, C. Bruder, J. I. Cirac, C. W. Gardiner, and P. Zoller. Cold bosonic atoms in optical lattices. *Phys. Rev. Lett.*, 81(15):3108–3111, 1998.

[89] T. Kinoshita, T. Wenger, and D. Weiss. A quantum newton's cradle. *Nature;*, 440(7086):900–903, 2006.

[90] M. Kollar and M. Eckstein. Relaxation of a one-dimensional mott insulator after an interaction quench. *Phys. Rev. A*, 78(1):013626, 2008.

[91] C. Kollath, A. M. Läuchli, and E. Altman. Quench dynamics and nonequilibrium phase diagram of the bose-hubbard model. *Phys. Rev. Lett.*, 98(18):180601, 2007.

[92] K. Kudo and T. Deguchi. Level statistics of xxz spin chains with a random magnetic field. *Phys. Rev. B*, 69(13):132404, 2004.

[93] A. Lamacraft. Quantum quenches in a spinor condensate. *Phys. Rev. Lett.*, 98(16):160404, 2007.

[94] L. D. Landau and E. M. Lifshits. *Quantum mechanics - non-relativistic theory*, volume 3 of *Course of theoretical physics*. Pergamon Press, third edition, 1977.

[95] E. Lieb, T. Schultz, and D. Mattis. Two soluble models of an antiferromagnetic chain. *Ann. Phys. (N.Y.)*, 16:407, 1961.

[96] S. R. Manmana, S. Wessel, R. M. Noack, and A. Muramatsu. Strongly correlated fermions after a quantum quench. *Phys. Rev. Lett.*, 98(21):210405, 2007.

[97] P. Mazur. Non-ergodicity of phase functions in certain systems. *Physica*, 43(4):533 – 545, 1969.

[98] B. McCoy and T. Wu. *The Two Dimensional Ising Model*. Harvard University Press, Cambridge, Massachussets, 1973.

[99] A. Messiah. *Quantum mechanics*, volume 2. North-Holland, Amsterdam, 1962.

[100] M. Moeckel and S. Kehrein. Interaction quench in the hubbard model. *Phys. Rev. Lett.*, 100(17):175702, 2008.

[101] M. Moeckel and S. Kehrein. Crossover from adiabatic to sudden interaction quenches in the hubbard model: prethermalization and non-equilibrium dynamics. *New J. of Phys.*, 12(5):055016, 2010.

[102] S. Mondal, K. Sengupta, and D. Sen. Theory of defect production in nonlinear quench across a quantum critical point. *Phys. Rev. B*, 79(4):045128, 2009.

[103] C. Monthus and T. Garel. Many-body localization transition in a lattice model of interacting fermions: Statistics of renormalized hoppings in configuration space. *Phys. Rev. B*, 81(13):134202, 2010.

[104] V. Mukherjee, U. Divakaran, A. Dutta, and D. Sen. Quenching dynamics if a quantum xy spin-1/2 chain in presence of a transverse field. *Phys. Rev. B*, 76:174303, 2007.

[105] V. Mukherjee, A. Dutta, and D. Sen. Defect generation in a spin- 12 transverse xy chain under repeated quenching of the transverse field. *Phys. Rev. B*, 77(21):214427, 2008.

[106] G. Mussardo. *Statistical field theory. An Introduction to Exactly Solved Models in Stastical Physics.* Oxford. Oxford University Press, 2009.

[107] N. Nagaosa. *Quantum Field Theory in Strongly Correlated Electronic Systems*. Springer-Verlag, Berlin, 1999.

[108] V. Oganesyan and D. A. Huse. Localization of interacting fermions at high temperature. *Phys. Rev. B*, 75(15):155111, 2007.

[109] A. Pal and D. A. Huse. The many-body localization transition. `arXiv:1003.2613`, 2010.

[110] F. Pellegrini, S. Montangero, G. E. Santoro, and R. Fazio. Adiabatic quenches through an extended quantum critical region. *Phys. Rev. B*, 77(14):140404, 2008.

[111] A. Peres. Ergodicity and mixing in quantum theory. i. *Phys. Rev. A*, 30(1):504–508, 1984.

[112] P. Pfeuty. The one-dimensional ising model with a transverse field. *Ann. Phys. (N.Y.)*, 57:79, 1970.

[113] A. S. Pires and M. E. Gouvêa. Quantum fluctuations in low-dimensional easy-plane spin models. *Eur. Phys. J. B*, 44(2):169–174, 2005.

[114] D. Poilblanc, T. Ziman, J. Bellissard, F. Mila, and G. Montambaux. Poisson vs. goe statistics in integrable and non-integrable quantum hamiltonians. *Euophys. Lett.*, 22(7):537, 1993.

[115] A. Polkovnikov. Universal adiabatic dynamics in the vicinity of a quantum critical point. *Phys. Rev. B*, 72:161201(R), 2005.

[116] A. Polkovnikov. Microscopic diagonal entropy and its connection to basic thermodynamic relations. `arXiv:0806.2862`, 2008.

[117] A. Polkovnikov and V. Gritsev. Breakdown of the adiabatic limit in low-dimensional gapless systems. *Nature Physics*, 4:477, 2008.

[118] A. Polkovnikov, K. Sengupta, A. Silva, and M. Vengalattore. Nonequilibrium dynamics of closed interacting quantum systems. `arXiv:1007.5331`, 2010.

[119] D. A. Rabson, B. N. Narozhny, and A. J. Millis. Crossover from poisson to wigner-dyson level statistics in spin chains with integrability breaking. *Phys. Rev. B*, 69(5):054403, 2004.

[120] G. Refael and J. Moore. Entanglement entropy of random quantum critical points in one dimension. *Phys. Rev. Lett.*, 93:260602, 2004.

[121] C. Regal and D. S. Jin. Experimental realization of bcs-bec crossover physics with a fermi gas of atoms. `arXiv:cond-mat/0601054v1`.

[122] H. Rieger and F. Iglói. Quantum critical dynamics of the random transverse-field ising spin chain. *Europhys. Lett.*, 39(2):135, 1997.

[123] M. Rigol. Breakdown of thermalization in finite one-dimensional systems. *Phys. Rev. Lett.*, 103(10):100403, 2009.

[124] M. Rigol, V. Dunjko, and M. Olshanii. Thermalization and its mechanism for generic isolated quantum systems. *Nature*, 452(7189):854–858, 2008.

[125] M. Rigol, V. Dunjko, V. Yurovsky, and M. Olshanii. Relaxation in a completely integrable many-body quantum system: An ab initio study of the dynamics of the highly excited states of 1d lattice hard-core bosons. *Phys. Rev. Lett.*, 98(5):050405, 2007.

[126] M. Rigol and L. F. Santos. Quantum chaos and thermalization in gapped systems after a quench. `arXiv:1003.1403`, 2010.

[127] G. Rigolin and G. Ortiz. Adiabatic perturbation theory and geometric phases for degenerate systems. *Phys. Rev. Lett.*, 104(17):170406, 2010.

[128] G. Rigolin, G. Ortiz, and V. H. Ponce. Beyond the quantum adiabatic approximation: Adiabatic perturbation theory. *Phys. Rev. A*, 78(5):052508, 2008.

[129] D. Rossini, A. Silva, G. Mussardo, and G. E. Santoro. Effective thermal dynamics following a quantum quench in a spin chain. *Phys. Rev. Lett.*, 102(12):127204, 2009.

[130] D. Rossini, A. Silva, G. Mussardo, and G. E. Santoro. Long time dynamics following a quench in an integrable quantum spin chain: local versus non-local operators and effective thermal behavior. `arXiv:1002.2842`, 2010.

[131] S. Sachdev. *Quantum Phase Transition*. Cambridge University Press, 1999.

[132] S. Sachdev and A. P. Young. Low temperature relaxational dynamics of the ising chain in a transverse field. *Phys. Rev. Lett*, 78(11):2220, 1997.

[133] L. E. Sadler, J. M. Higbie, S. R. Leslie, M. Vengalattore, and D. M. Stamper-Kurn. Spontaneous symmetry breaking in a quenched ferromagnetic spinor bose-einstein condensate. *Nature*, 443:312, 2006.

[134] G. E. Santoro, R. Martoňák, E. Tosatti, and R. Car. Theory of quantum annealing of an Ising spin glass. *Science*, 295:2427, 2002.

[135] G. E. Santoro and E. Tosatti. Optimization using quantum mechanics: Quantum annealing through adiabatic evolution. *J. Phys. A: Math. Gen.*, 39:R393–R431, 2006.

[136] L. F. Santos and M. Rigol. Onset of quantum chaos in one-dimensional bosonic and fermionic systems and its relation to thermalization. *Phys. Rev. E*, 81(3):036206, 2010.

[137] U. Schollwöck. The density-matrix renormalization group. *Rev. Mod. Phys.*, 77(1):259–315, 2005.

[138] H. J. Schulz. Phase diagrams and correlation exponents for quantum spin chains of arbitrary spin quantum number. *Phys. Rev. B*, 34(9):6372–6385, 1986.

[139] R. Schützhold, M. Uhlmann, Y. Xu, and U. R. Fischer. Sweeping from the superfluid to the mott phase in the bose-hubbard model. *Phys. Rev. Lett.*, 97(20):200601, 2006.

[140] D. Sen, K. Sengupta, and S. Mondal. Defect production in nonlinear quench across a quantum critical point. *Phys. Rev. Lett.*, 101:016806, 2008.

[141] K. Sengupta, D. Sen, and S. Mondal. Exact results for quench dynamics and defect production in a two-dimensional model. *Phys. Rev. Lett.*, 100(7):077204, 2008.

[142] R. Shankar and G. Murthy. Nearest-neighbor frustrated random-bond model in d=2: Some exact results. *Phys. Rev. B*, 36(1):536–545, 1987.

[143] S. Sotiriadis, P. Calabrese, and J. Cardy. Quantum quench from a thermal initial state. *Europhys. Lett.*, 87(2):20002, 2009.

[144] M. Srednicki. Chaos and quantum thermalization. *Phys. Rev. E*, 50(2):888–901, 1994.

[145] B. Sutherland. *Beautiful Models*. World Scientific, 2004.

[146] A. K. Tuchman, C. Orzel, A. Polkovnikov, and M. A. Kasevich. Nonequilibrium coherence dynamics of a soft boson lattice. *Phys. Rev. A*, 74(5):051601, 2006.

[147] L. C. Venuti, C. D. E. Boschi, E. Ercolessi, G. Morandi, F. Ortolani, S. Pasini, and M. Roncaglia. Stable particles in anisotropic spin-1 chains. *Eur. Phys. J. B*, 53(1):11–18, 2006.

[148] G. Vidal, J. I. Latorre, E. Rico, and A. Kitaev. Entanglement in quantum critical phenomena. *Phys. Rev. Lett.*, 90(22):227902, 2003.

[149] N. V. Vitanov. Transition time in the landau-zener model. *Phys. Rev. A*, 59:988, 1999.

[150] N. V. Vitanov and B. M. Garraway. Landau-zener model: Effects of finite coupling duration. *Phys. Rev. A*, 53:4288, 1996.

[151] J. von Neumann. Beweis des ergodensatzes und des h-theorems in der neuen mechanik. *Z. f. Physik*, 57:30–70, 1929.

[152] A. Young. Finite-temperature and dynamical properties of the random transverse-field ising spin chain. *Phys. Rev. B*, 56:11691, 1997.

[153] A. P. Young and H. Rieger. Numerical study of the random transverse-field ising spin chain. *Phys. Rev. B*, 53:8486, 1996.

[154] V. Zelevinsky, B. Brown, N. Frazier, and M. Horoi. The nuclear shell model as a testing ground for many-body quantum chaos. *Phys. Rep.*, 276:85–176, 1996.

[155] C. Zener. Non-adiabatic crossing of energy levels. *Proc. Royal Soc. A*, 137:696, 1932.

[156] W. H. Zurek. Cosmological experiments in superfluid-helium. *Nature*, 317:505, 1985.

[157] W. H. Zurek, U. Dorner, and P. Zoller. Dynamics of a quantum phase transition. *Phys. Rev. Lett.*, 95:105701, 2005.